Improving Dike Slope Failure Assessments related to Groundwater Hydrology

Grondwater gerelateerde verbeteringen aan de beoordeling van macrostabiliteit van waterkeringen

(met een samenvatting in het Nederlands)

Proefschrift

ter verkrijging van de graad van doctor aan de
Universiteit Utrecht
op gezag van de
rector magnificus, prof. dr. H.R.B.M. Kummeling,
ingevolge het besluit van het college voor promoties
in het openbaar te verdedigen op

vrijdag 15 september 2023 des middags te 4.15 uur

door

Teun Antonius Andreas van Woerkom

geboren op 11 juni 1995
te Tilburg

Promotoren:
Prof. dr. M.F.P. Bierkens
Prof. dr. H. Middelkoop

Copromotor:
Dr. L.P.H. van Beek

Beoordelingscommissie:
Prof. dr. ir. M. Kok
Prof. dr. M.A. Hicks
Prof. dr. J.C.J. Kwadijk
Dr. A. Zech
Prof. dr. E. Stouthamer

Utrecht Studies in Earth Science 287

Improving Dike Slope Failure Assessments related to Groundwater Hydrology

Teun Antonius Andreas van Woerkom

Utrecht 2023

Faculty of Geosciences, Utrecht University

Promotoren:
Prof. dr. M.F.P. Bierkens
Prof. dr. H. Middelkoop

Copromotor:
Dr. L.P.H. van Beek

Examination committee:
Prof. dr. ir. M. Kok
Prof. dr. M.A. Hicks
Prof. dr. J.C.J. Kwadijk
Dr. A. Zech
Prof. dr. E. Stouthamer

ISBN 978-90-6266-658-4
Published by Faculty of Geosciences, Utrecht University, The Netherlands, in:
Utrecht Studies in Earth Sciences, ISSN 2211-4335

Cover images
Benthe Göbel & Teun van Woerkom
Scared sheep hope the humans did a good job in assessing uncertainties and calculating the stability of their dike, as it seems about to breach.

Design/Lay-out
Teun van Woerkom

Frontcover & Invitation design
Margot Stoete

Print
Ipskamp Printing BV

This research is part of the All-Risk project, which is supported by funding from the Netherlands Organisation for Scientific Research (NWO-TTW, grant No. P15-21). Chapters 2 to 4 are first-author versions of previously published articles. More information and citation suggestions are provided at the beginning of these chapters.

Correspondence to: teunvanwoerkom@live.nl

Geen gelul
De dijken moeten hoger
Geen gelul
De dijken moeten hoger

31 januari 1953
Dat nooit meer

Geen gelul
De dijken moeten hoger
Geen gelul
De dijken moeten hoger

Word wakker

(Hang Youth, 2020)

Contents

Samenvatting

Dijken en duinen beschermen momenteel meer dan 9 miljoen mensen in Nederland tegen overstromingen ten gevolge van extreme rivierwaterstanden of stormen op zee. In 2050 moeten alle primaire waterkeringen (3500 km) aan de nieuwe waterveiligheidsnorm (vastgesteld in 2017) voldoen, maar anno 2021 moet 1500 km nog worden versterkt. Deze versterkingen zullen moeten worden getoetst om te beoordelen of ze aan de nieuwe eis voldoen. Hierbij wordt de faalkans van een dijk gezien als een combinatie van meerdere mechanismen die tot een dijkdoorbraak kunnen leiden. Een van de belangrijkste faalmechanismen is macrostabiliteit: het afschuiven van het talud van een dijk, vaak als gevolg van verminderde schuifweerstand door een verhoogde grondwaterstand. Het grondwater reageert op de verhoogde rivierwaterstanden door directe infiltratie in het rivierwaartse talud en door infiltratie in de ondergrond, waar overdruk kan worden opgebouwd in watervoerende lagen die in directe verbinding staan met de rivier. In de huidige toetsing van dijkstabiliteit worden de grondwaterstanden geschat met analytische benaderingsmethoden. Deze vereenvoudigde benadering houdt echter slechts in beperkte mate rekening met hydrologische eigenschappen, heterogeniteit in natuurlijke ondergrond en de door de mens aangelegde rivierdijk, en de hoogwatergolfvorm. Bovendien is de ondergrond in het rivierengebied als de Rijn-Maas Delta vaak zeer heterogeen, wat de grondwaterstroming verder beïnvloedt. De variabiliteit van deze parameters heeft een grote invloed op de grondwaterstand, en deze negeren kan leiden tot foutieve berekeningen van de dijkveiligheid.

Het hoofddoel van dit onderzoek is daarom om te bepalen en kwantificeren wat in een deltagebied de bijdrage van verschillende parameters is aan de onzekerheid in de faalkansen van dijken als gevolg van variabiliteit in de grondwaterstanden. Hiertoe combineerde ik een grondwatermodel van een rivierdijk en zijn omgeving met een geomechanisch model voor dijkstabiliteit. In deze modellen varieerde ik verschillende parameters, met de hypothese dat ze een effect hadden op de dijkstabiliteit door de grondwaterstanden te beïnvloeden.

Het belang van materiaaleigenschappen en geometrie, gegeven stationaire grondwatercondities, werd bestudeerd met een uitvoerige gevoeligheidsanalyse. De gevoeligheidsanalyse omvatte vijftien parameters met betrekking tot geometrie, drainagecondities en materiaaleigenschappen. Van deze parameters was de dijkstabiliteit het meest gevoelig voor de helling van het dijktalud, gevolgd door het type materiaal in de ondiepe ondergrond. Er bestaan complexe niet-lineaire relaties tussen het dijkmateriaal en het ondergrondmateriaal, doordat ze beide de dijkstabiliteit zowel direct beïnvloeden via de geomechanische eigenschappen als ook indirect via de grondwatercondities. Deze bevindingen zijn echter slechts valide als de grondwaterstroming tijdens een hoogwaterevent stationair wordt, wat niet noodzakelijkerwijs het geval is.

Om het effect van niet-stationaire grondwaterstroming mee te nemen, werd de bijdrage van onzekerheid in de hoogwatergolfvorm bestudeerd. Deze onzekerheid werd afgeleid uit een database met extreme hoogwatergolven, en het dynamisch

grondwatermodel werd gekoppeld aan een probabilistische dijkstabiliteitsbeoordeling (FORM). Enerzijds resulteren tijdsafhankelijke grondwatercondities in lagere faalkansen voor macrostabiliteit in vergelijking met stationaire grondwatercondities. Anderzijds leidt het meenemen van de totale onzekerheid in hoogwatergolfvormen tot hogere faalkansen ten opzichte van de selectie van een enkele golfvorm. Derhalve kan de onzekerheid in hoogwatergolfvorm even belangrijk zijn als de onzekerheid in de geomechanische grondeigenschappen, en is het van belang dat deze wordt meegenomen in de dijkbeoordeling.

Een extra bron van onzekerheid is daarnaast heterogeniteit in de dijkconstructie en de natuurlijke ondergrond. De huidige rivierdijken hebben vaak een oude kern die door de tijd werd versterkt en verhoogd, met een heterogene opbouw als gevolg. Een object- en procesgebaseerd algoritme (DETRIS; Dike Erection Tessellation using Regionally Inherited Statistics) werd ontwikkeld die de heterogeniteit in materiaal en geometrie zoals we die observeren in huidige historische rivierdijken na kan bootsen. Archeologische dwarsdoorsneden van rivierdijken en eventueel beschikbare lokale ondergrondgegevens vormen de basis van het algoritme. Door meerdere simulaties van DETRIS dijken te gebruiken voor grondwater- en dijkstabiliteitsberekeningen ontstaat een probabilistische stabiliteitsbeoordeling inclusief de interne dijkheterogeniteit. Door relatief doorlatende lagen of zwakke zones in de dijk expliciet mee te nemen ontstaat een meer realistische benadering van dijkstabiliteit.

Heterogeniteit in de natuurlijke ondergrond in een laaglanddelta, zoals de Rijn-Maasdelta, bestaat vaak uit een complexe architectuur met zandige stroombanen in kleiige komafzettingen, maar bevat ook kleinschalige variatie. In de huidige praktijk wordt grondwaterstroming door deze complexe afzettingen vaak gebaseerd op een vereenvoudigde geologische schematisatie en gereduceerd tot twee dimensies loodrecht op de rivier. In vergelijking met een 3D grondwatermodel inclusief complexe geologie kan 2D-modellering leiden tot ernstige onderschatting van de grondwaterstanden, vooral als de riviergeul (in 3D) verbonden is met een watervoerende laag, maar deze verbinding niet aanwezig is in de 2D dwarsdoorsnede. Een vereenvoudigde geologische schematisering heeft in een 3D schematisering daarentegen slechts voor een kleiner en meer lokaal effect op de grondwaterstanden. Uit onze analyse voor een representatief gebied in de Nederlandse delta blijkt een 2D-grondwatermodel de dijkstabiliteit vaker te onderschatten dan een 3D model met een simpelere geologische schematisatie.

Deze afzonderlijke thema's onderworpen aan onzekerheid in grondwatercondities en dijkstabiliteit zijn gecombineerd in één gevoeligheidsanalyse. Het freatisch vlak in de dijk is het meest gevoelig voor (heterogeniteit in) de dijkopbouw, en de stijghoogtes in de watervoerende laag zijn het gevoeligst voor de materiaaleigenschappen van de ondiepe ondergrond. De dijkstabiliteit, als functie van zowel grondwater als geomechanische eigenschappen, heeft een vrijwel gelijke gevoeligheid voor de hoogwatergolfvorm, de dijkopbouw, het materiaal van de ondiepe ondergrond en de dimensie (2D/3D) van het grondwatermodel. Aangezien klimaatverandering zeer waarschijnlijk zal leiden tot extremere waterstanden in rivier en dientengevolge extremere grondwaterstanden en mogelijk dijkfalen, is het van belang goede richtlijnen op te stellen voor het meenemen van onzekerheid in grondwaterstanden in een beoordeling van dijkstabiliteit.

Summary

Dikes and dunes currently protect over 9 million people in the Netherlands from floods as a result of extreme river water levels or storms at sea. Under the current river flood protection assessment (active since 2017) all 3500 km of primary flood defenses must comply with this new safety standard in 2050, but currently (anno 2021) 1500 km needs to be reinforced to meet that requirement. Clearly, these reinforcements will be assessed to meet the new safety requirements. In this assessment, dike failure probability is seen as a combination of multiple mechanisms that can lead to dike failure. One of the main failure mechanisms is dike slope instability: the mass movement of soil on the slope of a dike, often as a result of decreased sliding resistance by increased groundwater pressure heads. The increase in groundwater pressure during high water levels in the river is caused by direct infiltration of the water through the outer slope of the dike into the dike body, and by infiltration via the subsurface of the dike from an aquifer that has a direct connection to the river. In the current dike safety assessment, the groundwater conditions are estimated using an analytical approximation. However, this simplified method overlooks many parameters that influence the groundwater conditions, such as hydrological parameter properties, heterogeneity in the natural subsurface and human-made river dike, and the shape of the flood hydrograph. Additionally, the subsurface in the Rhine-Meuse delta is often very heterogeneous, affecting groundwater flow. As a result, by ignoring the naturally present variability of these parameters, false estimates of dike safety will be made.

The main objective of this research is therefore to assess and quantify the contribution of various parameters to the uncertainty in dike failure probabilities resulting from the variability in groundwater conditions in a delta setting. To achieve this, I coupled a groundwater model of a river dike and its surroundings with a geomechanical model that calculates dike slope stability. In these models, several parameters were varied, which were expected to influence dike slope stability by affecting groundwater conditions.

The importance of subsurface and geometry properties for dike slope stability under steady-state groundwater conditions was studied by means of a global sensitivity analysis. The sensitivity analysis encompassed fifteen parameters related to geometry, drainage conditions and material properties. Of these parameters, dike slope had the largest influence on dike slope stability, followed by the type of subsurface material. Interesting non-linear relations were observed between the dike and subsurface material, which both influence dike slope stability directly via their geomechanical properties and indirectly via the groundwater conditions. However, these results are limited to the assumption that pressure heads reach steady-state conditions during a high water event, which is not necessarily the case.

The importance of subsurface and geometry properties for dike slope stability under steady-state groundwater conditions was studied through a global sensitivity analysis. The sensitivity analysis included fifteen parameters related to geometry,

drainage conditions, and material properties. Among these parameters, the slope of the dike had the largest influence on dike slope stability, followed by the type of subsurface material. Interesting nonlinear relationships were observed between the dike and subsurface material, as they directly influenced dike slope stability through their geomechanical properties and indirectly through the groundwater conditions. However, these results are limited to the assumption that pressure heads reach steady-state conditions during a high water event, which may not always be the case.

An additional source of uncertainty is the heterogeneity in the human-made river dike and natural subsurface. The current river dikes often contain an old core that has been reinforced multiple times with new material, resulting in a heterogeneous dike. An object-based and process-based model, called DETRIS (Dike Erection Tessellation using Regionally Inherited Statistics), was developed to replicate the patterns of material heterogeneity observed in current river dikes with historical cores. This algorithm utilizes archaeological cross-sections of river dikes and can be conditioned to locally available ground truth data. By incorporating a set of heterogeneous DETRIS-simulated river dikes into hydrological simulations and dike slope stability calculations, a probabilistic stability assessment considering internal dike heterogeneity is achieved. This approach reduces dike slope stability uncertainty by more realistically incorporating permeable layers or weak zones in the dike.

The natural subsurface in a lowland delta, like the Rhine-Meuse delta, exhibits complex architecture with sandy channel belts and clayey floodplain deposits, including smaller-scale variations. Current practices in groundwater estimations often simplify the groundwater flow to two dimensions perpendicular to the river, based on a simplified geological schematization. However, 2D modelling can significantly underestimate groundwater conditions when the river channel is connected to a permeable deposit in three dimensions but not captured in the 2D cross-section. Conversely, using a simplified geological model in a 3D groundwater model has a minor effect on simulated groundwater levels, mainly near the simplification. Our analysis of a representative area in the Dutch delta suggests that a 2D groundwater model is more prone to underestimating dike slope stability compared to a 3D model with a simplified underlying geology.

These distinct factors, which are subject to uncertainty regarding groundwater conditions and dike slope safety, were ultimately combined. The most sensitive factor for the phreatic level within the dike (including its heterogeneity) is the interior composition of the dike itself, while the material type of the cover layer plays the most significant role in determining pressure heads in the subsurface. When considering these effects in conjunction with the geomechanical parameters of the material types, none of the following factors - flood wave shape, dike interior, material of the subsurface layer, or the dimension of the groundwater model - exhibit a significantly greater overall impact on dike slope safety than the others. Given the high likelihood of climate change leading to more extreme high flow conditions and the crucial role of groundwater conditions in potential dike failure, I strongly recommend the establishment of comprehensive guidelines for incorporating uncertainty in groundwater conditions within dike slope safety assessments.

1 Introduction

Along Europe's major rivers approximately 60,000 km of dikes protect the safety of people living behind them. A breach of one of these dikes has massive consequences, as testified by 45 major flood events that occurred in Europe between 1950 and 2005, each of which resulted in more than 70 fatalities or a minimum economic damage of $7.6{\cdot}10^8$ euro (Tourment, 2018). Within the Netherlands, over 9 million people live in flood-prone areas but, owing to dikes and dunes, they are currently safe from storms at sea or extreme river water levels. Flood protection in the Netherlands also has a long history, as the earliest dikes were constructed in the early Middle Ages, and at the start of the 16th century, most river branches were bordered by dikes (Figure 1.1B). Throughout history, these river dikes were made progressively higher and stronger to withstand more extreme conditions. In addition, the flood safety assessment also progressed significantly, from a more reactive philosophy (we react when a flood happens), via a pro-active philosophy (we act to prevent flooding), to a water level based approach (we can build higher dikes than expected water levels) in the recent past. Presently, an acceptable risk approach is adopted (we might not always keep dry feet) (TeBrake, 2002; Kok et al., 2017). The current Dutch Flood Protection Program will face major challenges in efficiently strengthening many of the primary flood defenses to meet the new risk safety standards over the next three decades. This risk-based approach encompasses multiple failure mechanisms for river dikes and requires considering all factors influencing these failure mechanisms. Therefore, understanding the influence of past processes, time-invariant and future changes (such as earlier snow melt or an increase in extreme precipitation events due to climate change (IPCC, 2022) leading to more extreme expected water levels) on the required safety standard in terms of dike failure probability is crucial.

1.1 Current state of river flood protection assessment

Where the previous safety standards for river dikes relied on a certain exceedance probability of hydraulic loads that the river dike could withstand, the new safety standards since 2017 are based on acceptable failure probabilities for sections of flood defenses (Figure 1.1A). safety in terms of dike failure probability is calculated in four steps: In a flood hazard analysis (1) the frequencies of hydraulic loads (peak flows, water levels, waves) are determined by hydraulic modelling and extreme value statistics. Given the hydraulic load conditions, the reliability analysis of the flood defence system (2) is considered for several failure mechanisms (for example piping or overtopping). Then, given a dike failure, hydrodynamic models assess the dike breach growth and inundation (3). Last, economical damage and life loss in the event of flooding (4) is assessed in terms of three risk categories; individual risk, societal risk and economic risk. A maximum acceptable risk is calculated for each of these three categories per dike section, for example 10^{-5} per year (or 1 person per 100,000 years) for individual risk (the annual probability of being killed by a flood at a certain location). The highest risk of these three criteria is used to derive the safety standard for the flood protection system accordingly (Jonkman et al., 2018).

All flood protection measures must meet the new safety standards by 2050; however 1500 km of the total of 3500 km of primary flood defenses did by the end of

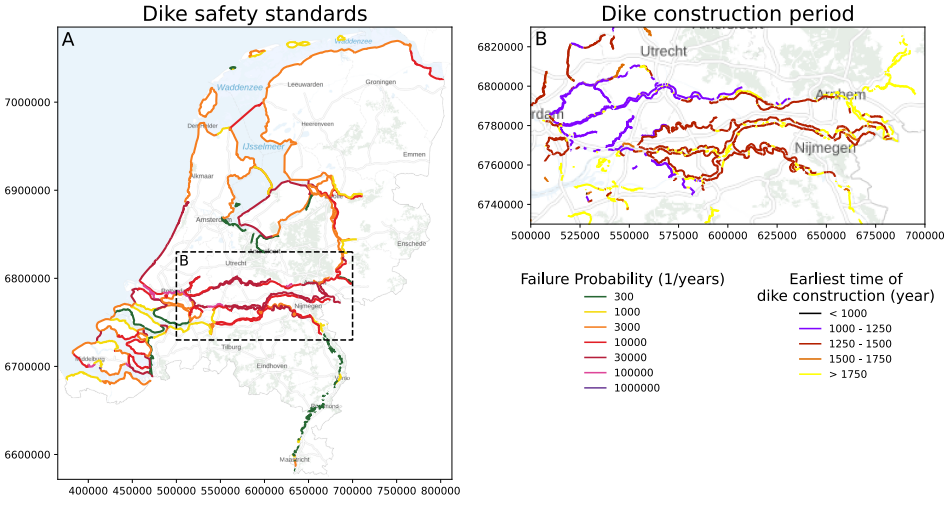

Figure 1.1 Overview of the primary flood defenses in the Netherlands, including the maximal acceptable failure probability of a flood defence system according to the current (since 2017) dike safety standards (A) and the age of some of these flood defenses (B). It indicates that, although flood protection has been on the agenda since the Middle Ages, the way we look at flood protection still evolves.

2021 still not comply with the acceptable failure probability requirement specified in the Dutch Flood Protection Program (in Dutch: Hoogwaterbeschermingsprogramma) (HWBP, 2022). Clearly, a major task for the HWBP will be the coordination of many new dike reinforcement projects, while at the same time the new standards of maximum acceptable failure probability must be enforced, considering multiple failure mechanisms and the underlying processes. Due to the high cost of dike reinforcements (3-20 million euros per km) and the limited space in the densely populated delta, enhanced knowledge of dike failure mechanisms and the processes leading to dike failure reduce the cost of dike reinforcements and support more societally acceptable flood defense measures.

1.2 Dike failure mechanisms

Four main groups of failure mechanisms can be distinguished that may lead to dike failure: *Overtopping*, *dike erosion*, *piping* and *slope instability* (Figure 1.2A). *Overtopping* indicates that water flows over the crest of the dike, inundating the area behind the dike. This can be caused by either river water levels becoming higher than the dike crest or by wave-runup and overtopping. Furthermore, the water flowing down over the inner (landward) dike slope may cause *dike erosion* of the top layer, decreasing the stability of the dike. In addition, wave impact on the outer (waterward) slope may have a similar effect.

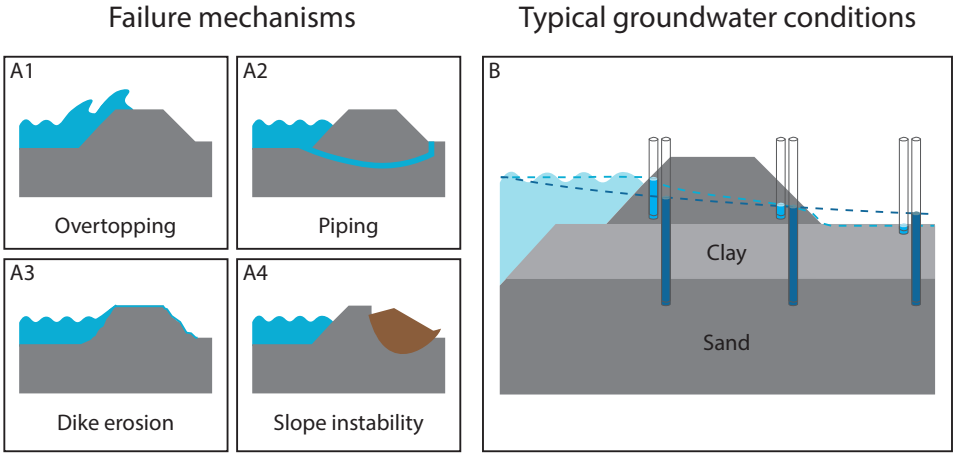

Figure 1.2 Of the processes that may lead to dike failure (A), piping and slope instability (A2, A4) have a strong link to local groundwater conditions. Whereas in a homogeneous situation, these groundwater conditions (B) can be approximated by the aquifer pressure heads (dark blue piezometers) and the phreatic level (light blue piezometers), this estimation is less reliable if there is spatial or temporal heterogeneity in the river water levels or material characteristics.

The other two main groups of failure mechanisms do not necessarily require water levels to reach the dike crest elevation. These mechanisms are driven by groundwater flow building up pressure heads below and within the dike body. *Piping* (Figure 1.2-A2) creates a subsurface channel underneath the dike that threatens its structural stability. It occurs high river flood stages cause a strong gradient in pressure heads between the river and land side of the dike to build up in a sand body overlain by a clayey cover layer, and consists of three stages: First, at the landward side of the dike the cover layer ruptures due to the high pressure, then the underlying sand fluidifies as it is no longer kept in place and finally erosion of the sandy layer occurs due to the high pressure head gradients (van Gerven, 2004). *Slope instability* (Figure 1.2-A4) considers multiple mechanisms (for example liquefaction and erosion due to seepage at the exit point), but mostly focuses on inner slope failure (STBI) and outer slope failure (STBU).

Slope failure is defined as the mass-movement of soil on the slope of a dike and results primarily from the downslope component of the soil weight. After dike slope failure, the dike crest height might be lowered to a level below the river water level or the more vulnerable dike core might be exposed, leading to dike breaching. Failure is often triggered by a reduction in the soil resistance in combination with a loss of lateral support at the toe of the dike when groundwater levels in the dike rise in response to the elevated river stages during and following a flood ('t Hart et al., 2016). Given a certain set of geotechnical parameter values and hydrological conditions, dike slope stability is expressed in a safety factor F. If some of these geotechnical parameters

or the groundwater conditions are uncertain, the safety factor becomes uncertain as well, resulting in a probability distribution of F that is often translated to a failure probability, i.e. the chance that the dike becomes unstable (which occurs if $F < 1$).

1.3 Groundwater conditions related to slope instability and current estimations

Somewhat simplified, the groundwater conditions that are important for dike slope stability can be described by a phreatic surface and several pressure heads in the deeper subsurface. The phreatic surface in the dike and the groundwater level in the subsurface will rise during high water levels in the river due to direct infiltration of the water through the outer slope of the dike into the dike body, and due to infiltration via the subsurface of the dike from an aquifer that has a direct connection the river. The phreatic level will be high in the dike and approximately at the surface elevation on the landward side, whereas pressure heads in the subsurface can remain higher than the surface elevation (Figure 1.2B)

The prescribed assessments of groundwater conditions for slope instability (Rijkswaterstaat, 2021) are based on analytical solutions and the pore pressures derived from steady-state groundwater models (U.S. Army Corps of Engineers, 2003; TAW, 2004). In the Dutch case, this method provides an analytical approximation that combines four typical subsurface scenarios with the dike geometry and subsurface hydrology: a clay dike on a thick clay layer, a clay dike on a sandy layer, a sand dike on a clay layer, and a sand dike on a sandy layer. Given a certain subsurface scenario, estimates of groundwater conditions are provided at two depths: a phreatic level in the dike and a pressure head inside a sandy aquifer several meters underneath the dike (Figure 1.2B). The estimations are furthermore based on data that can easily be derived, such as the dike geometry, the expected river water level, the presence of ditches, and the location of river to aquifer groundwater infiltration. However, this analytical method has three major simplifying assumptions that do not always comply with actual local conditions: (1) the dike interior is homogeneous, which is not the case for most dikes that have a long history of improvement; (2) the subsurface is homogeneous, which is unlikely for dikes bordering rivers in a lowland deltaic setting where changes in the depositional conditions over time and space can lead to changes in material over short vertical and horizontal distances, and (3) hydrological conditions are quasi steady-state conditions, which due to the transient (dynamic) nature of a flood wave are unlikely to be attained. Thus, the analytical approximation ignores different sources of uncertainty, without which estimates of dike safety may be in error and that should be considered to assess the failure probability of dikes.

1.4 Uncertainty in parameters influencing groundwater conditions and dike slope stability

The current estimation of groundwater conditions is subject to uncertainty in two ways: First, the values of some of the input parameters needed to describe groundwa-

ter flow and slope stability are not exactly known as they are difficult to determine, and second the relation between these parameters and the resulting groundwater conditions and dike slope stability are sometimes poorly understood and therefore result in an uncertain outcome too. This is seen as epistemic uncertainty: the uncertainty due to the imperfection of our knowledge. In addition, there is also aleatoric uncertainty, which is caused by the inherent variability of the natural system. The epistemic uncertainty can be decreased by indicating these uncertainties and increasing the knowledge of the processes behind the uncertainty. By doing this we can better assess the impact of the simplifications mentioned before on dike slope stability. Regressing from 'know' to 'no-know' various levels of uncertainty can be distinguished (Walker et al., 2003): determinism, statistical uncertainty, scenario uncertainty, recognized ignorance and total ignorance.

1.4.1 Determinism

Determinism indicates that there is no uncertainty, it represents the situation in which we know parameters precisely (Walker et al., 2003). Related to groundwater conditions, deterministic parameters are mostly surface parameters, for example land surface topography, dike slope angle or the presence and dimension of surface water drainage channels. Most of these parameters are expected to have a large impact on dike slope safety, as for example constructing less steep dike slopes results in more stable dikes and increasing the hinterland drainage rate can lead to lower groundwater levels beneath the dike. However, these parameters can often be determined in high detail (for example with LIDAR surveys or ground-based geodetic instruments), thus even with a large sensitivity of dike slope safety to these parameters the dike slope stability will also remain deterministic.

1.4.2 Statistical uncertainty

Statistical uncertainty indicates that the uncertainty can be captured by statistical properties. Related to dike stability, the variables of concern are mostly the subsurface parameters such as saturated conductivity, angle of internal friction, or shear strength increase exponent.

Such properties are either derived from a combination of cores and lab tests, from geophysical data, and from field tests. The distribution of the values around a most likely value is strongly related to the sampling error, the degree to which a certain number of measurements is representative for the corresponding (geological) unit. Nonetheless, data is always acquired as point observations, especially in the horizontal direction. Consequently, these parameter values are often applied in a probabilistic analysis (Gui et al., 2000; Cao et al., 2016) to assess their probable response on dike hydrology and stability, or a representative deterministic value is derived from the probability density.

1.4.3 Scenario uncertainty

Scenario uncertainty implies that there are multiple plausible outcomes, but the mechanisms leading to these outcomes are expected to be inherently random or not well

understood. As such, these scenarios indicate what might happen and are all assumed to be equally likely. Related to groundwater conditions, these are subsurface architecture, dike buildup and flood wave shape.

The variable three-dimensional architecture of the delta and the overlying dikes are difficult to determine in high detail. The heterogeneity of the natural subsurface (the Rhine-Meuse delta) is the result of the delta's development in the past 8000 years. After the last glacial period rapid sea level rise occurred until 6000 years BP, which created a large accommodation space for river and coastal deposits (Berendsen and Stouthamer, 2000). By this time, the most inland position of the shoreline was reached (Stouthamer et al., 2011) and the previously present barrier island system gradually changed into a beach barrier system. This system resulted in calm conditions behind the beach barrier, allowing for a phase of extensive peat formation that lasted up to 2000 years BP (Pierik et al., 2018). Meanwhile, the Rhine River continued to bring fluvial material to the delta, which resulted in channel-belt sand bodies accompanied by finer levee and overbank deposits. Increased sediment load after 3000 years BP in the Rhine River triggered a series of avulsions, increased overbank deposition and new river branch development (Erkens and Cohen, 2009). These new systems partly eroded the previously formed peat, until the last major avulsion occurred 1400 yr BP. After the completion of an extensive dike network along the rivers around 700 yr BP, fluvial sedimentation was confined to the floodplain. Currently, the Holocene deltaic wedge increases from 1 m near the delta apex to over 15 m near the shoreline. The sandy channel belt deposits, finer levee and overbank sediments and extensive peat deposits alternate and at many locations similar deposits from different river systems (with different material characteristics) are interconnected (Gouw, 2008). At a regional scale, the architecture of these deposits is well known because a significant amount of subsurface data has been collected (Stafleu and Dubelaar, 2016; Cohen, 2017), for example through cores. However, the 3D subsurface, when used in dike safety calculations, is often represented by 1D subsurface profile scenarios (Hijma and Lam, 2015). These scenarios consist of depth-sequences of geological units and are sometimes assigned a probability of occurrence, but this is not always feasible; thus, we classify this aspect as scenario uncertainty.

The dike core heterogeneity is a result of its history as well, as many river dikes in the Netherlands have a long history and are still located where they were first erected in the Medieval ages. These dikes often consist of layers of different materials, which were reinforced in several phases using soil material chosen based on availability rather than engineering properties. Often, the construction material for the dike cover layer was extracted from a clay pit in the floodplain next to the dike (van Heiningen, 1978). Although the maintenance and improvement of the river dikes were governed by water boards, local landowners were still responsible for the upkeep up to the 19th century. However, few documents from that time survived, and thus accurate documentation on the reinforcements of the dike and the resulting inner structure of the dike body is often unavailable.

Furthermore, flood wave shape variability is large as it is determined by many factors, such as rainfall over the river basin, antecedent moisture conditions within the basin, the presence of hydropower dams or weirs in the upstream basin, upstream

inundation, and local floodplain roughness, among others. Several methods are proposed to provide statistical uncertainty for the flood wave shape, such as a single design discharge wave given a maximum expected water level (Butera and Tanda, 2006), or probabilistic methods coupling for example the probability of the peak flow discharge and duration (Balistrocchi et al., 2019). Such methods generally simplify several parameters (Hegnauer et al., 2014), thereby not fully accounting for the actual uncertainty associated with flood wave shapes and groundwater conditions. To still classify the uncertainty of flood wave shapes, the GRADE dataset (Hegnauer et al., 2014) provides flood waves derived from a combination of rainfall-runoff modelling and hydrodynamic river models for the Rhine River. However, although this provides scenarios of flood wave shapes, all these scenarios are possible, and no single scenario is more valid than any other. Changing river regimes due to climate change also falls into this category.

1.4.4 Recognized ignorance and total ignorance

Recognized ignorance can also be seen as knowledge uncertainty and relates to a fundamental lack of understanding of the mechanisms and relationships at stake. Total ignorance implies a deep level of uncertainty, but there is little to say on aspects belonging to total ignorance, as any aspect mentioned here would not totally be ignored.

Whereas the previous levels of uncertainty focused on the uncertainty in determining values for driving variables, recognized ignorance uncertainty is present in the relation between these driving variables, the groundwater conditions, and the dike slope stability. The basic influence (e.g. material with a higher permeability often results in higher pore pressures) is relatively well understood, but large uncertainties arise when the system becomes more heterogeneous, for example when adding multiple layers, a spatially heterogeneous geological architecture, or a complex and heterogeneous dike body.

Numerical, physics-based groundwater models are used to represent groundwater flow through and below dikes during high-flow events. Yet, as the simulated groundwater conditions are coupled to 2D plane-strain stability models, most of the time only a 2D transect perpendicular to the river is used (Meehan and Benjasupattananan, 2012; Lanzafame et al., 2017). As highly heterogeneous subsurface characteristics in combination with large pressure head gradients between the river and the area behind the dike are known to deflect groundwater flow paths, 2D groundwater models are not representative for the pore pressure distribution in and below a dike (Jafari et al., 2016). While this is widely acknowledged, 3D groundwater models are in practice rarely used and little is known about the impacts of this simplification in model dimension on pressure head estimates used in slope stability assessments of dikes.

1.5 Objective and research questions

This research is part of the larger research program All-Risk that aimed to support the reinforcement of flood defences at an increased pace and decreased cost while

considering the implementation's governance and legal aspects (Kok et al., 2022). Therefore, this research is strongly entangled with decreasing the recognized ignorance of uncertainty related to groundwater conditions for dike slope stability: in the end, we want more efficient dike reinforcements while not knowing all parameters exactly, thus knowledge of relations and processes is required. By using a physics-based numerical groundwater model, whether in 2D or 3D, we can highlight important relations between input parameters, such as lithological heterogeneity in the dike and the subsurface, and groundwater induced slope stability.

The lack of detailed knowledge on groundwater conditions near river dikes and understanding their implications for dike safety, especially in relation to the parameters mentioned above, was the main reason for this research. This research contributes to providing innovative techniques, novel methods and improved understanding of processes related to dike failure mechanisms and dike reinforcement projects. The main objective is **to assess and quantify the importance of various parameters leading to uncertainty in dike failure probabilities resulting from variability in groundwater conditions in a delta setting**. To this end, based on the above-mentioned types of uncertainty, the following research questions are addressed, each focusing on different parameters and potential contributors to uncertainty in dike stability assessments:

RQ 1 *Which subsurface and geometrical properties influence dike stability estimates the most under steady-state conditions?*

RQ 2 *What is the influence of flood wave shapes on probabilistic dike slope stability under transient groundwater conditions?*

RQ 3 *How can we incorporate the heterogeneous dike interior?*

RQ 4 *To what extent do the downgraded information from 2D groundwater simulations and simplified geological schematizations bias the results of a hydrological model and stability assessment?*

1.6 Research approach

The research questions are all wedged between the complex variability of the natural (and anthropogenic) environment and the simplified physics-based simulations of groundwater and dike slope stability. In my approach I explored step by step how different components (and their variability and uncertainty) contribute to the final uncertainty in dike slope stability predictions by including these components in a numerical groundwater flow model and dike slope stability analysis (Figure 1.3).

To determine which subsurface and geometry properties are most important under steady-state conditions (RQ 1), I performed a global sensitivity analysis of dike slope stability with a comprehensive hydro-stability model under steady-state hydrological conditions (chapter 2). The sensitivity analysis encompasses fifteen parameters related to geometry, drainage conditions and material properties. I prioritized the main parameters, identified trends over the assessed parameter ranges and qualified interaction between these parameters.

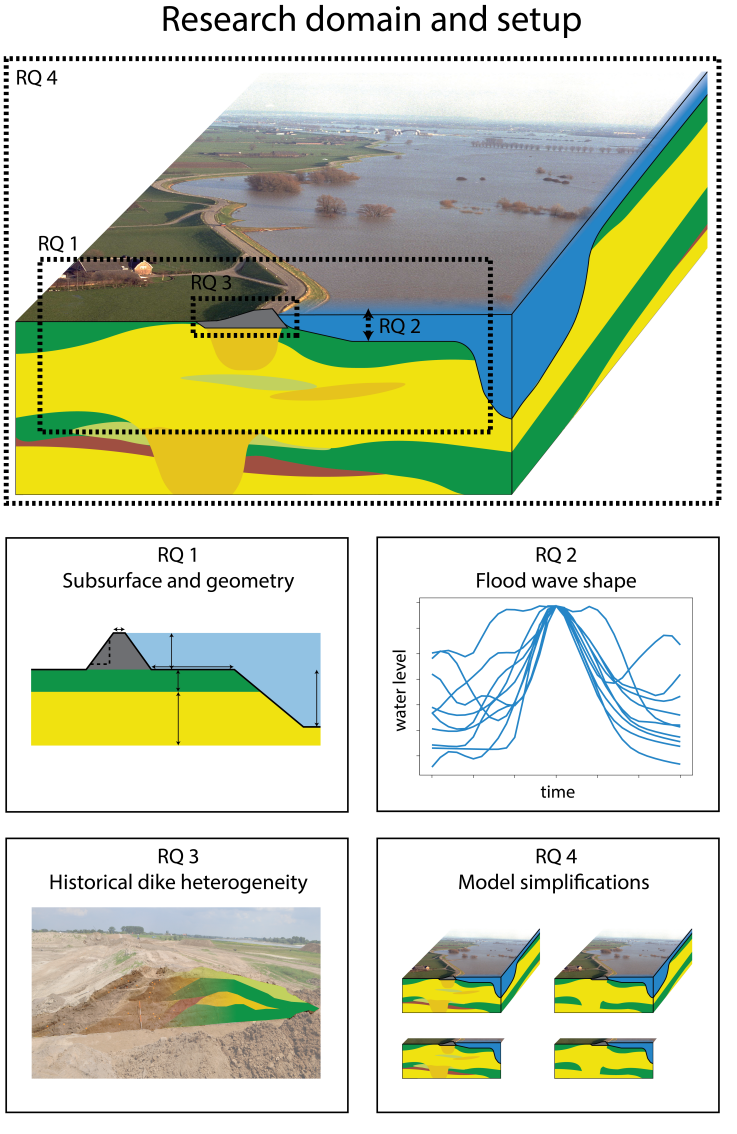

Figure 1.3 Overview of the spatial domain in which the research questions are positioned and corresponding simplified visualization of each of these research questions.

The next step aimed to determine the influence of time-dependent flood wave shapes on dike stability (RQ 2). For this purpose a set of flood wave shapes was derived from a database of hydrographs, and subsequently evaluated for their effect on probabilistic safety estimates of slope stability with transient groundwater conditions, using a modeling chain consisting of a groundwater flow model and a probabilistic dike slope safety assessment (chapter 3). These results were compared to current analytical estimations and steady-state solutions and the importance of various wave shape characteristics for dike slope stability was determined.

To incorporate the heterogeneous dike interior in stability analyses (RQ 3), I developed an object-based and process-based model (DETRIS; Dike Erection Tessellation using Regionally Inherited Statistics) that simulates dike bodies, based on the construction history of archaeological dike cross-sections, yielding patterns of heterogeneity similar to those observed in real dikes, and applied it in a dike safety assessment (chapter 4). As many current river dikes still contain a core of medieval Age, this model can more realistically and accurately incorporate dike interior heterogeneity in the dike safety assessment.

As final step I explored to what extent realistic groundwater conditions can be estimated using conventional simplifications, such as 2D groundwater simulations and simple geological schematizations (RQ 4). This was done by comparing pressure heads resulting from a multiplicity of groundwater models in 2D and 3D on both a simple or complex geological schematization (chapter 5). As current methods for estimating groundwater conditions for dike slope stability often use one (or both) of these simplifications, this assessment can determine to what extent these simplifications are acceptable.

Finally, chapter 6 integrates the results of this thesis, provides answers to the research questions, and contains recommendations for further research and knowledge implementation. It also provides an exemplary case study, in which the importance of the various parameters for groundwater related dike safety is compared.


LET OP
INSTORTINGS
GEVAAR

2 Global Sensitivity Analysis of Groundwater Related Dike Stability under Extreme Loading Conditions

Based on: Teun van Woerkom, Rens van Beek, Hans Middelkoop, and Marc F. P. Bierkens (2021). Global Sensitivity Analysis of Groundwater Related Dike Stability under Extreme Loading Conditions. Water, 13(21):3041

Abstract

With up to 15% of the world's population being protected by dikes from flooding, climate-change-induced river levels may dramatically increase the flood risk of these societies. Reliable assessments of dike stability will become increasingly important, but groundwater flow through dikes is often oversimplified due to limited understanding of the important process parameters. To improve the understanding of these parameters, we performed a global sensitivity analysis on a comprehensive hydro-stability model. The sensitivity analysis encompassed fifteen parameters related to geometry, drainage conditions and material properties. The following three sensitivity settings were selected to characterize model behavior: parameter prioritization, trend identification and interaction qualification. The first two showed that dike stability is mostly dependent on the dike slope, followed by the type of subsurface material. Interaction quantification indicated a very prominent interaction between the dike and subsurface material, as it influences both groundwater conditions and dike stability directly. Despite our relatively simple model setup, a database containing the results of the extensive Monte Carlo analysis succeeded in finding most of the unsafe sections identified by the official inspection results. This supports the applicability of our results and demonstrates that both geometry and subsurface parameters affect the groundwater conditions and dike stability.

2.1 Introduction

Over 45 major flood events occurred in Europe between 1950 and 2005 that each resulted in more than 70 fatalities or a collected economic damage of $7.6{\cdot}10^8$ euro (Tourment, 2018). As a result, many flood prone areas have an extensive network of artificially elevated levees or dikes, which, along Europe's major rivers, add up to a length of approximately 60,000 km (ICOLD, 2018). To ensure the safety of people living behind dikes, continuous maintenance and reinforcements are needed to warrant the stability of dikes and their proper functioning during high water events. Climate change, e.g., earlier snow melt or an increase in extreme precipitation events in the upstream drainage area (IPCC, 2022), poses a new threat that may increase the risk of a society to flooding (Middelkoop et al., 2001). To maintain safety levels under changing climatic conditions, major investments are needed for dike maintenance and reinforcement, of which the costs for the latter are in the order of 1–20 million euro per kilometer (Tourment, 2018). Improved knowledge of the processes during and following a high-water event that can result in dike failure is crucial for more cost-effective dike reinforcements, which may reduce the total expenditures on dike reinforcements substantially and can support more societally acceptable flood defense measures (Eijgenraam et al., 2014).

Many dike failure mechanisms are related to local groundwater conditions and pore pressures in the dike body. In response to elevated river stages, changing groundwater conditions may increase the pore pressure and, thus, reduce the effective normal strength, while, at the same time, the lateral load of river water pushing against the dike is increased. Therefore, parts of its inner or outer slope may slip, or the dike may slide along its base (soil slip sensu lato), threatening the structural integrity of the dike. Accordingly, when analyzing a dike failure hazard in relation to high groundwater levels and river stages, multiple failure mechanisms must be considered.

Although we acknowledge that critical groundwater heads in dikes are primarily driven by the occurrence and nature of high-water events, their variation in space and time also depends on surface geometry and subsurface properties. Previous research on this topic can roughly be divided into the following three categories: research focusing purely on hydrology, research focusing on single cases or research assessing variability in either surface geometry or subsurface properties. An extensive analysis of only the hydrology near a river dike was provided (Meehan and Benjasupattananan, 2012; Polanco and Rice, 2014). Research on a single case (Stanisz et al., 2017) was often also focused on the effect of artificial reinforcements (Mateo-Lázaro et al., 2016; PEÑUELA, 2013). Attempts including a local sensitivity analysis investigated the influence of material properties (Lanzafame et al., 2017) or geometry (Vahedifard et al., 2017) on the stability of embankments. In sum, none of these previous studies conducted a full analysis that considers both variations in hydrological parameters as factors influencing the stability of a dike.

Such a full analysis has already been widely applied in landslide probability modelling (Canli et al., 2018; Collison and Anderson, 1996; Malet et al., 2005). Nonetheless, whereas slope hydrology is mostly dependent on rainfall infiltration, flow as a result of elevated river water levels mostly occurs horizontally and is often affected

by intersecting aquitards, resulting in very different patterns of groundwater flow and pore pressure buildup. These differences inhibit the direct application of results from landslide modelling to river dike failure scenarios. Nonetheless, to assess variations in hydrological parameters as factors influencing the stability of a dike, a comprehensive hydro-stability system needs to be modelled.

To quantify the model and parameter uncertainty, local sensitivity approaches estimating the partial derivatives of the model at a specific point in the parameter space are no longer sufficient (Iooss and Lemaître, 2015). Alternatively, a global sensitivity analysis can handle nonlinearity and local variations expected in more complex models. A global sensitivity analysis considers the entire variation of the input factors (Saltelli et al., 2008). Global sensitivity analysis recently gained interest in environmental modelling (Ferretti et al., 2016), and the different goals and methods related to global sensitivity in environmental models have been extensively reviewed (Pianosi et al., 2016; Song et al., 2015). Hydrological models have seen a similar rise in interest for global sensitivity analysis, both from a methodological point of view (Borgonovo et al., 2017; Ciriello et al., 2019; Ratto et al., 2007) and for analyzing geo-hydrological systems (Bianchi Janetti et al., 2019) and slope stability uncertainty (Guo et al., 2019; Hamm et al., 2006; Xu et al., 2020). Though some attempts have been made to analyze the global sensitivity of dike stability based on the uncertainty in its internal characteristics (Lanzafame et al., 2017; Guo et al., 2019), no complete sensitivity analysis covering both geometrical and subsurface characteristics has yet been made.

Thus, to assess both geometrical and subsurface characteristics of dikes, we created a coupled high-resolution groundwater model and a limit equilibrium stability analysis. To constrain our results and to highlight first-order relationships, we evaluated the stability under the most critical loading conditions and the maximum pore water pressures. Three failure mechanisms that affect the macro-stability of a dike were considered, being inner slope stability, outer slope stability and basal sliding, as their occurrence is directly linked to the geometry of a dike and its composition.

To add to previous research on both river dike hydrology and global sensitivity analysis, the goal of our analysis was to identify the overall stability of a dike in terms of its factor of safety F under different hydrological loading conditions, subsurface geometries and material properties, and including pore pressure calculations. In this work, our research goal translates into the following three sensitivity settings to characterize model behavior: parameter prioritization, trend identification and interaction qualification. We aim to provide insights in each of these settings while maintaining a reasonable computation time. For parameter prioritization we used the Elementary Effect (Morris, 1991) and the delta-importance measure (Borgonovo, 2007). As we are mostly interested in those factors that could lead to unstable dikes, we used a regional sensitivity analysis (RSA) to perform trend identification and identify regions in the parameter space with a safety factor below one. For interaction qualification, we focused on the subsurface, and used response surfaces to analyze the interaction activate between hydrology, material characteristics and dike stability. Moreover, the outcome of this global sensitivity analysis can be used to inform semi-qualitative assessments

of dike stability as often applied in regional inventories, and the conducted set of model runs is used for a direct comparison to a case study site in the Netherlands.

2.2 Materials and Methods

2.2.1 Case-study schematization

We applied the global sensitivity analysis on a cross-section from the river to the hinterland behind the dike. Fifteen parameters (Table 2.1) describe the cross-section, subdivided in the following three groups: topographical parameters, subsurface parameters and human management parameters. The topography is described by the following six parameters: the dike height (D_h), dike crest width (D_w), dike slope (D_s) and floodplain width (F_w), riverbed slope (R_s) and river depth (R_d) (Figure 2.1). The subsurface is described by five parameters, which divide the subsurface in three units with uniform characteristics. The dike is schematized by its material type (D_{typ}), in addition to the previously mentioned geometry parameters D_{typ}, D_w and D_s. The upper subsurface layer is schematized by a thickness (U_{thck}) and material type (U_{typ}). The same applies to the lower subsurface layer (L_{thck}, L_{typ}). Two parameters describe human management by specifying the drainage conditions behind the dike (Figure 2.1), which are drain spacing (Dr_s) and drainage depth (Dr_d).

2.2.2 Coupled hydrology-stability model

Hydrological model setup

We added a stability module to a groundwater model to examine the stability of the schematized cross-section. The MODFLOW 6 software (Hughes et al., 2017; Langevin et al., 2019), a Modular Three-Dimensional Finite-Difference Groundwater Flow Model, simulates the groundwater conditions, which are included in the structural stability using the Generalized Limit Equilibrium Method (GLEM) (Fredlund and Krahn, 1977; Fredlund et al., 1981). The MODFLOW 6 hydrological model is constrained by the river water level and drainage depth. On the river side, the imposed river stage at the top of the dike constitutes a head-controlled boundary condition

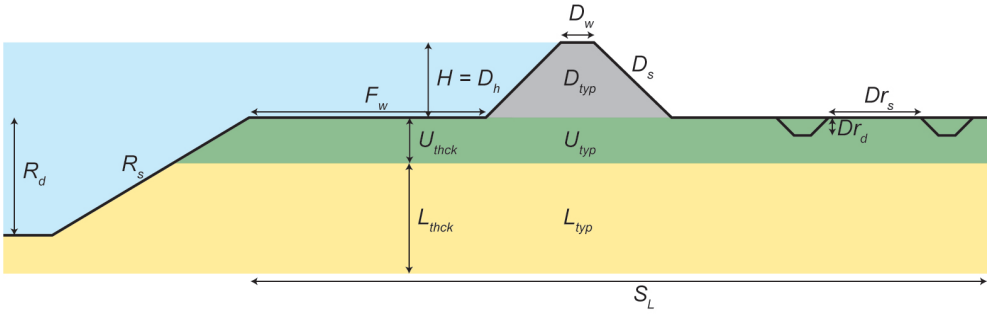

Figure 2.1 Schematization of model inputs, indicating the setup of the hydrological model. See for their meaning, values and possible ranges Table 2.1 and Table 2.2.

Table 2.1 Name, symbol and range of the model parameters. A visualization of each of the parameters is shown in Figure 2.1. Layer type descriptions are found in Table 2.2

Parameter	Symbol	Range	Unit
Dike height	D_h	3-10	m
Dike crest width	D_w	2-5	m
Dike slope	D_s	0.2-1	m/m
Dike type	D_{typ}	C-CL-L-SL-S	-
Upper layer thickness	U_{thck}	0.3-1.9	m
Upper layer type	U_{typ}	C-CL-L-SL-S	-
Lower layer thickness	L_{thck}	5-10	m
Lower layer type	L_{typ}	C-CL-L-SL-S	-
Foreland width	F_w	0-100	m
Drainage depth	Dr_d	0.1-2	m
Drainage spacing	Dr_s	1-20	m
Riverbed slope	R_s	0.33	m/m
River depth	R_d	0.9*(U_{thck}+L_{thck})	m
Flood height	H	D_h	m
Drawdown time	T_d	1	days

that is regulated by the MODFLOW river package. A head-controlled boundary on the inner side of the dike is regulated by the MODFLOW drain package, which creates outflow-only seepage points (Hughes et al., 2017). Seepage is possible if the hydraulic head at the surface is higher than the surface elevation. In addition, at a distance of Dr_s behind the dike, a ditch is located with a depth of Dr_s (Table 2.1), enabling faster drainage of deeper layers.

The cell size is 0.5 m in all directions, which enables the assessment of small-scale spatial variation while retaining the computational efficiency needed. The model first performed a steady-state simulation, in which the river stage (H) was set at the dike crest elevation. It was assumed that under these conditions, the pore pressures reach their most critical values. After the steady-state simulation, a rapid drawdown of H from the dike crest to the dike toe in a time period (T_d) of one day was transiently simulated with a 3-hour timestep. As pore pressures in the dike do not immediately follow river water level changes and the stabilizing effect of the high river water levels is absent, these conditions might provoke outer slope failure. An exploratory sensitivity analysis showed a time step of 3 h does not significantly impact results when compared to smaller time steps.

Dike slope stability model setup

Dike stability is expressed by the factor of safety (F), which is calculated separately for inner slope failure, basal sliding and outer slope failure using the Generalized Limit Equilibrium Method (Fredlund and Krahn, 1977; Fredlund et al., 1981), resulting in the following three safety factors: F_{inner}, F_{lat}, F_{outer}. This method solves both moment and force equilibrium on a slip surface for different ratios between the vertical

Table 2.2 Subsurface types and their abbreviations used in the model, related to the D_{typ}, U_{typ} and L_{typ} parameters. The subsurface type is linked to the hydraulic conductivity (K_{sat}), drained cohesion (c'), effective friction angle (ϕ), the bulk unit weight (γ) and the saturated bulk unit weight (γ_{sat}).

Subsurface type	Abbr.	K_{sat} (md^{-1})	c' (kPa)	ϕ (^{o})	γ (kNm^{-3})	γ_{sat} (kNm^{-3})
Clay	C	0.13	5.0	17.5	17	17
Clay-Loam	CL	0.18	4.0	22.5	18	18
Loam	L	0.19	1.0	30.0	20	20
Sandy Loam	SL	1.54	0.5	31.25	19.5	19.5
Sand	S	8.94	0.0	32.5	18	20

and horizontal inter-slice shear forces. The relationship between the magnitude of the inter-slice shear and normal forces is assumed to be constant (Morgenstern and Price, 1965). The factors of safety presented in this paper always represent the factor of safety of the most critical circular slip surface, derived by an effective critical slip surface minimization technique adapted from (Malkawi et al., 2001). To constrain the slip surface for inner and outer sliding the slip surface is forced to enter on the dike crest or on the corresponding dike side. For basal sliding an infinite slump radius is assumed, which results in a horizontal slip surface and enables the calculation of F using only force equilibrium. To ignore very small slumps not causing dike breaches, a minimum cross-sectional slip surface area of 5 m^2 is imposed.

2.2.3 Workflow and Parameters for Global Sensitivity Analysis

As conducting the entire global sensitivity analysis with all parameters was not a feasible option due to increasing computation times, we first screened our inputs using the Elementary Effect test (EE) (Morris, 1991; Campolongo et al., 2007). Hereby, we identified which input parameters have a small contribution to the output variation in high-dimensional models and can, therefore, be set to a fixed value. Subsequently, the global sensitivity analysis was performed using a Monte-Carlo (MC) approach, as it captures the entire range of possible combinations, while facilitating parameter interaction understanding (Figure 2.2). The Delta Moment-Independent measure (DMI) (Borgonovo, 2007) was used to quantify the sensitivity of the factors contributing significantly to the variation in the model output.

All variable parameters defining the cross-section are screened using the Elementary Effect test (EE). As no information is available a priori, the parameters are sampled from a uniform distribution within their possible range (Table 2.1). The material types (D_{typ}, U_{typ}, L_{typ}) each represent a single lithological class (Figure 2.3), having deterministic attributes used in the coupled hydrology-stability model. We selected the values for these attributes (Table 2.2) based on characteristic values in the literature. The hydraulic conductivity (K_{sat}) is derived from the geometric mean of multiple laboratory K_{sat} measurements of soils with a relatively high density(Pachepsky and Park, 2015). The cohesion (c'), the effective friction angle (ϕ),

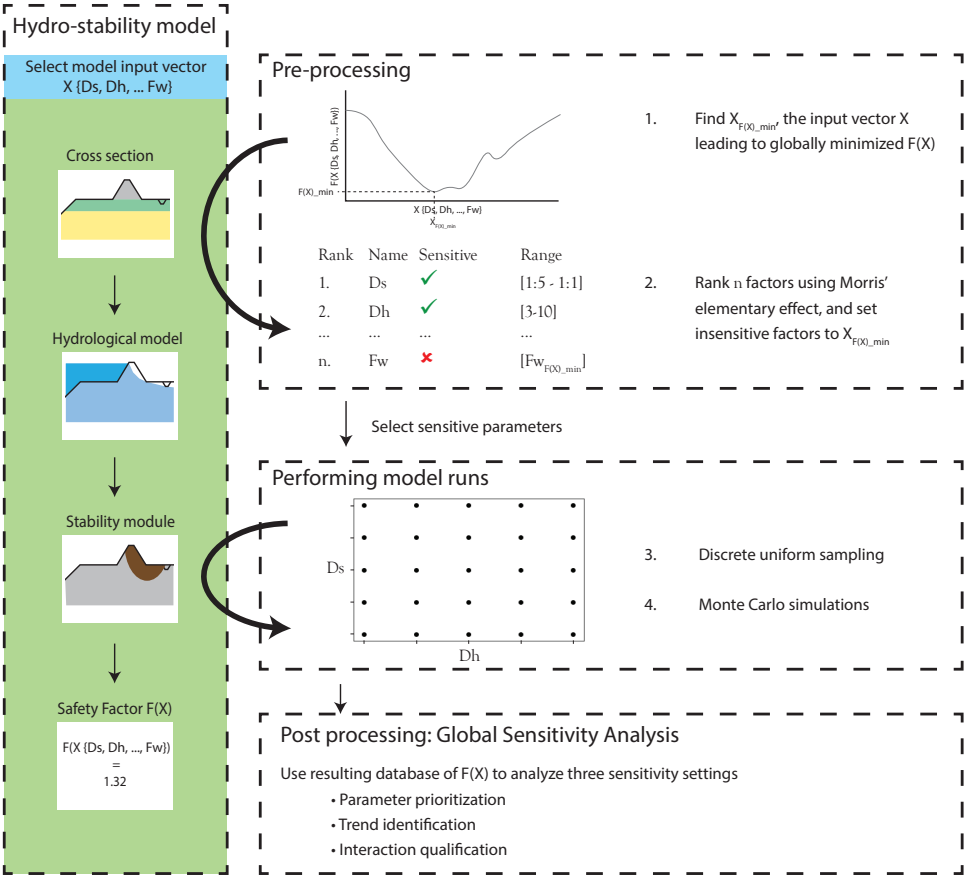

Figure 2.2 Workflow of Global Sensitivity Analysis, focusing on the pre-processing by factor fixing and performing the model runs. The specific measures used to qualify and quantify sensitivity are discussed in Figure 2.4.

the bulk unit weight (γ) and the saturated bulk unit weight (γ_{sat}) are in line with the European standardized characteristics for soil stability (CEN, 2004).

2.2.4 Parameter Prioritization

This sensitivity setting focuses on identifying the input factor (parameter) that has the largest effect on the model output, e.g. the input factor that, when fixed, decreases output variability the most. For this we used the Elementary Effect test (EE) and the Delta Moment-Independent measure (DMI).

The Elementary Effect test (Campolongo et al., 2007) is an effective sensitivity analysis (SA) method that is widely used for screening practices, as it provides relatively good results at small sample sizes (Morris, 1991). This method is basically a

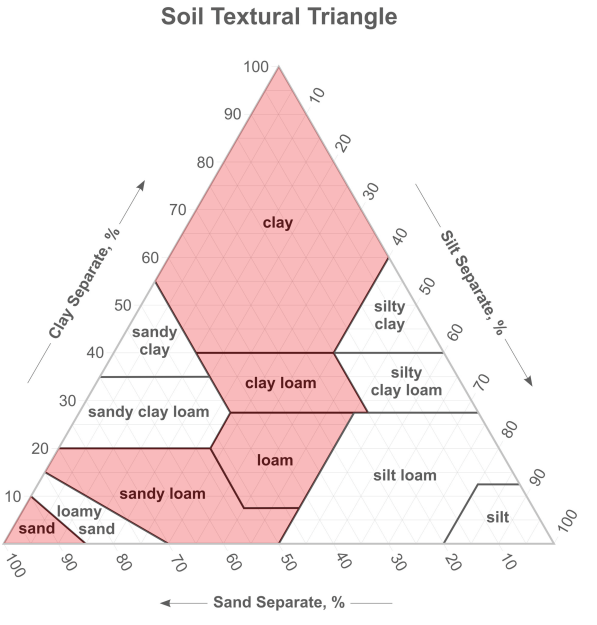

Figure 2.3 Subsurface types used in the analysis as seen in the soil textural triangle, modified from (Soil Science Division Staff, 2017).

One-At-a-Time analysis, which is extended to the full input factor space. The original method (Morris, 1991) measures sensitivity in terms of μ, indicating the first order influence or elementary effect, and σ, indicating second order influences, being nonlinearity or interaction effects. For each input factor, random baseline points are selected from which the others are varied (Figure 2.4A). Given function "y" (in our case the calculation of F), step size Δ and a random baseline sample X, the elementary effect of input factor X_i is given by

$$EE_i(X) = \frac{y(X_1, \ldots, X_{i-1}, X_i + \Delta, X_{i+1}, \ldots, X_k)}{\Delta} \tag{2.1}$$

The final μ for any input factor is the mean of the EE_i at all baseline points X. Non-monotonic models result in both positive and negative EE's for a given input factor, which average out when taking the mean. Therefore (Campolongo et al., 2007) introduced μ^*, which is the mean of all absolute elementary effects and is found to be suitable for input factor ranking.

$$\mu_i^* = \frac{1}{r} \sum_{j=1}^{r} |EE_i(j)| \tag{2.2}$$

where $|EE_i(j)|$ is the elementary effect for input factor X_i using the j-th step with step size Δ, with r being the number of steps in the parameter space. A μ_i^* value

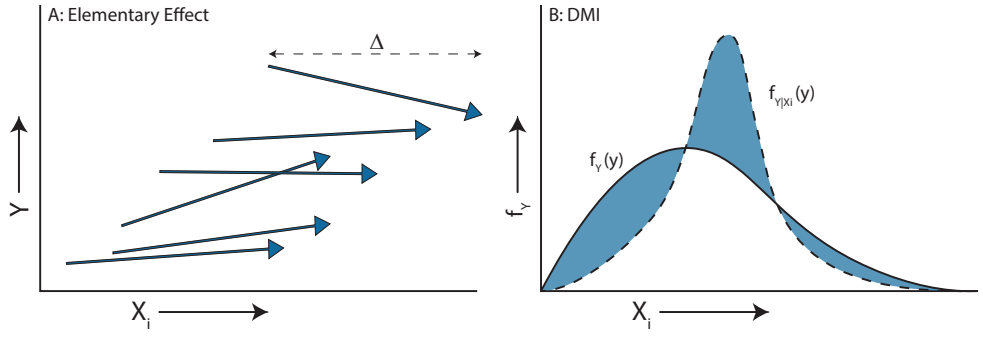

Figure 2.4 Visual explanation of both SA methods used. The elementary effect EE (A) uses a fixed step (δ_i, equation 2.1) of input factor X_i from random starting points and measures the change in result Y. Note that all arrows are of the same size in the X direction, representing the fixed step size. The DMI method (B) is based on the area difference (highlighted in blue) between the continuous unconditional probability density function $f_Y(y)$ and a conditional unconditional probability density function $f_{Y|X_i}(y)$, which is based on a sample of the unconditional input vector.

near zero indicates that the parameter has a small general effect on the output. This measure is used in the Insensitive Factor fixing procedure.

The Delta Moment-Independent measure (DMI) (Borgonovo, 2007) is based on shifts in the probability density function $f_Y(y)$, contrary to most SA techniques, which are variance-based. Variance-based sensitivity, according to classical utility theory, is not suitable to describe uncertainty in case of a non-normal probability distribution and in case of a non-quadratic utility function. Moreover, the probability density function provides a more complete overview of sensitivity than variance-based techniques. DMI returns the measure δ_i, which represents the non-overlapping area between an unconditional input vector X_i, including all parameter values, and a conditional input vector X_i, consisting of a subset of parameter values (Figure 2.4B). Mathematically it is expressed as:

$$\delta_i = \frac{1}{2} E_{X_i}[s(X_i)] \tag{2.3}$$

with

$$E_{X_i}[s(X_i)] = \int f_{X_i}(x_i)[\int |f_Y(y) - f_{Y|X_i}(y)|dy]dx_i \tag{2.4}$$

which shows that the input factor specific δ_i depends on the shift in probability density function for multiple conditional inputs X_i and on the underlying probability of that shift to occur. As in our method a uniform probability function is used, the mean of the separate shifts represents the final δ_i.

2.2.5 Factor Fixing procedure

Factor fixing is often used as a SA setting in itself, where the goal is to simplify the model and prevent overparameterization (Ratto et al., 2007). In this research, it was just a means by which we aimed to keep MC simulation runs to an acceptable level, i.e., by fixing the least influential parameters to some nominal value. To provide evidence for the identification of the least influential parameters for the model output, we used an iterative version of the SA repeatability test (Andres, 1997), previously successfully adapted for environmental models (Nossent et al., 2011; Tang et al., 2007). This approach focuses on testing the predictive capacity of parameters.

First, 1200 samples of all model parameters are created. The test then consists of the comparison of two conditional input samples, $X2$ and $X3$, to the previously created unconditional sample, $X1$. Set $X2$ fixes the input factors deemed insensitive at a predetermined value, while $X3$ fixes the input factors deemed sensitive. Afterwards, the unconditional result $F(X)$ is compared with the conditional results $F(X2)$ and $F(X3)$. If a correct classification of important and non-important parameters was used, the correlation coefficient (r^2) between $F(X2)$ and $F(X1)$ approaches 1, while the correlation coefficient of $F(X3)$ and $F(X1)$ approaches 0, as the parameters fixed in $X3$ should have a small influence on the results. We iteratively applied this approach, starting with only the most important factor classified as sensitive, and consecutively also classifying the next important parameter as sensitive, until the correlation coefficient $r^2_{F(X2)|F(X1)}$ exceeds a certain threshold. A threshold $r^2_{F(X2)|F(X1)}$ of 0.95 has been successfully applied (Nossent et al., 2011) to limit the dimensionality of a problem, while retaining sufficient model variability.

To initially rank the parameters from sensitive to insensitive, we used the enhanced Elementary Effects method (Campolongo et al., 2007) on the initial sample $X1$. The iteration was performed for each failure mechanism separately, but we used an inclusive selection strategy, indicating that only those parameters that were found to be insensitive for all failure mechanisms were excluded from the MC-parameters. Although the inclusive approach increases the dimensionality of our problem, it also enables an easy comparison between the different failure mechanisms. As we used a threshold for $r^2_{F(X2)|F(X1)}$ of 0.95 as the closing criterion for the iterative Factor Fixing procedure, this threshold being lower than 1 indicated that the factors to be fixed still influenced the model outcome, though their influence was limited.

As this research was investigating worst case scenarios, any factor to be fixed should have been set at a value that resulted in relatively low safety factors. This value is selected from the input vector $X(allparameters)$ that results in the globally minimized $F(X)$ within the specified parameter ranges (Table 2.3) for each failure mechanism separately. Initiated at a random starting point, a modification of Powell's method (Powell, 1964) performs the minimization operation. This method performs a bi-directional search in one dimension, meaning it searches for the local minimum $F(X)$ by changing only one input parameter. The input parameter is updated to the value resulting in the minimum $F(X)$, and the bi-directional search is applied to the next input factor. After minimizing all input factors, the intermediate model output is stored, and the first factor is again selected. When the difference between the previous and current intermediate output is lower than a given threshold, the

Table 2.3 Minimum $F(X)$ per failure mechanism and parameter values of input vector X resulting in that minimum $F(X)$. See Table 2.1 for the abbreviations and units of the parameters.

	Basal sliding	Inner slope stability	Outer slope stability
F_{min}	0.69	0.00	0.26
D_h	9.97	9.74	9.34
D_w	2.14	3.50	4.61
D_s	1:1	1:1	1:1
D_{typ}	Sand	Sand	Sandy Loam
U_{thck}	0.31	1.10	1.82
U_{typ}	Clay	Clay-Loam	Loam
L_{thck}	5.07	7.50	5.25
L_{typ}	Clay	Clay-Loam	Clay-Loam
F_w	50	50	85
Dr_d	-1.05	-1.05	-0.62
Dr_s	20.0	10.5	20.0

globally minimized input vector X is found. Though we acknowledge that fixing only a single input factor to value in the globally minimized input vector does not necessarily result in the local minimum $F(X)$ at any given point in the parameter space, we believe that it results in a safety factor near the real minimum at that point.

2.2.6 Factor Sampling

As neither the real parameter probability density functions of the selected model parameters were known and no information was available on their correlation, we used a uniform uncorrelated sampling strategy. The sensitive factors were sampled using a discrete uniform distribution in their possible range (Table 2.1), which suggested a known, finite number of outcomes that were equally plausible. We used five steps (n) at which to sample discrete values from the minimum value (a) to the maximum value (b) in the possible range given parameter p, i.e.,

$$x_p = a, a + \frac{b-a}{n-1}, a + 2\frac{b-a}{n-1}, \ldots, b \tag{2.5}$$

Afterwards, each possible combination of the parameter values was selected for the MC analysis, resulting in a number of P^n model runs, with P being the number of selected parameters.

2.2.7 Trend identification and interaction qualification

For trend identification and to increase our understanding of model sensitivity, we explored whether any change toward higher parameter values would also lead to a larger safety factor. To this end, we performed a regionalized sensitivity analysis

(RSA), which aimed to identify regions in the input space that result in output in a specified zone (Ratto et al., 2007). In our case, the selected zone was $F \leq 1$, as it was intuitively the most interesting region of model outcomes; that of dike failure. To indicate this regional effect, we used $p(F \leq 1)$ as a measure, which is the probability for a fixed parameter to result in $F \leq 1$ given the variations of the other parameters. This measure can be easily calculated as a result of the uniform discrete sampling distribution. Interaction qualification uses response surfaces, which directly show the correlation between material properties, groundwater and dike stability. As we focused on a qualitative description and interpretation of these interactions, no quantitative statistical measures were used.

2.3 Results

2.3.1 Exemplary results of the hydro-stability model

The typical model results that highlight the interplay between the model input factors, groundwater hydrology and macro-stability are presented in Figure 2.5. Focusing on changes in groundwater conditions, the phreatic surface in the dike after the steady-state simulations (t_0) seems to be more influenced by dike geometry than material properties. Due to increased drainage, steeper and narrower dikes seem to result in a generally lower phreatic level, as the hydraulic heads at the center of the dike are more directly affected by gradient changes near the surface. Lower river water levels after draw-down also affect the phreatic level, but the amount of lowering depends on the possibility to drain the excess pore pressure. This is reflected in lower groundwater levels at steeper and thus smaller dikes, at dikes on a sandy substrate and in case of longer drawdown times.

For inner slope stability, these results have a more direct effect, as the minimum factors of safety F are always found at t_0, when the pore pressures are the highest. For basal sliding, this is the case as well, although this is also influenced by the still high river water levels, which apply a lateral force. As a result, the dike's stability related to basal sliding increases to infinity at t_e, as the river water level is at the dike toe and no driving force is exerted by it. For outer slope stability, the opposite argument applies, and due to a decrease in the lateral river water pressure, the lowest F is most often found at t_e (Figure 2.5).

These example results clearly show that not only the safety factor, but also the slip surface area and location are dependent on the hydrological conditions. Higher pore pressures are likely to result in larger slumps that result in a greater chance of dike breach, in addition to lower stability. The results also indicate an effect of drawdown time, which is related to the flood wave shape, but in this study the drawdown time (T_d) was kept constant.

2.3.2 Parameter prioritization

Factor Fixing on globally minimized input vector

The values used to fix the insensitive factors are derived from the input vector X that results in the globally minimized $F(X)$. The globally minimized factor of safety

(F_{min}) is 0.69, 0.00 and 0.26 for basal sliding, inner slope stability and outer slope stability respectively, of which the corresponding input vectors are shown in Table 2.3. The iterative factor fixing is performed in the order of the mean absolute elementary effect (μ^*) of each input factor per failure mechanism (Figure 2.6A). If the dike slope, dike height, dike material type, upper subsurface type, lower subsurface type, upper subsurface thickness, drainage spacing and foreland width are classified as sensitive, the $r^2_{F(X2)|F(X1)} \geq 0.95$ for all failure mechanisms. These eight factors (Figure 2.6) are thus selected for the MC-analysis. Using the final $F(X2)$ and $F(X1)$, a mean error in F of -2.76·10^{-1}, 7.86·10^{-3} and -1.81·10^{-2} is observed for basal sliding, inner slope stability and outer slope stability respectively, and a combined $r^2_{F(X2)|F(X1)}$ of

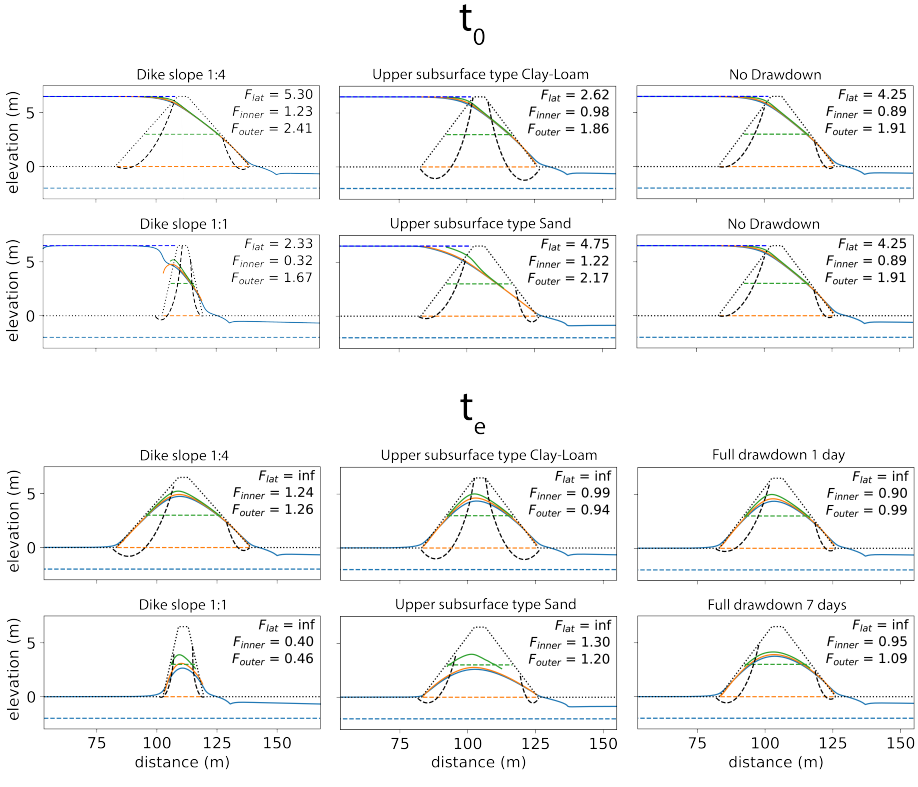

Figure 2.5 Example results of the coupled hydro-stability model. Left two columns: steady state with maximum loading equal to dike crest. Right two columns: falling water levels from dike crest to dike toe. Continuous colored lines indicate hydraulic heads at the depth of the dotted lines with a corresponding color. The black curved lines indicate the sliding planes on the inner and outer slope of the dike associated with the minimum safety factor. t_0 indicates the steady-state results at maximum pressure, and t_e shows the results with water levels returned to the dike toe elevation. For each situation the safety factors of basal sliding (F_{lat}), inner slope stability (F_{inner}) and outer slope stability (F_{outer}) are presented.

0.985 across all failure mechanisms. Based on these small errors and high correlation coefficient the drainage depth, lower layer thickness and dike crest will be fixed. Furthermore, most points in Figure 2.6B are above the 1:1 line, indicating that fixing these input factors either results in equal or lower factors of safety, which suits our goal of performing a sensitivity analysis under the most critical conditions and justifies the use of the global minimum as the fixing point.

Delta Moment Independent measure

The eight sensitive parameters are selected for the global sensitivity analysis, which results in 390,625 combinations for each failure mechanism. The DMI method (Figure 2.7), based on differences in output probability density functions, clearly indicates that for each mechanism, the dike slope (D_s) is most influential. The other dike parameters, namely its height (D_h) and material properties (D_{typ}), are also among the more important factors. Furthermore, some input factors have a different importance for the different failure mechanisms. For example, the foreland width F_w mainly influences the outer slope stability, while the spacing of drainage (Dr_s) mainly influences the inner slope. Other important differences include the relatively high influence of the U_{typ} for basal sliding, as the sliding surface at the dike base is in continuous contact with this upper subsurface layer. Two remarkable differences are the smaller influence of D_{typ} on outer slope stability, and the high standard deviation related to upper layer thickness regarding the inner slope stability (Figure 2.7). While these re-

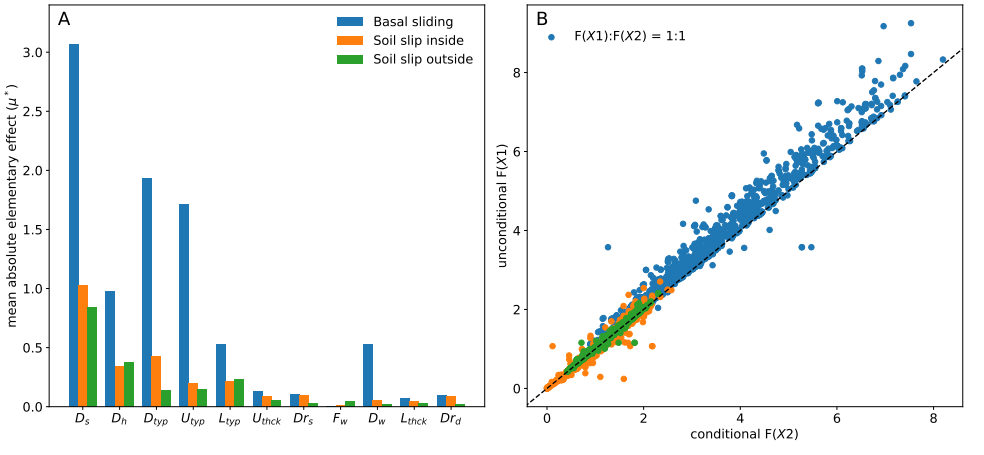

Figure 2.6 Factor Elementary Effects, leading to the factor rank per failure mechanism (A). Fixing the insensitive factors results in the final scatter plot between the results of the unconditional (unfixed) input, and conditional (partly fixed) input (B), leading to a combined r^2 of 0.985. Eight parameters (selection x-axis) are selected for the Monte-Carlo analysis, namely dike slope (D_s), dike height (D_h), dike material type (D_{typ}), upper layer material type (U_{typ}), lower layer material type (L_{typ}), upper layer thickness (U_{thck}), drainage spacing (Dr_s) and foreland width (F_w).

sults indicate the importance of several input parameters, they do not provide further information about their relation to dike failure and local variability.

2.3.3 Trend identification

To identify the trend, the probability of an unstable dike $p(F \leq 1)$ given a certain input factor value is determined (Figure 2.8). For basal sliding, only a small fraction of the input factors' combinations result in unstable dikes, making it the least important process of dike failure. For inner and outer slope stability, the effect is often similar, although critical safety factors are more often found for inner slope stability. Figure 2.8 reflects many of the DMI results (Figure 2.7), for example, a large influence of dike slope and dike height, where less steep sleep slopes and lower dikes are, in general, more likely to remain stable, and the small influence of U_{thck}. However, new insights become apparent too, as it is shown that an increase in foreland width (F_w) increases the outer slope stability only if the dike is less than 25 m away from the river. A similar effect is seen regarding drainage spacing (Dr_s), which mostly decreases the inner slope stability at small distances from the dike (<∼10 m).

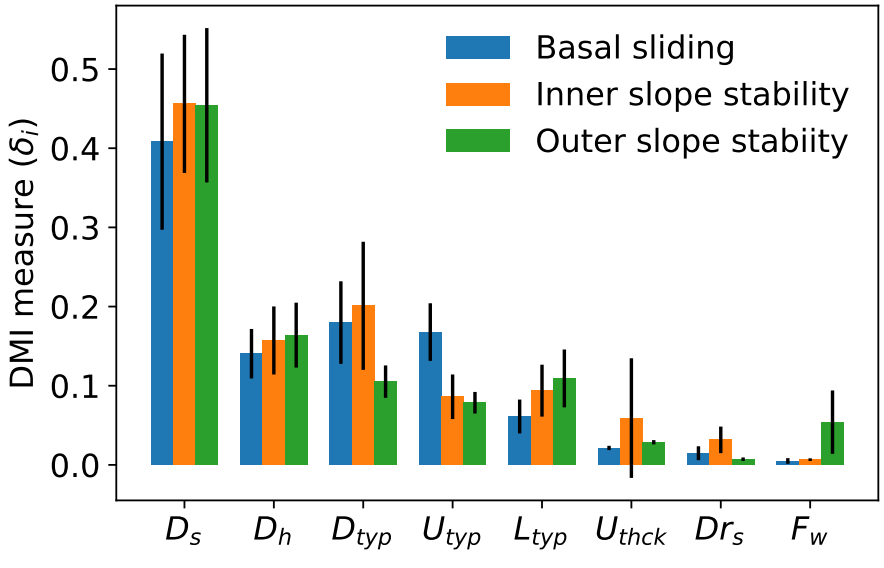

Figure 2.7 Results of global sensitivity analysis (DMI-method). The bars indicate the Delta Moment-Independent measure (δ_i) per failure mechanism where higher values indicate a greater sensitivity of the factor of safety to that variable (Table 2.1). Error bars show the values ± 1 standard deviation (1 σ). Wider error bounds indicate greater variance in the sensitivity for that parameter, possibly caused by parameter interaction.

The most important local variability, however, is observed for the material types, where a unidirectional change in the input factor does not necessarily result in a unidirectional change in dike stability. Where any shift towards a sandier subsurface will, on average, still result in a smaller p$p(F \leq 1)$ for outer slope stability, this is not the case for inner slope stability, which has its lowest $p(F \leq 1)$ at L_{typ} sandy loam. An even more striking trend is observed for D_{typ}, where the lowest failure probability $p(F \leq 1)$ for outer slope stability and the highest failure probability for inner slope stability both coincide at a sand dike. Although basal sliding results in failure less often, a similar local variability in the response can be observed.

2.3.4 Subsurface interaction qualification

To explain these results in more detail, the response surfaces of the average dike stability F at a given combination of material properties are compared with the corresponding pore pressure (Figure 2.9). The results are in line with the $p(F \leq 1)$, which, for example, shows that sand as D_{typ} results in a low F for inner slope stability, but reaches a high F for outer slope stability (Figure 2.9). The results also show that low stability is strongly linked to high pore pressures, in addition to material parameters related to strength, such as cohesion or friction angle. This is mostly the case for basal sliding, where the low factors of safety are reached at both a clay dike/sand cover layer and a sand dike/clay cover, while high pore pressures are only observed in the latter situation.

However, for inner slope stability, there is a clear coincidence of high pore pressures, sand dikes and low F values. As shown in Figure 2.5, the dikes are least stable at t0, which, due to the initial steady state, shows maximum groundwater heads for a dike type of sand, as it is more permeable. Sand dikes generally have low cohesion and rely largely on frictional strength, but friction is lost as the high pore pressures

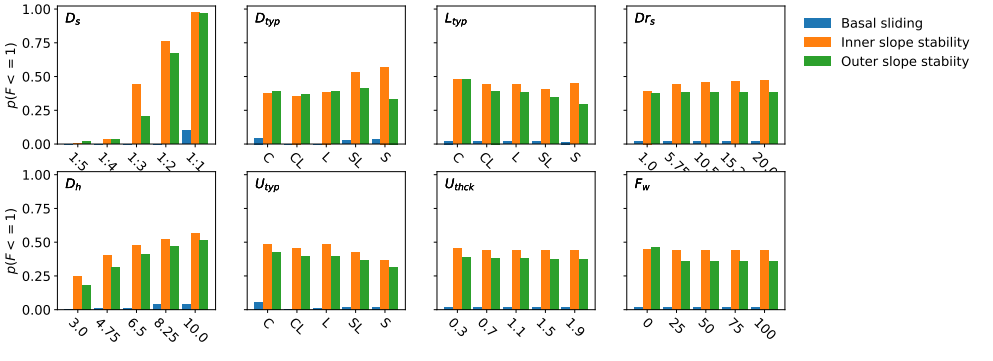

Figure 2.8 Probability of failure $p(F \leq 1)$ given that the selected input factor is fixed at the given value on the x-axis, and all other input factors are not fixed. Where $p(F \leq 1)$ equals 0 all calculated dikes are stable, and with a $p(F \leq 1)$ of 1, all calculated dikes fail. A large difference in the probability of failure between neighboring bars indicates a strong local importance of that factor.

reduce the effective normal stress. As the largest part of the slip surfaces intersects the dike and only slightly touches the cover layer, subsurface types U_{typ} and L_{typ} only have a minor influence on the dike's stability on the inside.

This is not the case for outer slope stability, which often finds its most unstable condition at the end of river water drawdown. In this case, the dike's stability is mostly dependent on the hydrological conditions, as lower stability coincides with higher pore pressures. Strikingly, low stability occurs most often for D_{typ} sandy loam, for which conductivity is high enough to become fully saturated during prolonged high river water levels, but low enough to prevent rapid drainage when the river level falls. This effect becomes more prominent when the material of the dike is more permeable than that of the underlying layers; therefore, the excess pore pressure during river level drawdown cannot dissipate to the underlying layers.

There are no apparent differences between shallow and deeper subsurface layers, although the explanation differs. In case of a shallow subsurface layer (U_{typ}), the lower permeability directly inhibits drainage into this layer, while an impermeable deeper subsurface layer (L_{typ}) inhibits flow to the lateral drainage channels installed behind the dike.

2.4 Discussion and Practical Application

2.4.1 Global sensitivity indices for groundwater induced dike failure

Using the relations derived from the MC simulations, a database is constructed including the input factors and related factors of safety. For each failure mechanism, 390,625 parameter combinations are in this database, of which $p(F \leq 1)$ was 0.02, 0.443 and 0.379 for basal sliding, inner slope stability and outer slope stability, respectively. It follows that our assumptions of an infinitely long period of high-water level at the dike crest followed by a rapid drawdown both favor inner and outer slope failure. Nonetheless, the inner slope is generally more unstable, as its minimum stability is reached during the infinitely long high water, whereas outer slope failure only occurs during the drawdown. This rapid but transient drawdown decreases pore pressure, which thus increases friction and results in more stable conditions than on the inner slope. The larger fraction of simulations in the database with inner slope failures matches with practical experience (Stuij et al., 2017), which suggests the modelling assumptions in this paper result in groundwater conditions that are representative of real-world conditions. Combining all three mechanisms results in a total $p(F \leq 1)$ of 0.48 out of all the combinations, i.e., based on simulations that result in $F \leq 1$ for one or more mechanisms.

All the parameters involved in the analysis have at least a small effect on the dike stability. In general, the least influential parameters are F_w, L_{thck} and Dr_d. However, the foreland width becomes influential at small values (Figure 2.8). Furthermore, the inner and outer slope stability are insensitive to changes in the dike width given the steady-state groundwater conditions, while the dike width does affect basal sliding. In addition, drainage spacing influences inner slope stability mainly if drainage occurs close to the dike. As such, many parameters have a considerable effect on a part of their parameter space and a given failure mechanism, but few are important over

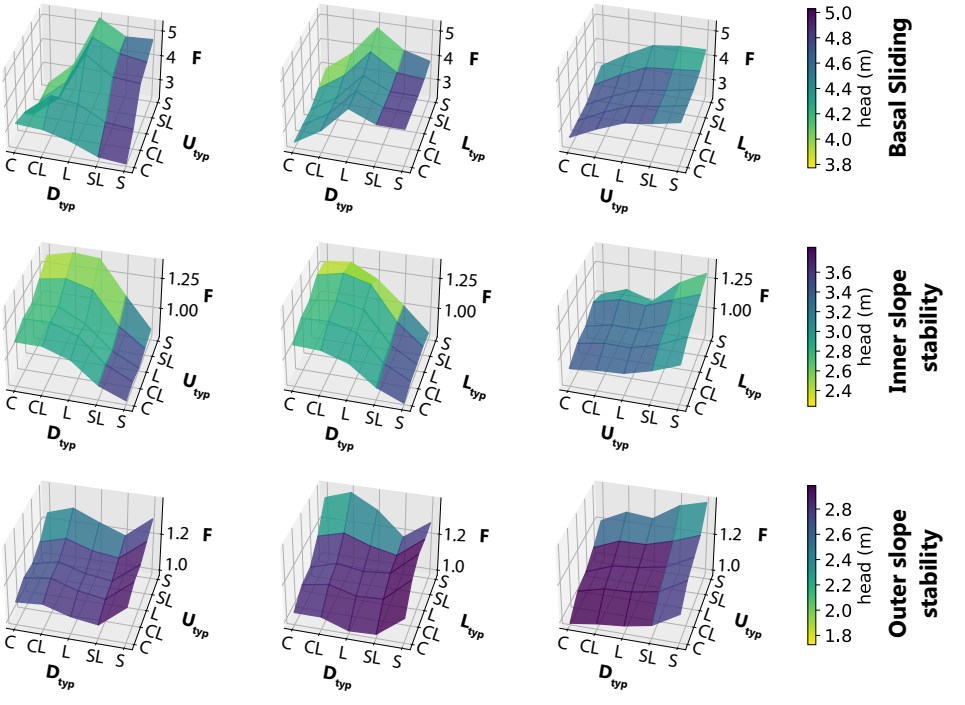

Figure 2.9 Response surfaces of dike stability F on different combinations of dike and subsurface properties. Low factors of safety clearly coincide with high (darker blue) hydraulic heads for each failure mechanism. Note the different scales for both the y-axis (F) as the colors (heads).

their entire parameter space and for all the failure mechanisms. This suggests that although global sensitivity analysis is a useful tool in determining the importance of parameters, the resulting sensitivity indices should be handled with care. In some cases, sensitivity indices such as the DMI (Borgonovo, 2007) underestimate the general importance of a parameter, as they provide a mean parameter sensitivity that does not necessarily reflect the abundance of strong local effects.

2.4.2 Toward flooding

The probability of flooding is not only related to the probability of dike instability, but also to the water levels at the time of failure and the volume of the instability. To analyze the occurrence of these properties, we select the set of model runs for dikes with a 1:3 slope, a height of 6.5 m and a cover layer thickness of 1.5 m. Of the 625 selected scenarios that remain in the database with these parameters fixed, the slip surface shape and phreatic water level are related to the upper substrate type (U_{typ}) for outer slope stability (Figure 2.10). In this example set, the area of failure

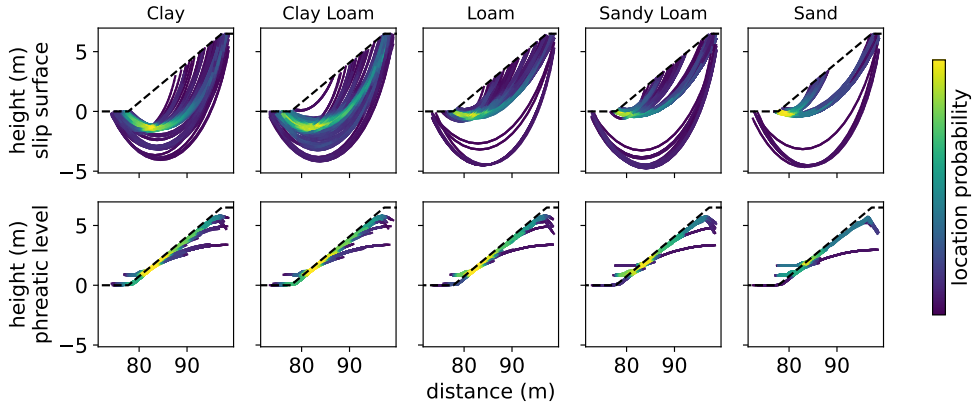

Figure 2.10 Probability of slip surface location and phreatic surface for different types of upper layer (U_{typ}) material. Brighter colors indicate a larger probability of, respectively, the slip surfaces or phreatic surfaces to occur at that location.

decreases from 59.2 to 26.4 m^2, while the mean phreatic level in the upper subsurface layer decreases from 2.36 to 1.93 m when the substrate material changes from clay to sand. Accordingly, the average safety factor increases from 1.06 to 1.29. This indicates not only that dike failure as a result of macro-instability is less likely due to occur with a sand subsurface, but also that potential instabilities are less threatening for a dike breach, as their volume is much smaller.

It should be noted that the groundwater model assumes a stationary response to the flood wave at the dike crest, but a transient response on the drawdown of this flood wave. From a hydrological perspective, the simulations thus start at a situation of minimal internal strength and, hence, minimal dike stability. However, as the high river water levels act as a stabilizing external force on the outer slope, this aspect of failure generally occurs after river water level drawdown. The breaches that subsequently occur create vulnerable dikes but, owing to the falling flood water levels, this is unlikely to lead to major dike beaches and flooding. Obviously, if this instability is followed by a second flood wave, the situation might become critical. Thus, additional research is needed in the transient dike response under very common multi-peak flood waves (Hegnauer et al., 2014).

2.4.3 Limitations regarding sampling, hydrology and subsurface uncertainty

First, this research used a uniform sampling strategy, not taking into account any possible correlations. We suggest, however, that by sampling each parameter uniformly over a range of possible outcomes and not taking account of possible but unknown correlations between parameters, we are likely to overestimate the possible range of outcomes. This conservative estimate of possibilities is deemed a rational choice, if no information is available about the a-priori joint probability distribution of parameters.

Second, we used the most adverse hydrological conditions for dike slope stability calculations, being steady-state conditions for inner slope stability. We acknowledge that this might not be the case when considering flood duration and transient groundwater conditions, as the infiltration curve might not reach the inner toe and the safety factor becomes more favorable. A similar argument applies to basal sliding.

Third, this study used many possible scenarios of subsurface material and surface geometry combinations. Still, the subsurface material in this study is assumed to be homogeneous and deterministic in each of the layers, and likewise the layer thickness and surface profile are constant per section. Due to the long history and continuous improvement of many dikes, their interior is presumably very heterogeneous (Meehan and Benjasupattananan, 2012; Polanco and Rice, 2014). In reality, the subsurface properties, induced by previous river systems, are also known to have a large spatial variability (Berendsen and Stouthamer, 2000; Bierkens, 1996). These heterogeneous topographic and subsurface properties have a large influence on both hydrological conditions (Wang et al., 2018) and stability (Hicks et al., 2014), while still ignoring the 3D slope effects (Gong et al., 2019). In addition, animal burrows and human measures inhibiting or enhancing groundwater flow may also affect the pore pressure evolution.

2.4.4 Suggestions for further research

Nonetheless, the simulations show that for all the mechanisms, the dike type and upper layer type have a large effect on the dike stability. Despite their importance for dike stability and the valid assumption that they are heterogeneous, these two subsurface parameters are often partly unknown. As such, extending this research with variable material properties (Lanzafame et al., 2017) may provide an even more extensive analysis of groundwater-related dike stability. In this way, the uncertainty of the material properties can be assessed too, which is important in real-world cases. In addition to assessing the uncertainty, decreasing it is of major importance when assessing dike stability (Deltacommissie, 2008); this is achieved by having more detailed subsurface data available. Thus, incorporating large scale subsurface heterogeneity (in 3D) is an important step in actively incorporating groundwater calculations in dike stability calculations, although we are confident that the large contrast in dike and subsurface materials used in this study, to a great extent, covers the large variation across many dikes. Furthermore, additional research is needed in the transient groundwater response given a certain flood wave instead of steady-state conditions. Finally, the database constructed and explored in this paper could be used for mapping those regions where factors of safety might reach critical values.

2.4.5 Case study: application of the database for fast high-resolution dike safety assessment

As a first attempt for identifying those regions, the created database was applied to a real-world case. This case concerns the area near the village of Ameide in The Netherlands (51.954594 N, 4.963298 E; Figure 2.11), for which an official preliminary assessment of the dike stability was made (Consortium DOT, 2014). The failure

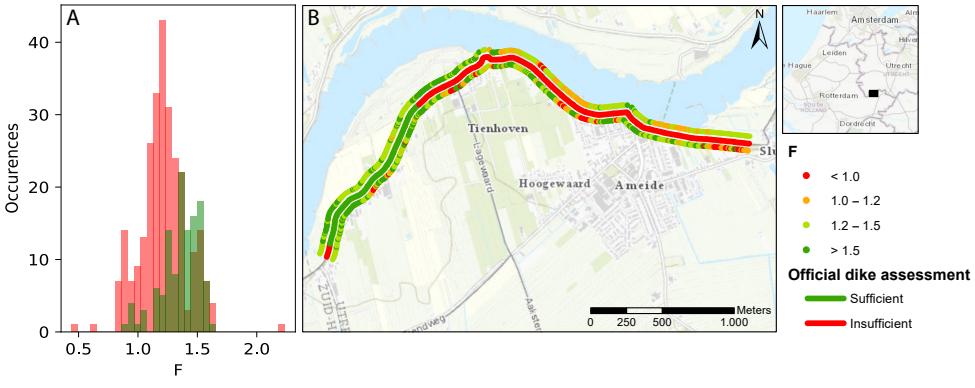

Figure 2.11 Comparison between official preliminary dike safety assessment and safety factors derived from our database. The histograms (A) of the safety factors corresponding to the sufficiently safe (green) or insufficiently safe (red) dike segments clearly show a clear distinction in our database between these segments. Spatially (B), both inner and outer slope stability show a much larger variation in safety factors than the official dike assessment suggests.

probability of the dike was calculated using Bishop's modified method (Bishop, 1955), and based on the characteristic values of material strength parameters. The phreatic level was simplified in the schematization and was roughly a straight line between the river water level and the ditch water level. In the assessment, larger segments with reasonably similar characteristics were tested against a failure probability of 1/360 years and assigned the final judgement. In a later stage, the precision of these judgements was drastically improved using local schematizations and locally derived characteristics for the important parameters; hence, the current assessment was seen as preliminary.

Case study methodology

The dike in this area was subdivided into segments with a length of 100 m, of which several failed to meet the expected failure probability. Here, we compared the values of the factor of safety for comparable situations in terms of dike geometry and composition from the Monte Carlo simulations with the assessment in order to test whether unsafe conditions were revealed by our approach. We hypothesized that using a pre-constructed database with factors of safety in combination with actual dike characteristics could provide a quick a priori analysis of the dike stability. To compare the official assessment with the database, those dike parameters should be selected from a database that corresponds to the actual dike. The parameters concerning geometry and composition of the dike and the subsurface were determined at an interval of 10 m along the entire dike crest. The dike height, crest width and slope were automatically derived from the high-resolution lidar-based AHN3 surface elevation model. The properties of the subsurface, being layer thickness and lithology,

were derived from the GeoTOP subsurface model (Stafleu and Dubelaar, 2016). An approximation of the dike material was made from publicly available cone penetration tests (BRO) using a simple but effective method proposed by (Begemann, 1965). When these parameters were assembled, the corresponding safety factor was selected from the database.

Case study results

First, as the acquisition of surface geometry and subsurface composition can have a high spatial resolution of 10 m, it provides more detailed information than the official assessment, which is conducted on a 100-meter resolution. On visual inspection, the calculated safety factors already clearly coincide with the official dike assessment (Figure 2.11B), although the variation of the calculated values is much higher, as the official safety assessments are carried out only per 100 m section, whereas the factor of safety is calculated here every 10 m. There is also a clear difference visible between the inner and outer slope stability. Those dike sections that are assessed as sufficiently safe have an average safety factor of 1.53 ± 0.31 and 1.44 ± 0.13 for their inner and outer slope stability, respectively. The insufficiently safe sections according to the official assessment have a calculated average safety factor of 1.41 ± 0.38 and 1.34 ± 0.20, respectively. Thus, according to our method, most of the sections found to be insufficiently safe have an $F > 1$ (Figure 2.11A). In the official assessment, 69.3% of the dike was found insufficiently safe against 10.8% in our analysis. Of this 10.8%, 9.5% is found on the insufficiently safe sections and 1.3% is found on those sections that were found to be safe enough.

Case study discussion and conclusions

These false positive assessments, all occurring on the inner dike slope, are most dangerous. Their lower safety factors are caused by a combination of steeper dike slopes and the presence of sandy dike material. Thus, in addition to showing high spatial variability in the expected factor of safety, the analysis also clearly shows those sections that, according to our calculations, are the most critical. These differences seem to be largely related to variations in dike material but can also be related to some of the parameters (drainage, dynamic river level) that are not included in our analysis. Moreover, it is likely the cause of different definitions of failure and the use of different stability calculation methods, such as drained or undrained loading (Soil Science Division Staff, 2017). In conclusion, the high-resolution database comparison could help to focus further research and data assembly, by indicating areas to improve local schematizations and derive local characteristics for the important parameters in a more detailed stage of dike reinforcement design.

2.5 Conclusions

In this study, an extensive global sensitivity analysis was carried out for dike stability using calculated groundwater heads and resulting pore pressures that represent a worst-case scenario. The following three sensitivity settings formed the basis of this

analysis: parameter prioritization, trend identification and interaction qualification. The results show that each of the three studied failure mechanisms, namely, basal sliding, inner slope stability and outer slope stability, can possibly result in dike failure, where failure on the inner slope of the dike is the most likely.

In the parameter prioritization settings, eight parameters were determined to be influential for any of the failure mechanisms, being dike slope, dike height, dike material type, upper layer material type, lower layer material type, upper layer thickness, drainage spacing and foreland width. In contrast, the dike crest width, drainage depth and aquifer thickness had a negligible effect on the stability. According to the Delta Moment-Independent measure (Equation 2.4), the dike slope was found to have the largest effect on dike stability, as it has both a direct effect on slope stability (Figure 2.5) and indirectly affects the slope stability by changing the pore pressure conditions (Figure 2.7). We conclude that the delta sensitivity index provides a clear indication of parameter importance. The Delta Moment-Independent measure does not provide information on parameter interaction and the underlying mechanisms.

A regional sensitivity analysis by means of the probability of failure $p(F \leq 1)$ was used to show local and process-dependent variability. This measure shows that dike slope and dike material are most influential for resulting in unstable dikes. Furthermore, it indicates local variability, such as that drainage spacing only affects the inner slope stability if the drainage location is close to the dike. Combining the Delta Moment-Independent measure indices and the $p(F \leq 1)$ showed that while basal sliding is most sensitive to changes in most parameters, it is least likely to result in dike failure.

In addition, we qualified the interaction between different material types, hydrology and stability. Most strikingly, a combination of a relatively permeable dike and impermeable subsurface inhibits the dissipation of pore pressures to the lower layers. Therefore, pore pressures remain high and dike instabilities are more likely to occur. This effect is more prominent for outer slope stability, as dissipating high pore pressures is mostly important during river level drawdown. The area of failure is often also larger in case of an impermeable subsurface, increasing the chance of severe flooding after a slope instability.

Applying the database containing geometry parameters, subsurface properties and safety factors to a real case resulted in high-resolution estimates of dike stability. These estimates show that the unsafe segments derived from the database are mostly on those segments also found to be unsafe by the official assessment, although there are some false positives, e.g., segments that are estimated to be unsafe but classified as safe in the assessment. Overall, the database estimates provide a more differentiated picture and allow for more targeted analyses and measures. Although three-dimensional subsurface buildup and variable flood waves can improve the simulation results, the comparison gives confidence that our results provide useful insights in the process of groundwater-related dike stability and that the underlying database can be used to focus additional local research. The analysis of groundwater-related dike failure with global sensitivity methods clearly shows the importance of high-resolution groundwater modelling for estimating dike slope stability.

Author contributions

T.v.W., R.v.B., M.F.P.B. and H.M. designed the research. T.v.W. and R.v.B. performed the primary data analysis and model development. H.M. and M.F.P.B. helped with result interpretation. All authors have read and agreed to the published version of the manuscript.

Data availability

A dataset containing the results and input parameters for the Monte Carlo analysis can be found online (van Woerkom, 2020).

Acknowledgements

We greatly appreciated the support of Edwin Sutanudjaja and Lukas van de Wiel providing the computational power needed for the Monte Carlo simulations.

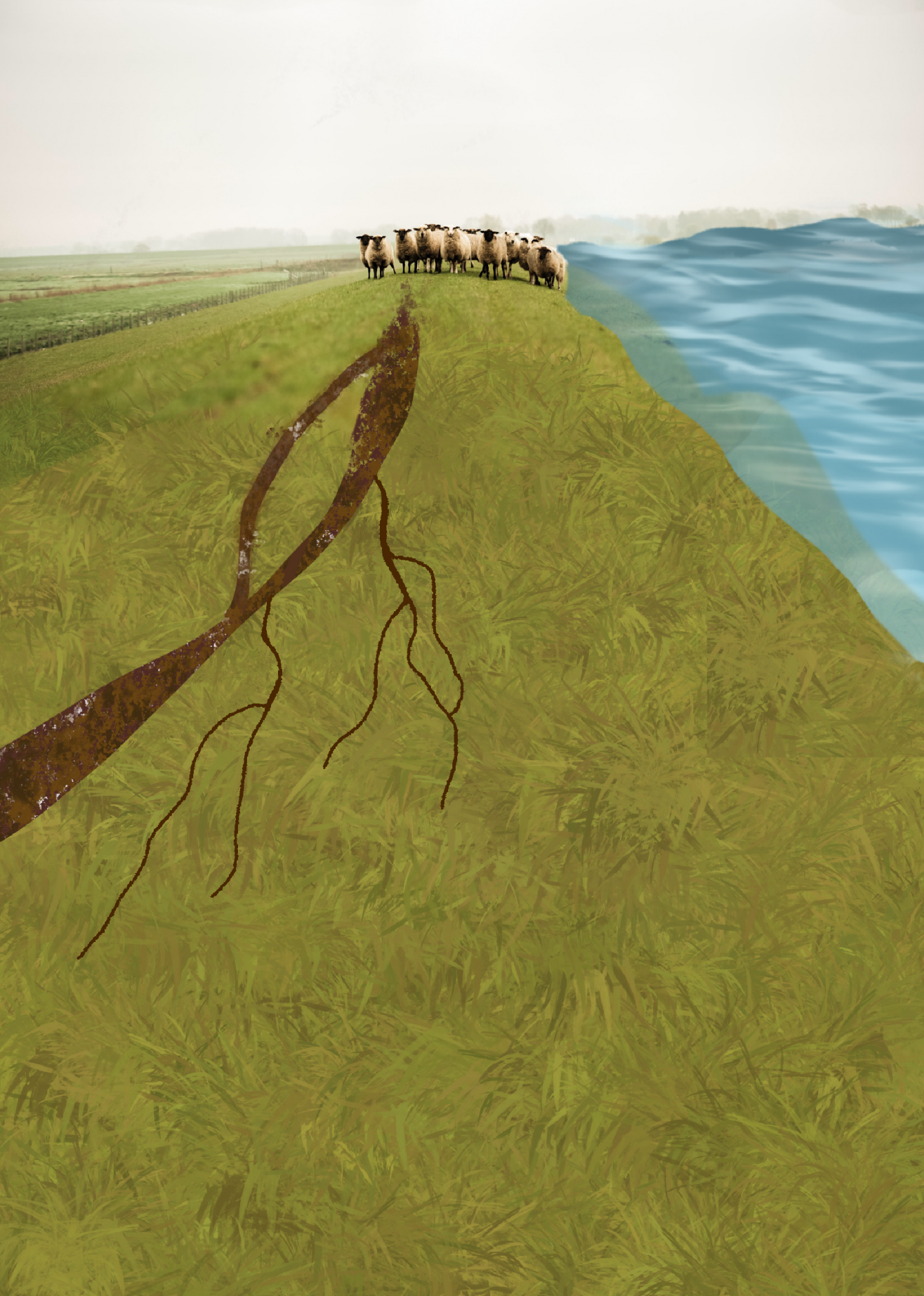

3 Effects of Flood Wave Shape on Probabilistic Slope Stability of Dikes under Transient Groundwater Conditions

Based on: Teun van Woerkom, Mark van der Krogt, and Marc F. P. Bierkens (2023). Effects of Flood Wave Shape on Probabilistic Slope Stability of Dikes under Transient Groundwater Conditions. Georisk: Assessment and Management of Risk for Engineered Systems and Geohazards, DOI: 10.1080/17499518.2023.2222540

Abstract

The time-dependent response of pore water pressures during floods largely determines the safety against geotechnical failure of dikes, which is deemed to be highly dependent on the uncertain shape (duration, maximum height, etc.) of the flood discharge wave. This paper derives the uncertainty of flood wave shape from a database of precalculated hydrographs (GRADE) and evaluates the effect of shape variability on probabilistic safety estimates of slope stability, using a modeling chain consisting of a transient hydrological model (MODFLOW) and a probabilistic dike slope safety assessment (FORM). Accounting for flood wave uncertainty with transient groundwater flow generally leads to higher reliability estimates for slope stability, compared to the steady-state groundwater condition and other conservative assumptions, but to lower reliability estimates compared to a single design flood wave. Furthermore, the uncertainty of the flood wave shape can be as important as the uncertainty in geotechnical properties. For the inner dike slope stability, the volume of the flood wave is the most important factor, while the outer dike slope stability depends mainly on the total water level drop after the peak. These two waveform characteristics are thus essential uncertainties to consider in probabilistic assessments of dike safety with transient groundwater conditions.

3.1 Introduction

Dikes (i.e., earthen flood defenses) form an extensive network along many major rivers around the world aimed at mitigating flood risk and preventing flooding. Climate change may increase the risk of a society to flooding (Middelkoop et al., 2001), for example through expedited snow melt or an increase in extreme precipitation events in the upstream drainage area (IPCC, 2022). Under current and future climatic conditions, slope instability during river floods is one of the major failure mechanisms of river dikes. Slope instability of these river dikes is associated with large uncertainties, mainly relating to soil properties (van der Krogt et al., 2019) and groundwater pore pressures (van Woerkom et al., 2021). The pore water pressure (pressure heads) in the dike and subsoil is also one of the main drivers leading to slope instability during floods.

When river water levels increase, water seeps into the dike and the subsoil, increasing the pressure heads and reducing the effective stress and strength of the soil. Pressure heads during floods are often assumed as steady state seepage conditions based on analytical solutions for typical conditions (TAW, 2004; U.S. Army Corps of Engineers, 2003; Lendering et al., 2018), which may lead to conservative estimates of dike safety. The development of pressure heads can be modeled more realistically using a time-dependent seepage analysis. In such an analysis the effects of soil layering, variable permeability, and flood wave shape can be considered. The hydrological forcing can be derived from a copula-based model considering variability of the peak flow discharge and flow duration (Balistrocchi et al., 2019; Curran et al., 2020) or from a single synthetic design flood wave (Butera and Tanda, 2006). However, they do not account for the full variability of flood wave shapes from variable weather conditions (Hegnauer et al., 2014). Thus, the impact of the flood wave shape uncertainty on the pressure head evolution and the resulting slope stability is currently unknown. The flood wave shape is strongly influenced by the river basin characteristics, and especially capturing multi-peak floods in statistical properties is not feasible (Yue et al., 2002). As such, we define flood wave shape uncertainty as a scenario uncertainty (Baecher, 2016), in which multiple pre-calculated flood wave shapes are assumed equally probable.

This paper thus explores the impact of the uncertainty of the flood wave shape on the probabilistic safety assessment of slope stability with transient groundwater conditions. A multiplicity of flood waves is obtained from a database of pre-calculated hydrographs (Hegnauer et al., 2014). First, a method is proposed to incorporate the variability of these flood wave shapes into the probabilistic reliability analysis for slope stability for a case study in the Netherlands in Section 3.2. This method includes the calculation of time-dependent pressure heads with the MODFLOW hydrological model. The results of this method are compared with dike slope reliability analyses based on pressure head assumptions used in standard engineering practice. Second, we assess the dynamic slope stability response to variability in flood wave shape for two simplified case studies in Section 3.3. The two cases are a permeable sand dike and a less permeable clay dike on a shallow aquitard blanket layer. Hereafter further findings of our research are discussed.

3.2 Methods

To account for the scenario uncertainty of flood wave shapes from variable weather conditions in dike slope stability calculations, multiple flood wave shapes should be considered. Using a combination of rainfall-runoff modelling and hydrodynamic river models, the flood wave shape at a given point on a river can be derived. Such a derivation for river discharge on the Rhine river at Lobith, the Netherlands, is available in the GRADE dataset (Hegnauer et al., 2014), which will be exemplarily applied in this manuscript.

3.2.1 Flood wave selection

The GRADE dataset (Hegnauer et al., 2014) consists of a database of 50,000 calculated flood wave shapes, each containing discharges at Lobith (the Netherlands) for 15 days before and 15 days after the simulated annual maximum discharge. The discharges are translated to water levels at the Lobith gauge station using a qf-rating curve (Bom and van Leeuwen, 2019), which considers steady flow, unsteady effects by water level hysteresis and the effect of weirs.

Given a particular flood wave, we define the maximum water level of that flood wave as h_{max}. Often, the expected maximum water level at a given location or return period is known (h_{max}), but the variation in flood wave shapes given that maximum water level is not. To derive the variation in flood wave shapes given a selected maximum (design) water level (h_{max}), first the 1000 flood waves with their maximum water level nearest to the selected water level are sampled from the dataset. Second, the sampled flood waves are scaled to the selected h_{max} resulting in a dataset of flood waves with equal maximum water levels, but varying shapes. Ideally all 1000 selected flood waves would be used, but to constrain calculation times the selected flood waves are divided in 50 subsets based on five flood wave shape parameters: H_0, A_{peak}, A_{tot}, ΔH_{ds}, Ds_{max} (Table 3.1, Figure 3.1A). The sub-setting is performed using k-means clustering on these parameters, which aims at minimizing the combined within-cluster variance. Finally, a random flood wave is drawn from each of the subsets and an occurrence probability of that flood wave is calculated following the size (number of waves) of the corresponding subset relative to the entire sample of 1000 selected flood waves.

The 50 selected flood waves are assumed to represent all possible flood wave shapes given the corresponding maximum water level. The flood waves that represent a larger group of waves with similar characteristics have a larger occurrence probability (Figure 3.1B). The resulting *sample set* (Figure 3.1C) contains flood waves with multiple peaks or various shapes of the rising and falling limb. The extreme flood wave shapes, for example those with a very wide peak or very steep rising limb, generally have a smaller occurrence probability than those central in the selection (Figure 3.1B). A more extensive analysis of the water level uncertainty can be found in the GRADE report (Hegnauer et al., 2014).

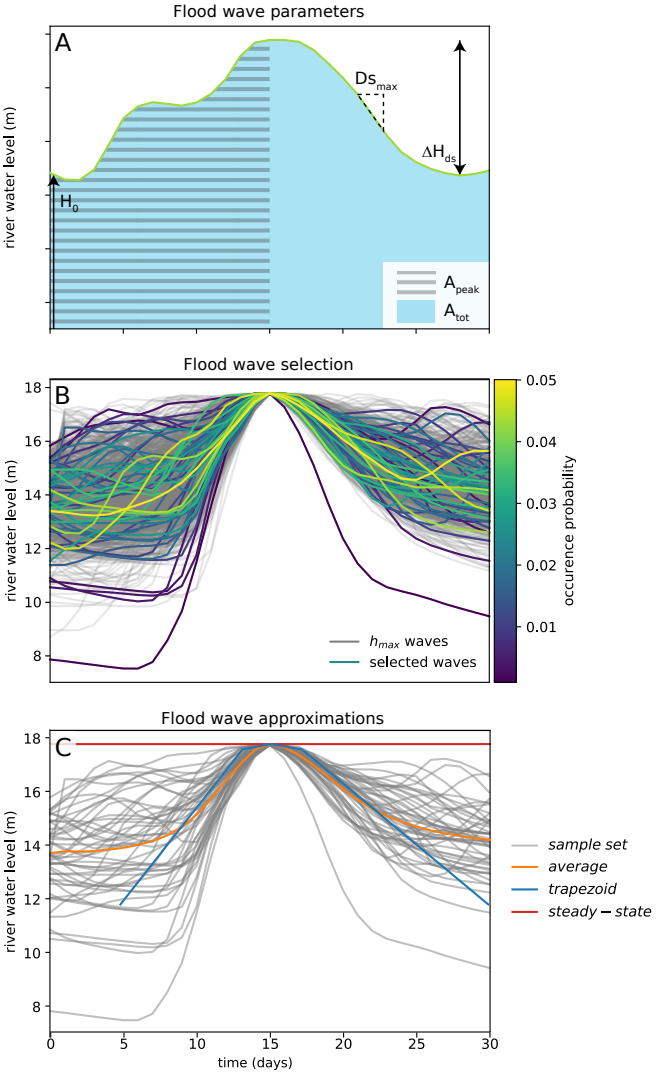

Figure 3.1 Visualization of the flood wave shape parameters (A), selection of 50 representative flood waves with occurrence probabilities given their representativeness (B), and a comparison of the 50 selected flood waves with several frequently used flood wave shapes for groundwater pressure head estimation (C).

Table 3.1 Selected flood wave shape parameters, which are visualized in Figure 3.1

Symbol	Definition	Unit
H_0	Starting wave height	m
A_{peak}	Wave area before peak	m
A_{tot}	Total wave area	m
ΔH_{ds}	Difference between peak discharge and minimum water level after the peak	m
Ds_{max}	Steepest gradient of decreasing water levels after peak	m/day

3.2.2 Combined reliability for multiple flood waves

To calculate the reliability for slope stability accounting for the uncertainty in the flood wave shape scenarios, we follow a three-step approach. First, for each of the 50 selected flood waves (denoted by w_i), we calculate the probability for slope instability for each time step t. Then we combine the failure probability of all time steps over the entire flood wave, to obtain the probability of failure conditional to the flood wave (shape): $P_f|w_i$, shortened to $P_{f,i}$. Finally, we weigh these probabilities with the likelihood of a flood wave shape $P(w_i)$. The probability of failure ($P_{f,i}$) for each time step (t_j) of each flood wave is calculated from the reliability index β (Hasofer, 1974) as

$$P_{f,i}(t_j) = \Phi(-\beta(t_j)) \tag{3.1}$$

where Φ stands for the cumulative distribution function of the standard normal distribution, and $\beta(t_j)$ is the reliability index conditional to the groundwater state at time t_j. Note that the failure probabilities throughout this paper represent a unitless conditional failure probability, for example given a certain groundwater condition or set of flood waves.

For the combination over the time steps $t_0, \ldots, t_n$, we assume that all time steps within one flood wave are fully dependent. First, because we only combine different time steps within one flood wave, and second because the geo-mechanical stochastic variables are time-invariant (at least on the time scale of a flood event) and thus highly correlated. Hence, the probability of failure (conditional to flood wave i), is the maximum probability of all time steps.

$$P_{f,i} = max\{P_{f,i}\,(t_0)\,,\ P_{f,i}\,(t_1)\,,\ \ldots P_{f,i}\,(t_j)\,,\ \ldots P_{f,i}(t_n)\} \tag{3.2}$$

with j the time step and n the number of time steps in the event. To combine the failure probabilities conditional to a given flood wave into a marginal failure probability including wave uncertainty, we assume the flood waves are mutually exclusive: if one wave shape happens, all other wave shapes cannot happen at the same time. Following the law of total probability, the combination is the sum of the probability conditional to the wave shape, weighted with the probability of each wave scenario to

occur $P(w_i)$, see eq. 3.3 and Figure 3.2E.

$$P_{f,combined} = \sum_{i=1}^{m} P\left(F|w_i\right) P\left(w_i\right) \tag{3.3}$$

Here m is the total number of flood waves analyzed (here 50) and $P(w_i)$ is the normalized occurrence probability of that given flood wave, which is estimated as the size (number of waves) of the corresponding subset relative to the entire sample of 1000 selected flood waves (see Section 3.2.1).

Thus, we perform the entire analysis above conditional to different values of the maximum water level of a flood wave $\max\left\{h_i\left(t_j\right)\right\}$, further denoted as h_{max}. Typically, existing methods (that neglect the variability in flood wave shapes) calculate annual failure probabilities. The presented conditional failure probabilities for a given event size h_{max} (eq. 3.3) can in theory be further converted to annual probabilities using the probability weighted sum of this conditional probability of failure for a given h_{max} and the probability density (pdf) of the annual maximum of that water level (1/year) (Schweckendiek et al., 2017).

3.2.3 Methods to estimate groundwater pressure heads

The method proposed in the previous section provides, given a sample of individual flood waves and their effect on groundwater pressure heads, a maximum failure probability conditional to a single flood wave (*sample set*) and a weighted failure probability of these maxima (*realistic*). This method takes the full variation in flood wave shapes from variable weather conditions (Hegnauer et al., 2014) into account. However, such a large dataset of flood wave shapes is often not present, thus current solutions are based on steady-state or analytical solutions for typical conditions (TAW, 2004; U.S. Army Corps of Engineers, 2003) or a single synthetic design flood wave (Butera and Tanda, 2006). We will compare the estimated failure probabilities of our analysis (including uncertain hydrograph shapes) with several frequently used methods to approximate pressure heads (Figure 3.2F, Figure 3.1C). These methods are described here, followed by the name they will be referred to, in *italic*. Each of the groundwater pressure head estimates relates to the maximum flood water level (h_{max}). Thus, the probabilistic dike reliability is calculated according to Section 3.2.5 and represents a failure probability conditional to the given maximum flood water level (h_{max}) and corresponding estimated pressure heads.

A steady-state method (*steady-state*) is based on a steady-state hydrological simulation, assuming an infinite duration of the maximum river water level. A second method, as prescribed for the Dutch flood safety assessment (TAW, 2004), approximates steady-state conditions. This method (*analytical*) provides an estimation of pressure heads at two depths; at the base of the dike and in the sandy aquifer, from which the other values within and underneath the dike are interpolated (TAW, 2004).

Synthetic design flood waves have an advantage over steady-state methods as they incorporate the temporal component of groundwater pressure heads, calculated by the method proposed in Section 3.2.5. Such a synthetic design flood wave has been previously determined for any location along the Dutch river branches (Botterhuis

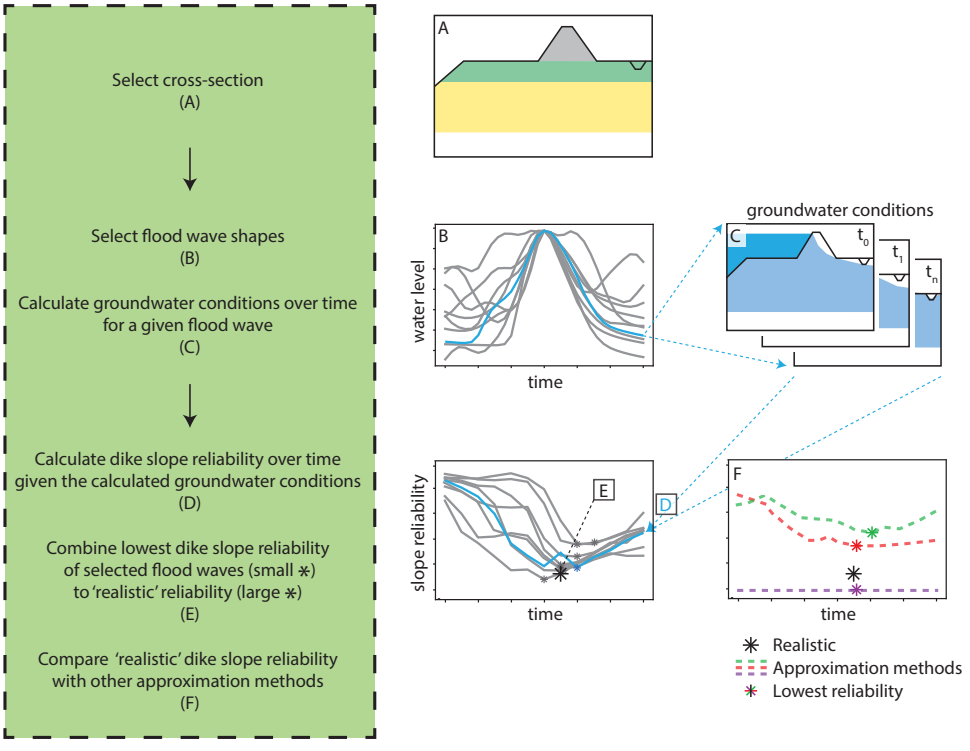

Figure 3.2 Workflow of the modelling chain and the comparison of its results with other methods.

et al., 2017) and has a default trapezoid wave shape (*trapezoid*) (Figure 3.1C). We add a second synthetic flood wave by taking the average for each individual time step of the initial selection of 1000 flood waves (*average*). As this choice is arbitrary, we cannot prove the accuracy of this representation, thus we only use it as an example of a synthetic flood wave.

3.2.4 Summary of the methodology: From flood wave shape to dike slope failure probability

Figure 3.2 provides the summary of the method devised to include flood wave shape variability and its transient groundwater response in probabilistic slope stability analysis, in four consecutive steps. First, a case location is selected, and a surface geometry and subsurface schematization are created of both the dike and the natural subsurface (Figure 3.2A). Second, representative flood wave shapes for that location are retrieved from a large selection of flood waves (Figure 3.2B). Third, time-dependent groundwater flow is simulated with a hydrological model given the surface geometry and subsurface schematization (Figure 3.2C). Fourth, coupling the hydrological out-

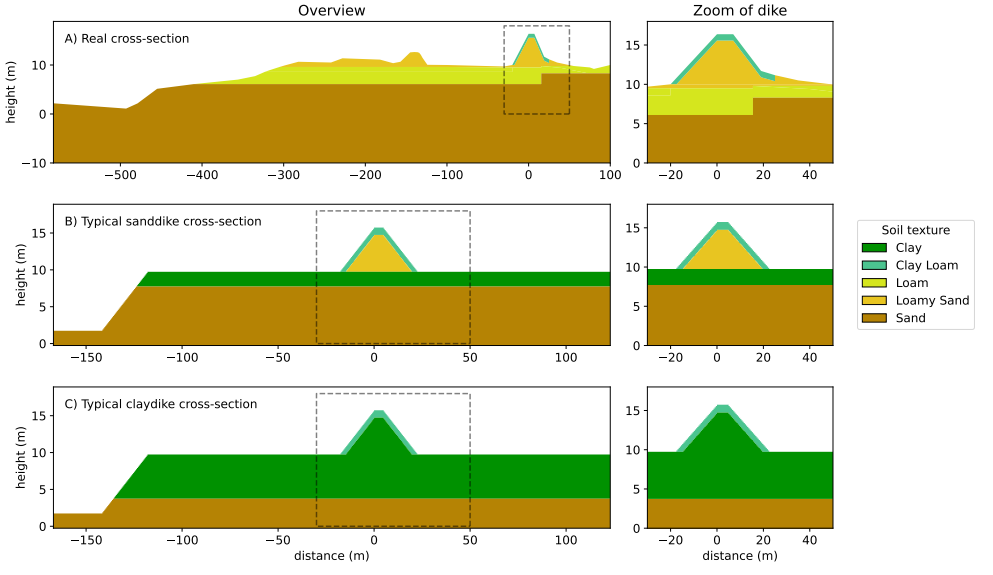

Figure 3.3 Three selected subsurface cases: One real cross-section and two hypothetical cross-sections that are typical for river dikes.

put with probabilistic slope stability analyses results in a dike slope failure probability (slope reliability) per flood wave (Figure 3.2D). These are finally combined into a single dike slope failure probability, which thus takes the variation in flood wave shapes into account (Figure 3.2C). In the following section, the entire workflow is laid out in more detail.

3.2.5 Modelling chain

The general approach as described in the previous sections, can in principle be applied to any location, using any groundwater simulation model code and slope stability algorithm. Here we describe the cases and modelling algorithms selected in more detail.

Selected cases; surface geometry and subsurface schematizations

We selected three cases: a real case study of an existing Dutch river dike and two simplified hypothetical cross-sections of typical dike archetypes (Figure 3.3).

The real case study (near Lent, the Netherlands (51.867 N, 5.884 E) has its floodplain elevation at approximately 10 m above mean sea level and the dike crest at 16.37 m above mean sea level. This case study consists of a loamy sand dike with a clay loam cover layer (Figure 3.3A). In the floodplain a layer of loamy sand is located on top of a clay loam aquitard with a thickness of 4 m. In the hinterland, the schematized aquitard thickness is approximately 1.5 m. A large sandy aquifer is

located below the aquitard, which is in contact with the river, located 300 m from the dike under non-flooding conditions.

The two simplified hypothetical case studies are typical for the Netherlands and consist of a standard dike and two idealized subsurface scenarios (Figure 3.3B-C). The surface geometry includes a 6 m high dike with a 1:3 slope and a crest width of 5 m, on a flat floodplain with an elevation of 0 m above mean sea level. The dike is located 100 m inland from the river channel. The two subsurface scenarios consist of a (loamy) sand dike on a thinner cover layer (Figure 3.3B) and a clay dike on a thick impermeable clay cover layer (Figure 3.3C). In both scenarios the dike has a clayey cover layer at the surface; due to weathering and roots of vegetation this cover layer is likely to be more permeable and less cohesive, hence it is schematized as clay loam.

Maximum flood wave water levels for selected cases

To quantify the influence of variable flood shapes on dike slope failure probability we use the real cross-section (Figure 3.3A) and a h_{max} of 15.96 meters above mean sea level, which is 0.41 m below the dike crest height, corresponding to its safety standard. To further assess the influence of subsurface material and maximum river water level on failure probability we use the hypothetical typical cross-sections (Figure 3.3B-C). For these cross-sections, three hypothetical maximum water levels are selected: a h_{max} of 2, 3.5 and 5 m above the floodplain, or respectively 4, 2.5 and 1 m below the dike crest height. These hypothetical maximum water levels cannot directly be related to a given safety standard but do provide an additional assessment of the influence of variable flood wave shapes under characteristic conditions and for various loads.

Hydrological model setup and parameters

The selected flood waves are used to simulate the pressure heads in the dike and subsurface (Figure 3.2C) using the groundwater model software MODFLOW 6 (Langevin et al., 2019). Initial groundwater conditions are provided by a steady-state MODFLOW simulation. These initial conditions are based on the average winter river water level and average winter excess precipitation. The time-dependent groundwater response to changing river water levels, provided by the selected GRADE flood waves, is simulated using a transient MODFLOW simulation. The model is run with a 2-hour time step, which was found to not impact results compared to smaller time steps. The hydrological model has a cell size of 0.5 m both horizontally and vertically.

On the river side, the MODFLOW river package enables river-groundwater interaction. On the landward side, the drain package (Hughes et al., 2017) enables outflow only if pressure heads become higher than the surface elevation. This package is also used to model a drainage ditch 20 meters behind the inner dike toe with a depth of 1 m. The average winter excess precipitation (2.25 mm day^{-1}) is simulated by the recharge package (Hughes et al., 2017). A saturated conductivity (K_{sat}) is assigned to the subsurface material types based on typical values (Table 3.2, Table 3.3).

Table 3.2 Geo-mechanical and hydrological model parameters for Lent real case study cross-section: saturated unit weight (γ_{sat}) angle of internal friction (φ), cohesion (c), saturated conductivity (K_{sat}), SHANSEP Undrained NC shear strength ratio (S) and SHANSEP shear strength increase exponent (n). In case of a probabilistic parameter the distribution type and standard deviation (SD) are also provided.

Material name	Soil type	Soil property	Unit	Distribution type	Mean	SD
Dike core (γ_{sat} 18.54 kNm^{-3})	Loamy Sand	φ	^{o}	Log-normal	34.8	1.4
		c	kPa	Deterministic	0	
		K_{sat}	md^{-1}	Deterministic	2.85	
Dike cover (γ_{sat} 18.54 kNm^{-3})	Clay Loam	φ		Deterministic	0	
		c		Log-Normal	7.5	1.75
		K_{sat}		Deterministic	0.86	
Blanket layer (γ_{sat} 16.82 kNm^{-3})	Loam	φ	*/above phreatic	Log-normal	35.7	2.0
		c		Deterministic	0	
		K_{sat}		Deterministic	0.1	
		S	*/below phreatic	Log-normal	0.31	0.04
		m	*/below phreatic	Log-normal	0.85	0.02
Aquifer (γ_{sat} 20.00 kNm^{-3})	Sand	φ		Log-normal	36.7	1.2
		c		Deterministic	0	
		K_{sat}		Deterministic	10.4	

Table 3.3 Geo-mechanical and hydrological model parameters for hypothetical cross-sections: saturated unit weight (γ_{sat}) angle of internal friction (φ), cohesion (c), saturated conductivity (K_{sat}). In case of a probabilistic parameter the distribution type and standard deviation are also provided. The stochastic properties of the geomechanical parameters are based on EC7 CEN (2004).

Material name	Soil type	Soil property	Unit	Distribution type	Mean	SD
Dike sand (γ_{sat} 19.5 kNm^{-3})	Loamy Sand	φ	^{o}	Log-normal	34.1	1.7
		c	kPa	Deterministic	0.5	
		K_{sat}	md^{-1}	Deterministic	2.85	
Dike clay (γ_{sat} 17.0 kNm^{-3})	Clay	φ		Log-Normal	21.0	2.1
		c		Log-Normal	7.5	1.5
		K_{sat}		Deterministic	0.05	
Dike cover (γ_{sat} 17.0 kNm^{-3})	Clay Loam	φ		Log-Normal	21.0	2.1
		c		Log-Normal	7.5	1.5
		K_{sat}		Deterministic	0.86	
Blanket layer (γ_{sat} 17.0 kNm^{-3})	Clay	φ		Log-Normal	21.0	2.1
		c		Log-Normal	7.5	1.5
		K_{sat}		Deterministic	0.05	
Aquifer (γ_{sat} 20.0 kNm^{-3})	Sand	φ		Log-normal	35.4	1.8
		c		Deterministic	0	
		K_{sat}		Deterministic	10.4	

Stability model setup and parameters

The hydraulic heads from the MODFLOW groundwater model are used as input for a detailed schematization of the groundwater pressure heads in D-Stability (Figure 3.2D). D-Stability (Deltares, 2019) is used to calculate the failure probability using the First Order Reliability Method (FORM, Hasofer and Lind (1974)) based on the following limit state function:

$$Z(u) = \frac{F_s(x(u))}{\gamma} - 1 \tag{3.4}$$

where $F_s(x(u))$ is the factor of safety, with $x(u)$ a realization of the stochastic variables in the geo-mechanical parameter space as a function of the realization u in standard normal space. FORM has been widely applied to structural reliability problems and involves a linearization of the limit state equation around a most probable failure point (design point) instead of the mean value. It aims to find the design point, and defines the reliability index (β, eq. 3.1) as the shortest distance between the origin in standard normal space and the failure surface (Hasofer and Lind, 1974).

The geo-mechanical parameters are assumed subject to uncertainty and treated as independent stochastic variables. The model uncertainty factor Y_d is also a stochastic variable (with a corresponding coordinate u), accounting for the inaccuracy of the Limit Equilibrium Method. The stochastic properties of the geo-mechanical parameters ϕ, c, S and m for the real cross-section (Table 3.2) are based on local data, i.e. the results of a Direct Simple Shear (DSS) tests on either normally consolidated or over-consolidated soils, provided by the governing organization. For the hypothetical cross-sections the values are based on EC7 (CEN, 2004) and summarized in Table 3.2.

The reliability is calculated for a fixed slip plane, which is iteratively selected by searching for the most critical slip plane in the probabilistic design point, see the procedure described in Huber et al. (2017). The Uplift-Van model (Van, 2001) was used for the slope stability calculation to account for long-shaped slip planes with strength loss due to uplifting of relatively thin clay blanket layers (with a particle swarm search algorithm to determine the most critical slip circle). The reliability is calculated for the landward (inner) side of the dike (STBI) and the (outer) side of the dike facing the river (STBU).

3.2.6 Estimating sensitivity of failure probability to waveform parameters

To evaluate to what degree the variability of flood wave shape contributes to the failure probability, and which flood wave shape parameters are most important, we use a first order variance-based sensitivity index (S_i). Given a generic model

$$Y = f(X_1,\ X_2,\ \ldots, X_k) \tag{3.5}$$

this sensitivity index determines the statistical dependence of Y and X_i by quantifying how much the model uncertainty is reduced if the input parameter X_i is set to a certain value (Ratto et al., 2007; Borgonovo et al., 2017). In our case, Y represents the failure probability and X_i parameters that determine this probability (flood wave

shape parameters and geo-mechanics parameters). If $V(Y)$ denotes the unconditional (total) variance of Y, $V(Y|X_i)$ denotes the variance of Y if X_i is set to a certain value. The expected value of $V(Y|X_i)$ over all possible values for X_i is $E_{x_i}(V[Y|X_i])$, which is related to $V(Y)$ by

$$V(Y) = E_{x_i}(V(Y|X_i)) + V_{x_i}(E(Y|X_i)) \tag{3.6}$$

where a large value of $V_{x_i}(E(Y|X_i))$ indicates a large contribution of X_i to the variability of Y and is called the first-order effect of X_i on Y (e.g. Saltelli et al. (2008)). This conditional variance can be normalized by the total variance to result in the first-order sensitivity index S_i by

$$S_i = \frac{V_{x_i}(E(Y|X_i))}{V(Y)} = \frac{V(Y) - E_{x_i}(V(Y|X_i))}{V(Y)} \tag{3.7}$$

where high values of S_i signals X_i to be an important parameter (Saltelli et al., 2008).

3.3 Results and discussion

3.3.1 Failure probability of the case study Lent using variable flood waves

Uncertainty and time-effects of wave-dependent failure probabilities

We analyzed the failure probabilities of a sample set of 50 flood waves (Figure 3.1). Each flood wave results in a different temporal development of failure probability; thus 50 different flood wave shapes lead to highly variable outcomes for dike slope reliability. The variability of the reliability is larger for inner slope stability (STBI) than outer slope stability (STBU), see Figure 3.4.

Furthermore, the *sample set* β's all have a similar development over time for STBI: the reliability indices are usually lowest several days after the peak water level (t_{15}). STBU reliability reaches its maximum at or just before the peak water level but has a highly variable development before and after this maximum, as a result of the variability of the flood wave. The minimum β is usually reached after the peak water level, although the reliability is hardly lower than before the peak.

The resulting *realistic* reliability, being the weighted average of the highest failure probability of each *sample set* wave (section 3.2.2), is shifted towards the waves with lower reliability indices (Figure 3.4). The *realistic* failure probability is thus dominated by only a few adverse flood wave shapes. The *realistic* β is lower for STBU than for STBI, which is mostly caused by the lower sloping berm on the inner side of the dike.

Comparison with other methods of groundwater pressure head estimations

The general development of the reliability index over time for the dynamic methods based on a synthetic flood wave shape (*average*, *trapezoid*) is comparable to the 50 individual selected flood waves. As such, the highest failure probability (lowest reliability index) of these dynamic estimation methods ($P_{f,i}$, Section 3.2.2) are also similar (Figure 3.4, crosses). The non-dynamic methods for pressure head calculation

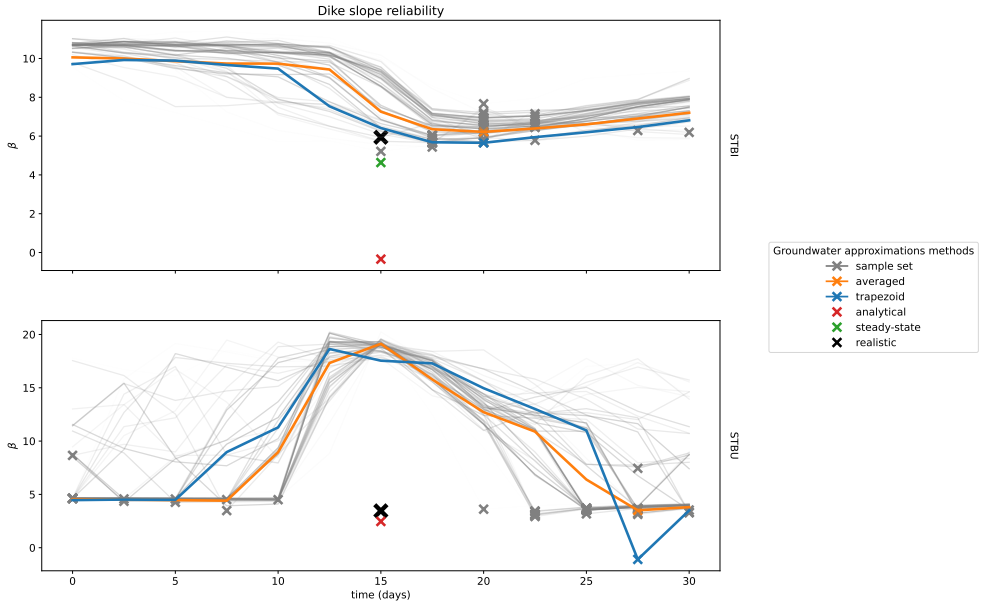

Figure 3.4 Temporal evolution (lines) and minimum value (crosses) for reliability indices of the real case over time for both inner side (STBI) and outer side (STBU) slope stability and multiple methods for approximating groundwater conditions (Figure 3.1C). Note that the *realistic*, *analytical*, and *steady-state* methods have no temporal component and are therefore plotted on t_{15}.

(*analytical*, *steady-state*) and the *realistic* method only have a single reliability index and thus no temporal component.

The *realistic* method has a β of 5.94 and 3.46 for STBI and STBU, the *average* method of 6.22 and 3.51 and the *trapezoid* method of 5.65 and -1.10 respectively. The *analytical* β is -0.34 and 2.46 for STBI and STBU and the *steady-state* β is 4.63 and $-\infty$ respectively. Both *steady-state* and *analytical* result in higher failure probabilities than the *realistic* method proposed in this paper, only the *analytical* method on STBU provides a failure probability estimate that is close to that of the dynamic methods.

3.3.2 Comparison between methods of the effects of subsurface properties and maximum river water level on failure probability

As the time step with the lowest reliability index β determines the failure probability for one flood wave, we only present the $P_{f,i}$ of the entire flood wave in the next sections (determined by the lowest reliability over all time steps). We compared the reliability for two cross-sections that are the same in terms of surface geometry but differ in subsurface properties (see Figure 3.5). We compare the reliability results for the various static and dynamic methods, and for flood waves with three different maximum water levels (section 3.2.3, 3.2.5).

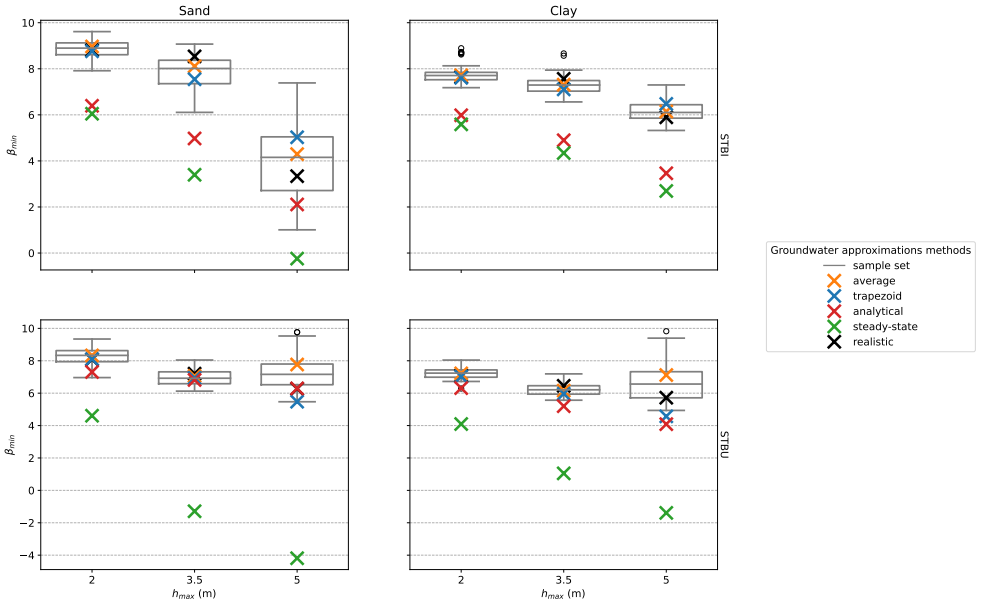

Figure 3.5 Reliability index (β) of the clay and sand dike cases conditional to various maximum river water levels (h_{max}) and according to multiple methods for groundwater pressure head approximation. The box-whisker plots indicate the variation of the 50 *sample set* flood wave shapes.

The reliability indices of the 50 flood wave shapes (*sample set*) generally decrease with a higher maximum water level. However, higher water levels also lead to a larger uncertainty of the dike slope reliability. For STBU with $h_{max} = 5$ the resulting *realistic* (weighted mean of the selected waves) reliability hardly decreases with respect to lower water levels. Sand dike inner slope stability (STBI) is most dependent on the maximum water level. Furthermore, in these two typical dike cases (Figure 3.3B-C) with the same inner and outer slope steepness, STBU has a lower reliability index in most cases.

As noted in the previous section, the combined reliability index from the 50 selected flood waves (*realistic*, Section 3.2.3) is again shifted towards the *sample set* waves resulting in lower reliability indices. The *realistic* reliability is again more similar to the dynamic methods than to the static approximations. For STBI, dike safety is overestimated by the *average* and *trapezoid* methods with respect to the *realistic* reliability. On the other hand, dike safety is underestimated by the *analytical* and *steady-state* methods, independent of the maximum water level. As the *analytical* method is based on steady-state conditions, we would expect it to be closer to the *steady-state* method. However, both phreatic levels as aquifer pressure heads are higher for *steady-state* than for *analytical*, thus leading to lower reliability indices. For STBU the *average*, *trapezoid*, and *analytical* methods all provide reasonable estimates of dike safety. On the other hand, a large underestimation of dike slope reliability

is made using the *steady-state* method. The reliability is thus often consistently either overestimated or underestimated using the selected methods, which illustrates the necessity of considering the uncertainty of the flood wave shape in dike safety calculations.

3.3.3 Further exploration of the dynamic slope stability response to flood wave shape

To further explore the influence of variable flood wave shapes on dike stability, we provide an analysis of:

- The variation in the selected flood waves and the influence of flood wave shape on groundwater pressure heads.
- The timing of lowest failure probability.
- The fraction of the failure probability uncertainty explained by the flood wave shape.
- The most critical flood waves and the most important flood wave shape parameters.

All these analyses are done separately for STBI and STBU and for the typical clay and sand dike cross-sections (Figure 3.3B-C).

Variability of the flood waves and the impact on groundwater conditions

The selected flood waves are normalized to have the same maximum water level after 15 days (t_{15}) (Figure 3.6, top row), but have different water levels before and after the peak. With $h_{max} = 5$, the mean and standard deviation of the river water levels at the start of the simulation (t_0) are -2.88 $\pm$ 1.44 m, -2.24 $\pm$ 1.74 m, and 1.24 $\pm$ 0.97 m, given a maximum water level at t_{15} of at 2, 3.5 and 5 m. 15 days after the maximum water level (t_{30}), the mean and standard deviation equal -2.29 $\pm$ 1.23 m, -1.53 $\pm$ 1.42 m, and 1.71 $\pm$ 0.84 m respectively. Thus, 15 days after the peak the water levels are generally higher than 15 days before the peak, but the variation is smaller.

The two flood waves with either the largest (high wave) or smallest area (low wave) under the curve are selected to analyze their effect on groundwater pressure heads. At the inner toe of the dike the resulting pressure heads of the high wave are much higher than those of the low wave, while at the outer toe this difference is much smaller. For both the high wave and low wave, pressure heads at the inner toe are on average highest at t_{30}, while at the outer toe pressure heads are highest during peak river water levels (t_{15}). This delay of pressure head response is more prominent in the clay dike case.

Furthermore, the pressure heads in the aquifer underneath the dike do not reach the same height as the river water level, but gradually increase towards t_{15}. The increase of pressure heads in the aquifer continues towards t_{30} for the clay dike case, even for the low wave in which river water levels decreased again substantially. For the maximum water levels of 2 and 3.5 m the observed pattern is similar, although

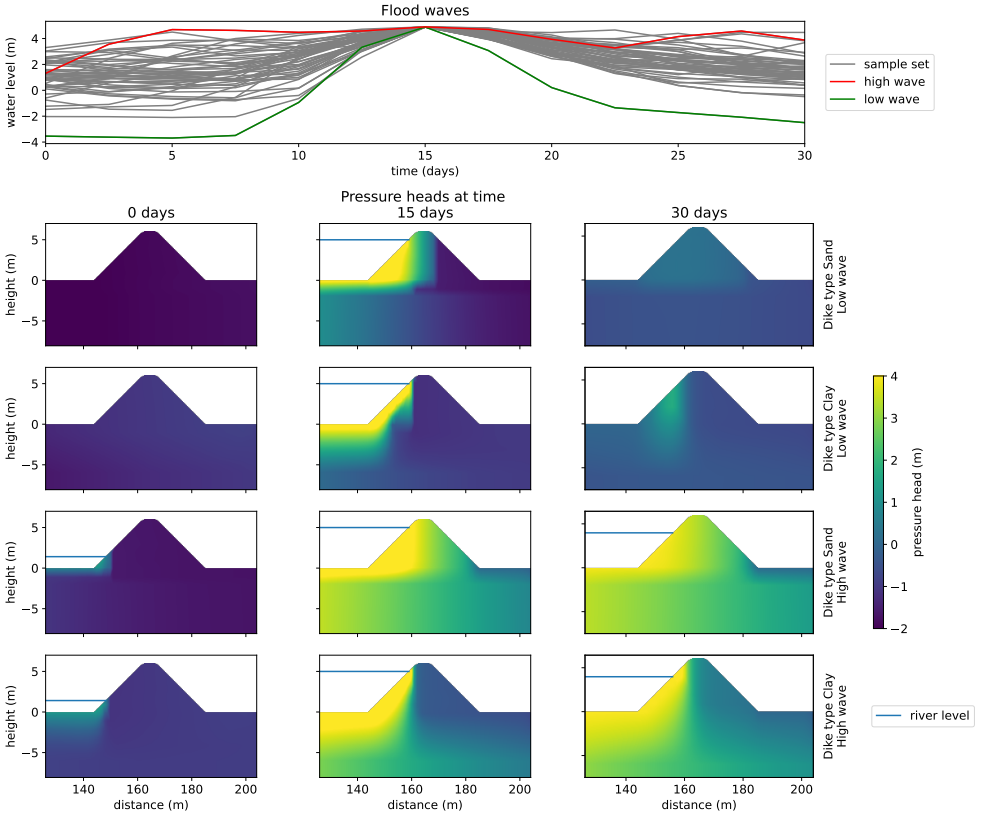

Figure 3.6 Various flood wave shapes and the response of the groundwater pressure heads in the sand dike case and clay dike case on two extreme shaped flood waves with a h_{max} of 5 m.

the response is smaller. For the real dike case (not shown), the groundwater response is closest to the hypothetical sand dike case.

Timing of lowest stability

The timing of the lowest dike stability is an important step to gain better insight into the stability response to flood waves. The timing of the lowest β ($T_{\beta_{min}}$) is >2.5 days after the occurrence of the peak water level for all cases. For STBI the median $T_{\beta_{min}}$ is 15 and 5 days after the peak water level for the clay and sand dikes cases respectively for the most extreme water levels (Figure 3.7). For STBU the median $T_{\beta_{min}}$ is 15 and 12.5 days after the peak water level for the clay and sand dikes cases respectively. The real delay of $T_{\beta_{min}}$ can be even larger as many selected flood waves reach the lowest stability on the last time step in the simulation. With lower maximum water levels, $T_{\beta_{min}}$ is usually closer to the timing of the peak water level. For STBI on the

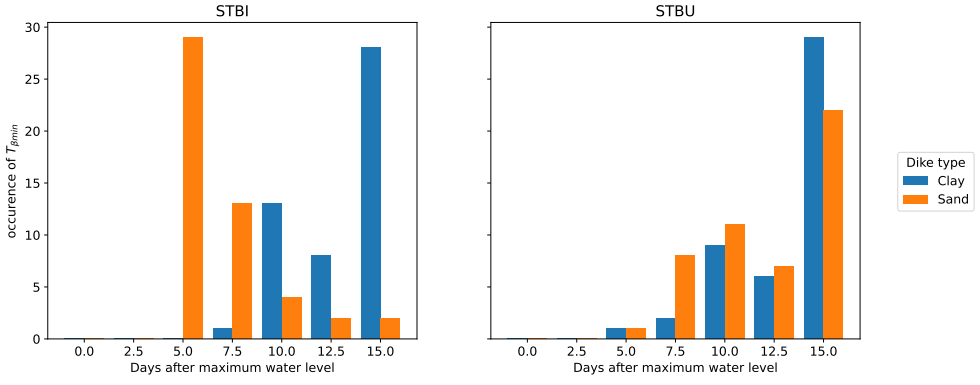

Figure 3.7 Timing of lowest reliability index for the most extreme simulated water levels ($h_{max} = 5$). For both STBI and STBU, and for both the clay dike and sand dike cases, the lowest reliability index occurs several days after the maximum river water level.

sand dike this is not the case, as the pressure heads decrease faster with decreasing river water levels, thereby also decreasing dike slope failure probability.

The delay of the lowest reliability index with respect to the peak river water for STBU has been widely acknowledged (van der Meer, 2020). On the other hand STBI is often assumed to be an instantaneous process, although a delay of several days has already been reported (Moellmann et al., 2011; van Leeuwen, 2019). Due to the delayed STBI failure, as water levels may have also dropped substantially by that time (van der Meer, 2020) extensive flooding after failure is less probable. This would reduce the economic damage and number of casualties after a slope instability and could lead to a reconsideration of dike safety in the flood risk framework, for example if it is combined with emergency repair to pose the risk of flooding by a quickly re-occurring high water level. As such, we recommend analyzing return times of high river water levels shortly after a possible dike failure (van der Meer et al., 2021).

Fraction of uncertainty in dike slope reliability explained by flood wave shape

To quantify the importance of flood wave shape and associated groundwater levels, we compare the uncertainty in dike slope reliability arising from flood wave shape with the uncertainty arising from geo-mechanical parameters (section 3.2.5) by means of the first-order sensitivity index (S_i). The analysis is carried out on the hypothetical cross-sections.

The influence of the flood wave shape increases with increasing maximum water levels (h_{max}) (Figure 3.8). The S_i of flood wave shape for the sand dike case increases from 0.15 and 0.18 to 0.56 and 0.52 for STBI and STBU respectively. The influence of variable flood wave shape increases fast towards $h_{max} = 5$ for or clay dike STBU, with a S_i of 0.55. For clay dike STBI on the other hand, the influence of variable flood wave shape hardly increases with increasing h_{max}. For both STBI and STBU, the remaining uncertainty resulting from the geo-mechanical uncertainty in the slope

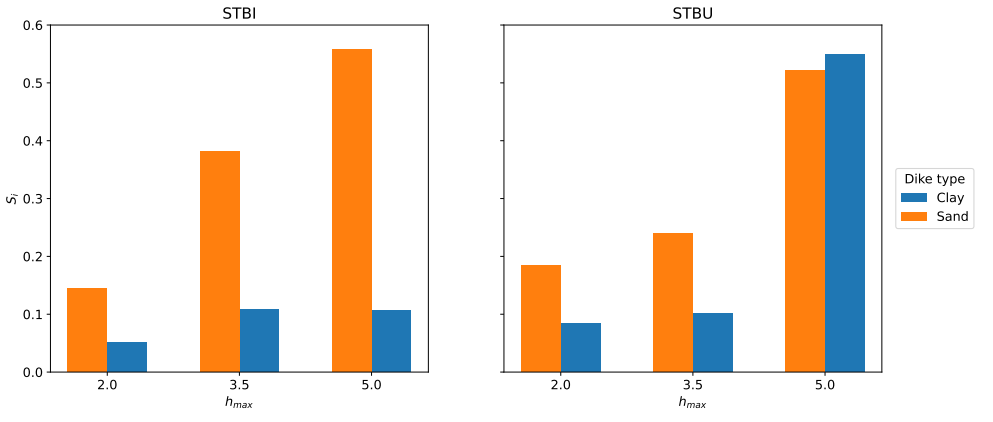

Figure 3.8 First order sensitivity indices (S_i) of flood wave shape for various maximum water levels. The values also represent the relative fractional influence of flood wave shape versus the influence of geo-mechanical material properties.

stability analysis is mostly caused by the friction angle of the cover layer (roughly 50%), with cohesion of the cover layer (roughly 25%) and model uncertainty (roughly 20%) being the other main drivers (Table 3.3).

The influence of flood wave shape variability on dike slope reliability is strongly correlated with the variability in pressure heads. For example, high pressure heads hardly develop on the inner slope of a clay dike (Figure 3.6), leading to a low S_i of flood wave shape for STBI. Contrary, the S_i for sand dikes is larger, probably because large pressure head differences are present between waves (Figure 3.6). The stabilizing effect of high river water levels is an additional explanation for the large influence of flood wave shape on STBU. To conclude, flood wave shape can contribute more than 50% to the uncertainty in a dike slope stability assessment with time-dependent groundwater analysis, pointing out the relevance of the entire flood wave shape, rather than only the maximum water level.

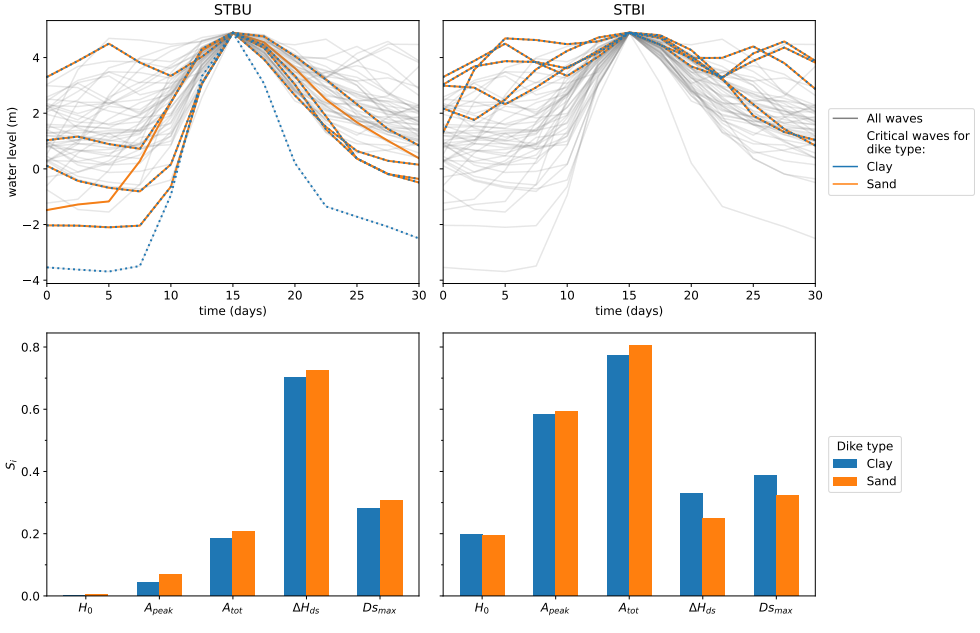

Figure 3.9 Most dangerous flood wave shapes (top row) and sensitivity of dike failure probability to several flood wave shape parameters (bottom row). Note that the sum of all S_i values is larger than 1, indicating dependency and interactions between parameters.

Critical flood waves and important flood wave shape parameters

Lastly, we focus on the most critical flood waves and determine to which flood wave shape parameter the reliability index is most sensitive. The first order sensitivity index (S_i) is used, focusing on flood waves with a maximum water level of 5 m. We selected the five flood waves that resulted in the highest dike failure probability.

The five most critical flood waves are almost the same for clay and sand dikes (Figure 3.9). The most critical waves for STBU differ before the peak water level, but all show a steep decline in river water levels after the peak. The most critical waves for STBI have relatively high water levels over the entire duration, but especially before the peak at t_{15}.

In line with this visual inspection, the maximum river water level difference in the declining limb (ΔH_{ds}) is most influential for STBU. Remarkably, it has over twice the influence of the maximum gradient of this decline (Ds_{max}), which is often assumed as more important (Gao et al., 2019). As expected (van der Meer, 2020), outer slope failure is less sensitive to the flood wave shape before the water level peak. The total wave area (A_{tot}) and flood wave area before the peak (A_{peak}) are the most important parameters for STBI. Contrary to STBU, all flood wave shape parameters have some influence on the STBI, but they mostly contribute to the total wave area (A_{tot}) and have an effect on the reliability as such (van Leeuwen, 2019).

3.4 Conclusions

In this work, a combined transient analysis of flood wave shapes, groundwater pressure heads, and dike stability, indicates that dike stability is not only influenced by the maximum water level, but by the flood wave shape as well.

- Combining multiple flood wave shapes into a single-event failure probability results in a failure probability that is more realistic than failure probabilities from a single design flood wave or a steady-state approximation.
- Considering only the average flood hydrograph in transient seepage analyses leads to overestimated reliability, urging to consider the variability in flood wave shapes.
- Steady-state and analytical approximations of groundwater pressure heads failure probability generally overestimate the failure probability for slope stability up to several orders of magnitude compared to estimates with transient seepage analyses.
- Higher maximum water levels result in higher failure probabilities due to higher groundwater pressure heads, but this relation is less strong for outer slope stability, which is more dependent on the difference between peak water level and minimum water level after the peak.
- In the considered case studies, the lowest stability always occurs > 2.5 days after the maximum water level. For inner slope stability and the sand dike case, the mode is 5 days after the maximum water level. Though this implies that

water levels will be lower at the time slope instability occurs, there is still a high risk of extensive flooding for example due to erosion. We recommend to further analyse when the delay is such that the risk of flooding can be lower, and how to incorporate it into safety assessments.

Author contributions

T.v.W. and M.v.d.K developed the research goals, and designed and performed the primary model development. M.F.P.B helped with results interpretations and feedback on the written manuscript.

Acknowledgements

The authors would like to thank Wim Kanning, Rens van Beek, Timo Schweckendiek, Hans Middelkoop and Willem Leeuwdrent for their assistance. In addition, the suggestions by anonymous reviewers and the journal's editors significantly improved this manuscript.

4 Assessing Lithological Uncertainty in Dikes: Simulating Construction History and its Implications for Flood Safety Assessment

Based on: Teun van Woerkom, Rens van Beek, Hans Middelkoop & Marc F. P. Bierkens (2022). Assessing Lithological Uncertainty in Dikes: Simulating Construction History and its Implications for Flood Safety Assessment. Journal of Flood Risk Management, e12848.

Abstract

Dikes often have a long history of reinforcement, with each reinforcement adding new material resulting in a heterogeneous dike. As data on the dike internal heterogeneity is sparse, it is generally overlooked in the stability assessment of dikes. We present an object-based and process-based model simulating dike construction history on archaeological dike cross-sections, yielding similar patterns of heterogeneity as observed in real dikes, and apply it in a dike safety assessment. Model predictions improve when being based on more accurate statistics of dike buildup, or when being conditioned to ground truth data. When incorporated in a dike stability assessment, multiple model runs can be coupled to hydrological simulations and dike slope stability calculations, resulting in a probabilistic stability assessment considering internal dike heterogeneity. While high-resolution observations are still sparse, good model accuracies can be reached by combining regional information on dike buildup with local point observations and this model provides a parsimonious basis to include information on internal dike heterogeneity in safety assessments.

4.1 Introduction

Current and future changes in climate likely lead to more extreme precipitation events and high-water levels, which demand major investments in dike reinforcement projects. To efficiently guide these expenditures, extensive research is carried out to determine the material properties of dikes (De Waal, 2016). This information is of great importance for dike stability, as the material type directly influences dike stability by the stability parameters (Cao et al., 2016), but also indirectly influences groundwater pressures and flow within the dike (Kuriqi et al., 2016; Butera et al., 2020; van Woerkom et al., 2021).

The material from which dikes are constructed is often very heterogeneous, as during their existence dikes were heightened and widened. To support this, a short overview of the river dike history of the Netherlands is presented, but a similar history can be expected elsewhere. The earliest dikes in the Netherlands were constructed in the early Middle Ages, and at the start of the 16th century all rivers were bordered by dikes. These dikes were owned by locals who could use the dike but were also responsible for its maintenance. A water board coordinated and inspected the maintenance works done by the local land owners (TeBrake, 2002). Large scale dike reinforcements only started in the 19th century with the mechanization of transport and construction and the establishment of a national institution for water safety (in Dutch: Bureau van de Waterstaat). In more recent times (following the 1953 storm surge) the Delta Law of 1958 led to an extensive round of dike reinforcement (Pleijster et al., 2014). Currently, new risk-based safety standards based on acceptable probabilities of flooding for various dike failure mechanisms are defined, again leading to a series of reinforcement projects. Differences in reinforcement methods, and the prolonged lack of institutionalized control, have resulted in very heterogeneous dikes (Figure 4.1), and locally the original lithological sequence in river dikes can be very discontinuous as a result of dike breaches.

It can be inferred from the sparse excavations of dikes (Figure 4.1) and from the more numerous cores and CPTs, that many dikes have been constructed during several phases of reinforcement and that often soil material was used that was chosen on the basis of availability rather than its engineering properties. However, their history is often undocumented and observations on dike composition are insufficient to reconstruct a single dike transect, let alone a spatial continuous mapping. Consequently, the stability of the river dike slopes is often very uncertain due to poor estimations of soil properties and groundwater pore pressures. Currently, only average properties of dike material are often derived, or a global statistical uncertainty is applied in a probabilistic analysis (Gui et al., 2000; Cao et al., 2016) to assess its probable response on dike hydrology and stability. Although this approach might be applicable for slope stability problems (van der Krogt, 2022), it ignores the internal structure and heterogeneity of the dike, in which a weak zone can significantly decrease dike macro-stability (Tabarroki et al., 2021). In addition, a wedge of sandy material can increase seepage and pore pressure heads, decreasing the shear strength of the material. Thus, to improve both pore pressure estimations and slope stability calculations internal heterogeneity needs to be included in dike buildup reconstructions.

Figure 4.1 Example of historical dike buildup as seen in the archaeological excavation in Vlaardingen (schematized in Figure 4.5, see Appendix A.1 for source). The variation in color is a first indication of variable material textures, which are mostly variations of clay-silt mixtures in this dike, with sandy to gravel deposits on the top, which form the road foundation.

Two complementary strategies can be deployed to increase information density and improve dike buildup reconstructions. The first strategy is to gather more field-based research, using e.g., geological cores and cone penetration tests (CPTs), but the resulting detailed point observations on layer depths and material properties are insufficient for a full reconstruction and in many cases, no local ground truth data of the dike is available at all. The second strategy focuses on point-data interpolation to simulate lithological sequences. Most common are the pixel or voxel-based techniques, for example kriging (Isaaks and Srivastava, 1989), Markov Chain (Li et al., 2004; Elfeki and Dekking, 2005) and multiple-point geostatistics (Feyen and Caers, 2006). Other techniques are object-based methods, which place preconstructed units with certain characteristics in the model domain consecutively (Deutsch and Wang, 1996) or process-based techniques, which simulate the construction or sedimentation process that formed the geological sequence (Pyrcz et al., 2009). However, most of the pixel or voxel-based techniques are less suitable for river dikes simulation given their very diverse and distinct, man-made lithological sequences. Moreover, some techniques

depend on abundant training data and local point data for simulation conditioning (Tahmasebi, 2018), which is virtually absent for dikes.

Thus, any proposed method for simulating dike heterogeneity should be capable of simulating the internal structure and composition of dikes and overcoming the lack of ground truth data by using general knowledge of dike buildup. In addition, the method should be able to incorporate ground truth data into the simulation, if any is present. These prerequisites require a combination of object-based and process-based techniques, as the process of iterative dike reinforcements can be understood from the general history of river dikes and object-based methods can most easily incorporate information on structural geometry.

In this work, we present a model to simulate multiple, equally probable versions of a dike's internal stratigraphy. The model uses general information to simulate layer geometry and lithology and can be conditioned on ground truth data where available. The goal of this study is to analyze the performance of this novel method for simulating non-natural discrete lithological sequences in dikes, which would improve pore pressure estimations and dike stability calculations when compared to methods using average properties with statistical uncertainties. We also apply the method to existing dikes to evaluate the effect of dike interior heterogeneity on groundwater flow under elevated river levels, as a key condition for dike failure. This application highlights the added value of a probabilistic representation of dike buildup in the current practice of dike safety assessments.

4.2 Methods

4.2.1 General methods

We developed DETRIS (Dike Erection Tessellation using Regionally Inherited Statistics) to simulate dike buildup, which uses general information on layer geometry and lithology from archaeological excavations of dike cross-sections (Figure 4.2). The performance of DETRIS is analyzed by its ability to simulate realistic dike buildups in terms of layer geometry and lithology types. The applicability of DETRIS for dike safety assessment is analyzed by coupling the algorithm to a groundwater flow model and dike safety and comparing these results to an expert assessment of dike slope stability.

4.2.2 Dike construction using DETRIS

Process-based dike construction based on historical assumption

Methods of dike construction in the Netherlands differed substantially throughout history, leading to different heterogeneity patterns of dike buildup. In addition, the inner (landward) and outer (riverward) sides of the dike are known to be constructed of different material: the outside needs to be resistant to wave erosion and therefore often mostly consist of clayey material, whereas the inner side is often a low sloping berm of more sandy material.

For this study, we distinguish four time periods with distinct construction methods (see Introduction) and sufficient sample points to derive meaningful characteristics.

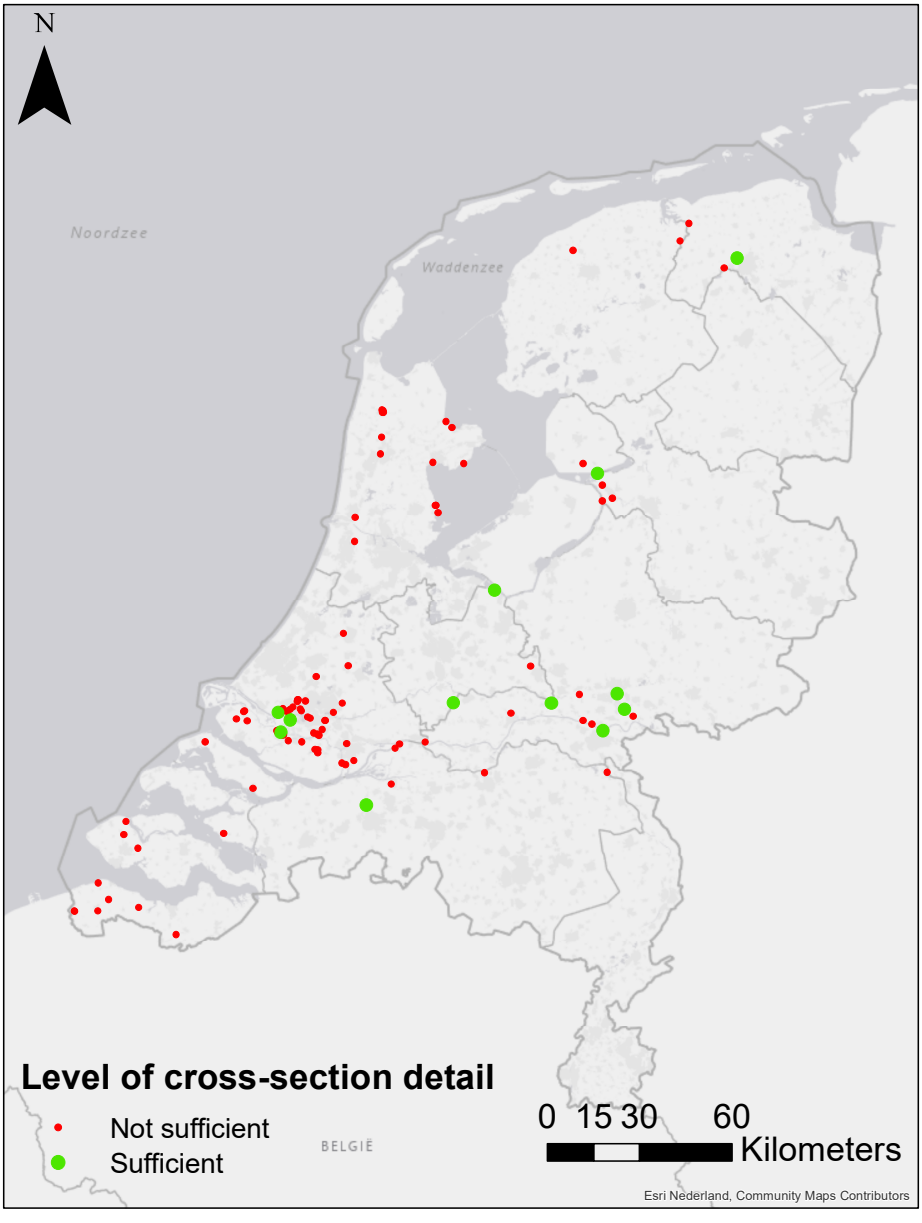

Figure 4.2 Location and level of detail of archaeological sources of dikes in the Netherlands. Those with sufficient quality are listed in Appendix A.1

A first period until the closure of the river dike network (1500 CE), a second period until the emergence of large-scale dike reinforcements (1800 CE), a third period covers further institutionalizations and the start large scale reinforcement projects and a fourth and final phase comprises modern reinforcement techniques starting from 1950. This last phase is often not present in the sampled dikes as it was of smaller interest from an archaeological point of view. We distinguish three geometrical zones along the dike: its outer (river-facing) side, its crest, and the inner side. The dike crest encompasses the top of the dike at those sample points where slopes are below 1:6 (vertical over horizontal distance). Sample locations with an absolute slope value ¿ 1:6 belong either to the outer or inner side. Creating geometrical zones based solely on slope is found sufficient, although some errors arose in the automatic classification. However, it has the advantage of rapid pre-processing of new data in case additional cross-sections become available. By intersecting the temporal and geometrical zones, a total of nine (3 periods x 3 dike zones) combinations is created (Figure 4.3C), each with distinct characteristics.

Deriving general information of dike characteristics

General statistics of dike buildup characteristics are derived from historical cross-sections of dikes, which are digitized from multiple archaeological reports (Appendix A.1, Figure 4.2). These cross-sections contain both high resolution layer geometry, detailed material description and dated ages of some layers. At a 10-cm spacing, sample points are created, at which the intersecting layer is selected (Figure 4.3). First, the layer material type at that location is determined. Second, the layer thickness (H) is sampled by calculating the length of the shortest line through the sample point connecting both sides of the layer. Third, the layer slope (α) is calculated as the perpendicular angle of that line with the horizontal. All sampled points are grouped in the corresponding combination of period and geometry (Figure 4.3C). For each combination, the statistics of layer material type are summarized into histograms and the statistics of layer thickness and layer slope are re-sampled to a continuous probability density functions using a kernel density estimate (Scott, 2015).

The statistics of layer material type, layer thickness and layer slope are derived per cross-section, and thus provide local information on dike buildup. Furthermore, regional statistics are derived by aggregating the statistics of all separate dikes. These regional statistics can be used to inform the model even at locations without local statistics on dike buildup.

DETRIS algorithm

We incorporated the general statistics of dike buildup characteristics per dike construction phase in DETRIS to hierarchically reconstruct the buildup of dikes in an object-based fashion. DETRIS starts with selecting either all local or regional statistics for slope, thickness, and material type. The local statistics are selected if they are available for that dike or a dike in the direct vicinity. Then, a simulation space is created (Figure 4.4) from the oldest known construction time period. If no information on construction periods is present, the current dike surface is used. Subsequently, the

statistics corresponding to that time period are selected. An initial dike is created and placed centered at the bottom of the simulation space.

DETRIS iteratively adds a new reinforcement layer on top of the already present dike until the simulation space is entirely filled. In this iteration, first the next reinforcement location (crest, inner, or outer) is selected on the principle of spatial accommodation, i.e., the larger the available space between the pre-simulated dike and the final known dike surface, the larger the chance that the next reinforcement stage will be on that location. Then, a new layer is created by sampling a thickness, slope, and material type from the statistics for the reinforcement location and added, until the outline of a dike construction phase is reached. If this is an intermediate phase, the statistics for slope, height and material type are updated to meet those of the next construction phase. If the final outline of the dike is completely filled, the process is completed. In this way, DETRIS simulates one possible realization of dike buildup. By creating multiple samples from the same probability density functions, DETRIS can generate many realizations of dike buildup, which are all equally probable.

Conditioning to ground truth data

If local point observations (e.g., cores, interpreted cone penetration tests) of the dike are available, each newly added layer that intersects with this ground truth data is assigned the observed thickness and material type (Figure 4.4). In case the thickness of the simulated layer is smaller than that of the ground truth data layer, the original thickness is kept, otherwise the thickness is reduced to that of the lowest intersecting ground truth data layer. If a simulated layer intersects with multiple ground truth data points, it must comply with all.

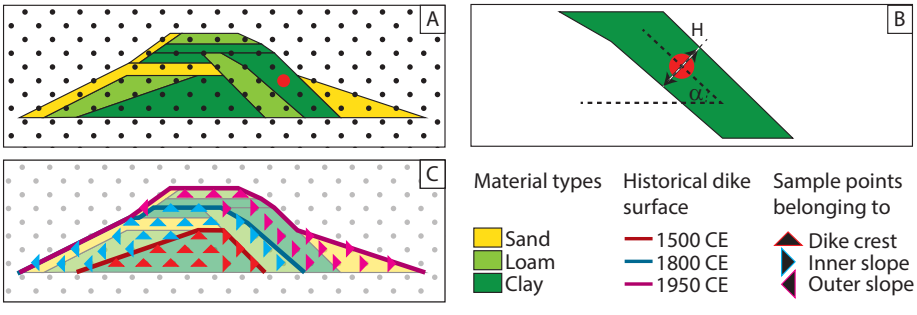

Figure 4.3 Derivation of dike statistics from archaeological dike cross-sections. First, a grid of sample points is created (A) at which the layer material type, layer thickness (H) and layer slope (α) are selected (B). These statistics are grouped given their age and location in the dike. For example, one group consists of points that were constructed as dike crest (upward triangle) between 1500-1800 CE (blue), as denoted by the combined symbol (blue upward triangle) in C. Here, the outer slope refers to the side of the dike next to the river, the inner slope is that on the side of the protected area (polder).

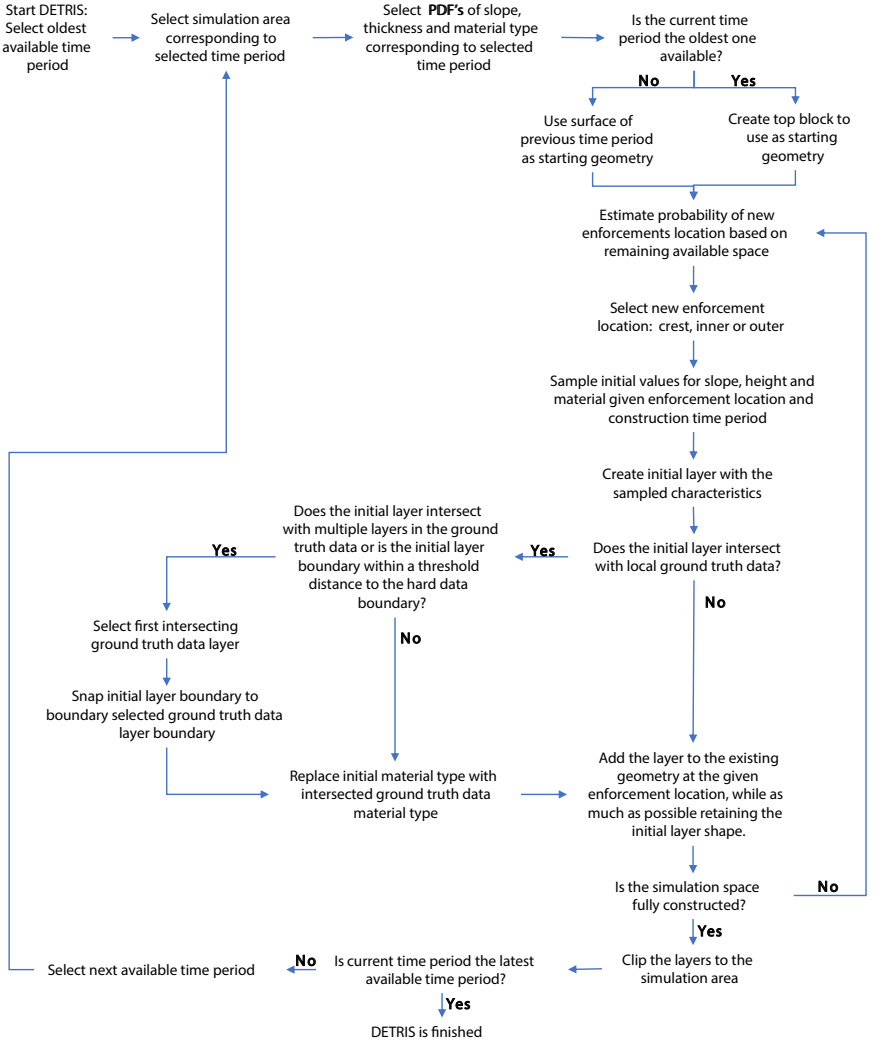

Figure 4.4 Workflow of DETRIS model, including the creation of a simulation space, parameter sampling and ground truth data conditioning.

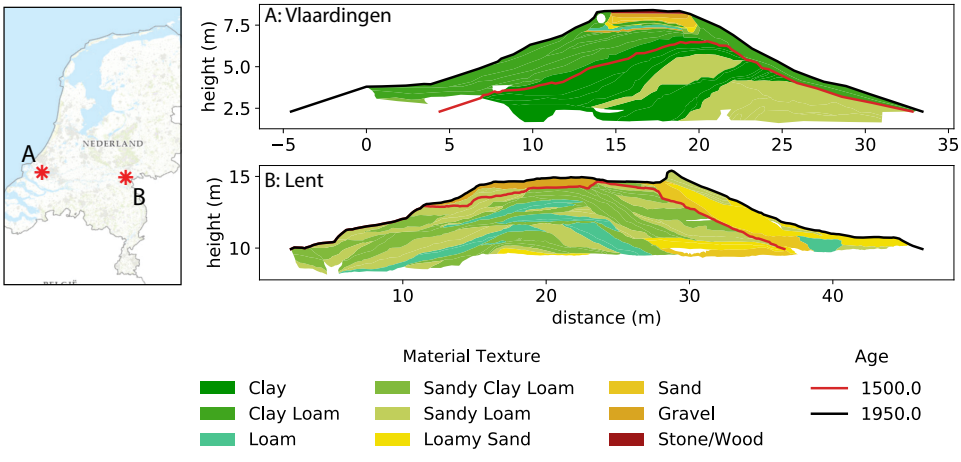

Figure 4.5 Overview of locations and cross-sections of the two known historical dikes used to measure the performance of the DETRIS algorithm. The age lines correspond to the location of the dike surface at that time (years CE). The presented heights are relative to the Dutch ordnance datum. Material types according to USDA classification system (Soil Science Division Staff, 2017).

4.2.3 Cross-section descriptions

Two cases are selected to analyze the performance of the DETRIS algorithm, and one case is selected to explore the added value in dike slope stability assessments.

Cross-sections for analysis of DETRIS performance

To analyze the material and shape heterogeneity and uncertainty related to DETRIS, two known cross-sections from the database (Appendix A.1) are selected: Vlaardingen (Maassluissedijk) and Lent (Bemmelsedijk). These are amongst the most complete historical cross-sections available and are located respectively in the more distal and proximal parts of the Rhine delta (Figure 4.5). The Vlaardingen dike is therefore mostly constructed of clay material, while the Lent dike has a strong variation of clays, sands, and silts. Furthermore, the Lent dike was almost entirely constructed before 1500 CE, while the Vlaardingen dike was raised and widened considerably after that time.

Cross-section for DETRIS application

The application of DETRIS in relation to the assessment of groundwater conditions and dike slope stability is shown for the northern Lek dike east of the village Nieuwegein (Figure 4.6A-B). A survey resulted in a complete lithological characterization of the natural subsurface (Figure 4.6C) and some point observations (ground truth data) on the dike interior from a cone penetration test (CPT, Figure 4.6D).

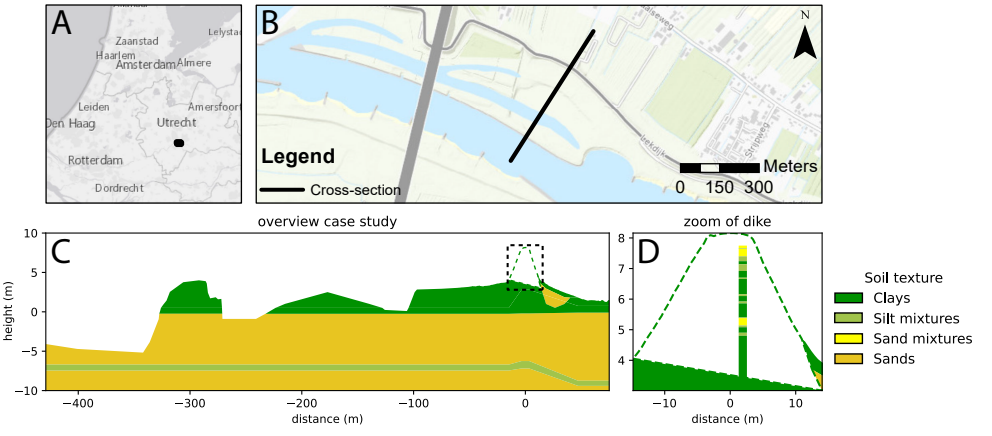

Figure 4.6 Overview of case study location and cross-section. The maps on the top row show the case location within the Netherlands (A) and a more detailed overview of the cross-section (B). The bottom row (C) shows the cross-section at that location, given the surface elevation and subsurface properties (Table 4.1). A zoom of the dike (D) is presented that focuses on the outline of the dike and the classified cone penetration test (CPT), which is used as ground truth data by the DETRIS algorithm. The presented heights are relative to the Dutch ordnance datum.

4.2.4 Performance of DETRIS

The performance of DETRIS is analyzed for the Vlaardingen and Lent dikes (Figure 4.5). The performance is assessed in terms of the ability of DETRIS to create similar patterns of heterogeneity as found in historical dikes, and the ability of DETRIS to simulate the correct material texture given variable quantities of available ground truth data.

In the assessments, local statistics of slope, layer thickness and material types, i.e., from the corresponding cross-section, and regional statistics, i.e., the aggregated over all cross-sections in the database, were evaluated. For each dike and selected set of statistics DETRIS created 100 hypothetical dike realizations using the dated outlines of the cross-sections for the construction phases.

Heterogeneity measures

The performance of DETRIS related to material and layer shape heterogeneity is analyzed on four simple quantitative heterogeneity metrics: fractal dimension D (O'Neill et al., 1988), relative contagion RC (Li and Reynolds, 1993), relative evenness RE and relative patchiness RP (Romme, 1982). They are frequently used in landscape characterization (Li and Reynolds, 1993) and represent different components of spatial heterogeneity. Fractal dimension (D) measures shape irregularity and is calculated using

$$A_k = P_k^{\frac{2}{D}} \tag{4.1}$$

where A_k and P_k are the area and perimeter of layer k. D is derived from a linear regression between the natural logarithms of A_k and P_k over all patches. Higher values indicate an increase in patch shape irregularity. The relative contagion (RC) measures patch continuity and spatial arrangement and is expressed as

$$RC = 1 + \frac{1}{2ln(n)} \sum_{i=1}^{n} \sum_{j=1}^{n} P_{ij} * ln(P_{ji}) \tag{4.2}$$

where n is the number of different lithologies present and P_{ij} is the probability that two adjacent pixels consist of lithology i and j. Higher values indicate a larger clustering of same-type patches or a larger patch size. The relative evenness (RE) specifies the proportions of each lithology type and is expressed as

$$RE = -\frac{1}{ln(n)} ln(\sum_{i=1}^{n} P_i^2) \tag{4.3}$$

where P_i is the probability of a random pixel being of type i. Higher values indicate a more uniform patch type distribution. The relative patchiness (RP) is a measure of the difference between adjacent layers and is expressed as

$$RP = \sum_{i=1}^{n} \sum_{i=1}^{n} E_{ij} \frac{\mid T_i - T_j \mid}{N} \tag{4.4}$$

where E_{ij} is the number of transitions from type i to type j, T is a unit chosen to indicate the dissimilarity for patch types i and j and N is the total number of transitions. The dissimilarity value T equals $log_{10}(K_{sat})$ corresponding to the material lithology (Table 4.1), as it is assumed representative of material type differences. Higher values indicate more and larger transitions between patches. These four metrics are compared between the simulated and observed cross-sections, and a combined performance is measured by the normalized root mean squared error ($NRMSE$) by

$$NRMSE = \frac{1}{N} \sum_{n=1}^{N} \frac{RMSE_n}{\bar{y}_n} \tag{4.5}$$

with N as the number of heterogeneity measures (four, as described above), $\bar{y}_n$ the average simulated value of a specific heterogeneity measure and $RMSE_n$ is the root mean squared error of that heterogeneity measure, calculated as

$$RMSE_n = \sqrt{\frac{1}{T} \sum_{t=1}^{T} (\hat{y}_n \ - \ y_{t,n})^2} \tag{4.6}$$

with T the total number of model runs, $\hat{y}_n$ the observed value for the heterogeneity measure and $y_{t,n}$ the simulated value for the heterogeneity measure.

Uncertainty quantification

The balanced accuracy (BA) is used to quantify the uncertainty of the DETRIS model. It can be used to address spatial differences (i.e., within the simulated dike) in accuracy, but also to address differences between multiple runs with different forcing. If each class is equally well predicted, or if there only is a single true value, this term is equal to normal accuracy. Otherwise, the value decreases as each sample is weighted according to its inverse prevalence. It is written as

$$BA = \frac{1}{2}\left(\frac{TP}{TP + FN} + \frac{TN}{TN + FP}\right) \tag{4.7}$$

in which TP equals the count of true positives, FN equals the count of false negatives, etc.

4.2.5 Application of DETRIS for dike stability assessment

The application of DETRIS is evaluated on a cross-section for which a dike slope stability assessment is performed, including estimates of groundwater conditions. As described in Section 2.3.2, this case study is located at Nieuwegein (Figure 4.6) and contains ground truth data (a CPT) to which DETRIS will be conditioned.

CPT classification

The CPT is classified into five lithological classes based on (Been and Jefferies, 1993): Sands, Sand mixtures, Silt mixtures, Clays and Organic soils (Table 4.1). These material types are used to simulate the dike buildup using DETRIS, and the originally used material type histogram (Figure 4.8) is reclassified to these units.

Basis of expert scenarios of groundwater conditions and dike slope stability

The available expert dike slope stability assessment is performed with the Dutch guidelines (Rijkswaterstaat, 2021) for dike slope stability assessment. These guidelines of this standard (TAW, 2004) specify two scenarios for the phreatic groundwater table in the dike and one for the pressure head in the underlying sandy aquifer.

The expert groundwater scenarios are imported in slope stability software D-Stability (Deltares, 2019). The Uplift-Van limit equilibrium method is used for slope stability calculations, which assumes a dual circular slip plane. The slip plane consists of an active circle, a passive circle and a compression bar in between (Van, 2001)). The slip plane has to start in the crest or the upper half of the landside slope. A C-Phi model for calculating shear stresses is used, and each layer in the DETRIS simulations is assigned a characteristic value of cohesion (c'), friction angle (ϕ), material weight (γ) and saturated material weight (γ_{sat}) given its simulated material type. The expert scenario dike is assumed homogeneous and is assigned a single value for each of the parameters (Table 4.1).

Calculating groundwater conditions and dike slope stability from DETRIS

The selected Nieuwegein cross-section (Figure 4.6) has no archaeological observations in its vicinity (Figure 4.2), so the DETRIS realizations are based on the regional

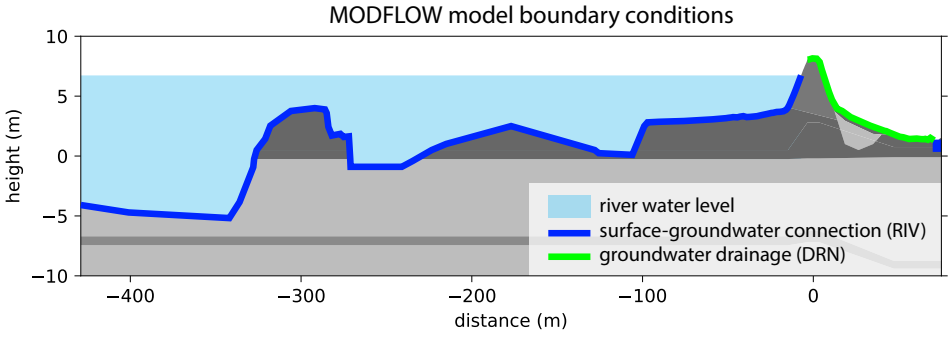

Figure 4.7 MODFLOW cross-section and boundary condition types. Boundaries without specified boundary conditions are no-flow boundaries. The different shades of grey are based on the lithology, which is more explicitly visualized in Figure 4.6C.

statistics. The classified CPT serves as ground truth data. DETRIS generates an ensemble of 100 possible dike realizations. For each realization steady-state pressure heads are calculated, and a dike slope stability calculation is performed on the DETRIS simulation and the resulting pore pressure heads.

The steady-state hydrological simulations of the entire cross-section are performed using the MODFLOW 6 software (Langevin et al., 2019). The 2D hydrological model is set up using a cell size of 0.2 m both vertically and horizontally and includes the dike and the subsurface (Figure 4.6C). At the left end the river has a connection with the lower aquifer. Here the imposed river stage constitutes a head-controlled boundary condition (Figure 4.3) handled by the MODFLOW river package(Hughes et al., 2017). On the inner side of the dike head-controlled conditions (Figure 4.7) are handled by the MODFLOW drain package that creates seepage points that permit outflow only (Hughes et al., 2017). A drainage ditch with a constant head 0.5 m below the surface is located on the landward boundary. The subsurface material types and simulated dike material types are assigned a saturated conductivity (K_{sat}) based on characteristic values (Table 4.1). In the steady-state simulation, the river is at a high stage, with a head of 6.73 m with respect to ordnance datum (recurrence interval of 1:30,000 years, the safety standard for this dike stretch).

The dike slope stability calculations are again performed in D-Stability software (Deltares, 2019). The DETRIS realization replaces the expert schematization of the dike material, while the natural subsurface is kept the same (Figure 4.6). Each layer in the DETRIS realization is assigned the C-Phi parameter values corresponding to its material type (Table 4.1). In addition, the resulting pressure heads from the steady-state MODFLOW model are inserted in the D-Stability software. From the DETRIS realization and corresponding pressure heads, the inner (landward) slope stability is expressed by the safety factor F (see Appendix A.2 for example calculation).

Table 4.1 Subsurface types used for case-study and corresponding hydrological and geotechnical parameters. Values of saturated conductivity are derived from (Pachepsky and Park, 2015) and geotechnical parameters are based on EC7 (CEN, 2004).

Material type	K_{sat} (md^{-1})	c' (kPa)	ϕ (^{o})	γ (kNm^{-3})	γ_{sat} (kNm^{-3})
Sands	5.75	0.0	32.5	18.0	20.0
Sand mixtures	0.26	0.0	30.0	18.5	20.5
Silt mixtures	0.05	1.0	30.0	20.0	20.0
Clays	0.01	5.0	17.5	17.0	17.0
Organic soils	0.10	3.75	15.0	12.5	12.5
Expert scenario dike material		0.0	30.0	18.9	18.9

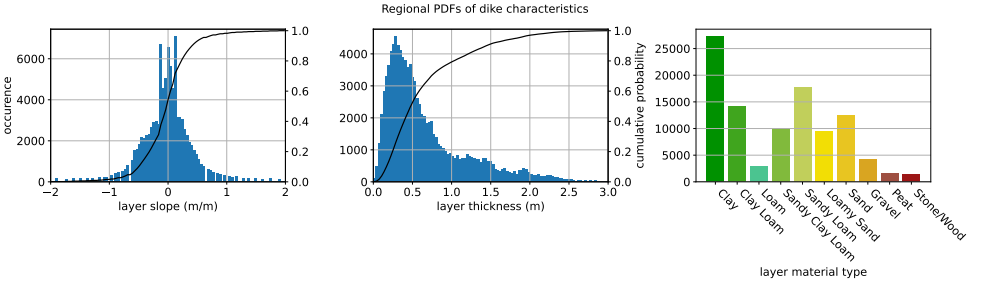

Figure 4.8 Histograms of regional dike properties from all high-detail cross-sections (Figure 4.2, Appendix A.1). The sampled properties are layer slope, layer thickness and layer material type. Negative layer slopes indicate inner side slopes and positive layer slopes indicate outer side slopes. Material types according to USDA classification system (Soil Science Division Staff, 2017).

4.3 Results

4.3.1 General characteristics of archaeological dike cross-sections

Out of the 66 digitized cross-sections, twelve cross-sections had sufficient detail to derive general statistics of dike buildup characteristics in the form of probability density functions for layer slope, layer thickness and layer material type. The layer slope is centered around a slope of zero, with negative values representing inner side slopes and positive values representing outer side slopes (Figure 4.8). The median layer slope is exactly zero, indicating inner and outer slopes are generally equally steep. The absolute median layer slope equals 0.21, roughly being equal to a vertical to horizontal ratio of 1 to 5. The median layer thickness is 0.50 meter, with 5 and 95 percentiles at 0.13 and 1.94 m. In our digitized cross-sections most dike layers consist of clay and loam (71%), with the largest remainder consisting of sand or gravel (26%). However, peat, wood and stone are also found in the historical dikes (3%).

4.3.2 Visual DETRIS example

To illustrate how DETRIS simulates construction history by consecutively selecting new reinforcement layers, the dated construction of the real Lent dike (Figure 4.9) is presented next to an arbitrary DETRIS realization of the same dike. The total construction period is divided into two phases: a first phase with construction and reinforcements made up to 1500 CE and a second phase with reinforcements made after 1500 CE. As outlined, these construction phases are linked to the different statistics to parameterize DETRIS, resulting in two separate simulation spaces that can be traced across the realizations.

The early reinforcements particularly consist of clayey to silty material in both the real dike and the DETRIS dike. The real dike equally extends the reinforcements to either side of the dike center, confirming our DETRIS assumption that the position of any next reinforcement is based on the principle of spatial accommodation, i.e., that there is no clear preference for one side. For the second (youngest) selected temporal period, both the DETRIS dike and the real dike have a larger occurrence of sand and gravel reinforcement layers. The DETRIS realization visually seems to mimic the construction history and resulting heterogeneity of the real dike relatively well, but a statistical analysis is needed to demonstrate this similarity on a larger set of realizations.

4.3.3 Performance of DETRIS algorithm

The performance of DETRIS in probabilistic terms is assessed on two known cross-sections (Lent and Vlaardingen, Figure 4.5), using statistics from both local and regional statistics. The performance is based on two indicators: The ability of DETRIS to create similar patterns of heterogeneity as found in historical dikes, and the ability of DETRIS to simulate the correct material texture given variable quantities of available ground truth data.

Performance of simulating dike heterogeneity

Four simple quantitative heterogeneity metrics (section 2.4.1), being fractal dimension (D), relative contagion (RC), relative evenness (RE) and relative patchiness (RP), are compared between 100 DETRIS realizations and the two known dike cross-section. The average normalized root mean squared error ($NRMSE$) of all heterogeneity indices between all the realizations and the real values are seen as a general indication of model performance (Figure 4.10).

The $NRMSE$ using local and regional statistics for dike buildup characteristics respectively are 0.18 and 0.21 for the Lent case and 0.20 and 0.23 for the Vlaardingen case. This indicates that a dike can be more precisely reconstructed by DETRIS if the local statistics of that dike are known. For both Lent and Vlaardingen cases, DETRIS performs best in the fractal dimension (D) measure, indicating that the simulated layer shapes match well with the layer shapes in the real dikes. For the tested cases, the RP of the local statistics generally tends to be low and of the regional statistics high, indicating that layer transitions given the regional statistics tend to be associated with shifts in material properties that are more abrupt than observed in

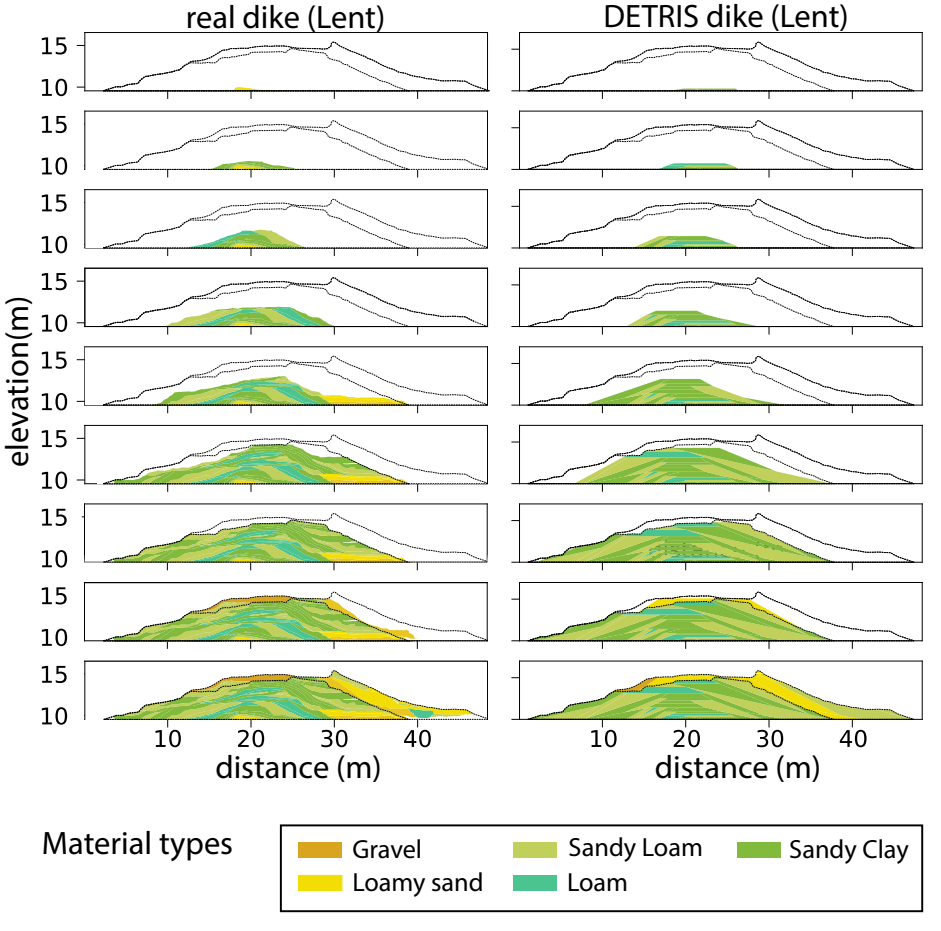

Figure 4.9 Historical evolution of a real dike (Lent) based on the archaeological excavation, and a realization of dike construction history by the DETRIS algorithm using the local statistics from the observed dike. The total construction period is approximately from 1200 CE to 1950 CE. The construction history is divided into two phases, separated by the dotted line, representing the historical dike surface at approximately 1500 CE and at 1950 CE.

reality. In line with this, the Vlaardingen *RE* is often too high, which might suggest that DETRIS is less suitable for simulating more homogeneous cross-sections.

Performance of model accuracy and effect of ground truth data conditioning

The DETRIS algorithm can also be conditioned on ground truth data, often available as vertical cores. These cores are often placed at the outer toe, at the dike crest or at the inner toe of the dike. Three scenarios are compared here: a scenario without ground truth data (Figure 4.11A, D), one location of ground truth data (Figure

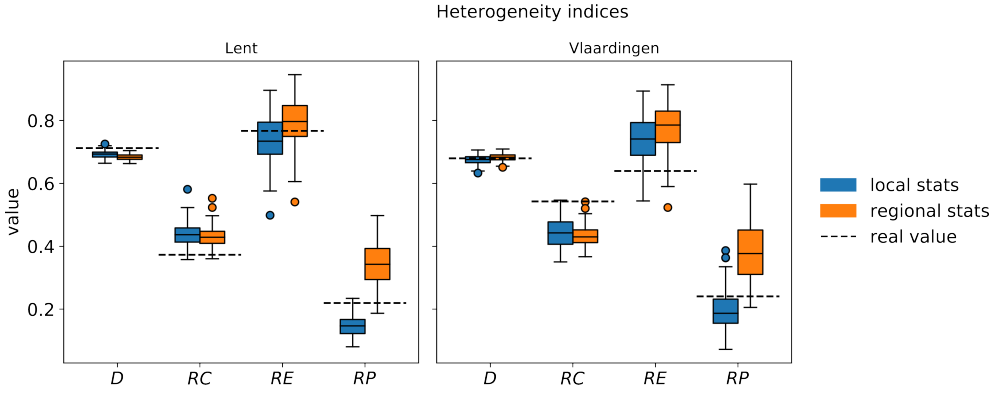

Figure 4.10 Comparison of heterogeneity indices of DETRIS algorithm based on local and regional statistics of dike buildup characteristics and the heterogeneity indices of the actual dikes: Fractal dimension (D), relative contagion (RC), relative evenness (RE) and relative patchiness (RP).

4.11, E) and three locations of ground truth data (Figure 4.11C, F) for DETRIS conditioning. For each scenario, 100 DETRIS realizations are performed using local and regional statistics for both Lent and Vlaardingen. The spatial balanced accuracy (BA) is only assessed on 100 realizations of Lent with local statistics (Figure 4.11D-F).

Independent of the use of local or regional statistics, the median BA increases when adding ground truth data, while the interquartile range of BA decreases. The local statistics result in a higher BA than the regional statistics, but this difference decreases when adding one core and almost diminishes when three ground truth data cores are used. There is a large difference in BA between the two presented cases, Lent and Vlaardingen, where the more uniform Vlaardingen case shows the largest relative improvement from no cores to one core, while the more heterogeneous Lent case shows the largest relative improvement from one core to three cores.

The BA increase of the DETRIS model is mostly caused by an increase in the proximity of the available ground truth data (Figure 4.11D-F), with $BA > 0.75$ for on average 1.7 meters on each side of the ground truth data. At locations further away from the ground truth data the BA stays the same or can even decrease compared to the non-informed (no cores) reconstruction.

4.3.4 Implications of DETRIS for groundwater levels and dike stability

The application of DETRIS is shown for a different cross-section (Nieuwegein, Figure 4.6). At this location, the regional statistics are used as no local information is available except a single CPT. For this location, two expert scenarios on groundwater conditions and the corresponding safety factors (F) for dike slope stability are available (see Section 2.5.2).

Based on the 100 dike buildup realizations by DETRIS, the simulated pressure heads in the aquifer beneath the dike are in general agreement with the schematized

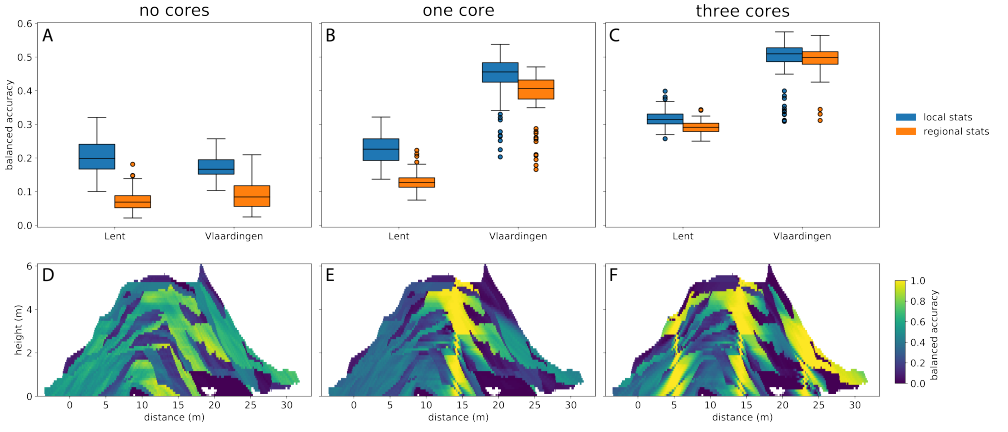

Figure 4.11 Performance of model predictions given one or multiple ground truth data locations for conditioning. The top row (A-C) shows the balanced accuracy (BA) on both cross-sections and local/regional statistics, and the bottom row shows the balanced accuracy (BA) spatially of the Lent dike based on local statistics.

expert scenario (Figure 4.12B). For the realizations, the variation of dike buildup material type results in a high variation of the simulated water tables in the dike. At the outer crest location (width = -3.5) the difference between the 5 and 95 percentile of the simulated phreatic lines equals 1.59 m, while the two expert schematized phreatic lines differ by 0.98 m. Around the CPT location and at the inner toe of the dike, the variability decreases. At the inner crest location (width = 3.5) the difference equals 0.48 m for the simulations and 1.05 m for the schematized phreatic lines, and this decreases even further towards the inner toe, as the dike is drained by the sandy wedge present. At the CPT location, the reduced 5-95 percentile range of groundwater pressure heads emphasizes that the effect of any ground truth data extends beyond decreasing the uncertainty in material texture (as shown in the previous section, Figure 4.11).

The two safety factors F for dike slope stability on the inner (landward, right side) slope are 1.12 with a high phreatic level and 1.53 with a lower phreatic level (Figure 4.12C). Based on the DETRIS realizations, the median dike stability F is 1.41, with a 5 and 95 percentile of 1.35 and 1.51. Thus, the simulated safety factors F are in between the two expert schematizations and have a smaller variation. Overall, the DETRIS-based values are nearer to the safety factor resulting from the schematized groundwater scenario with a lower phreatic level as the draining conditions near the inner crest strongly control the phreatic levels in this case.

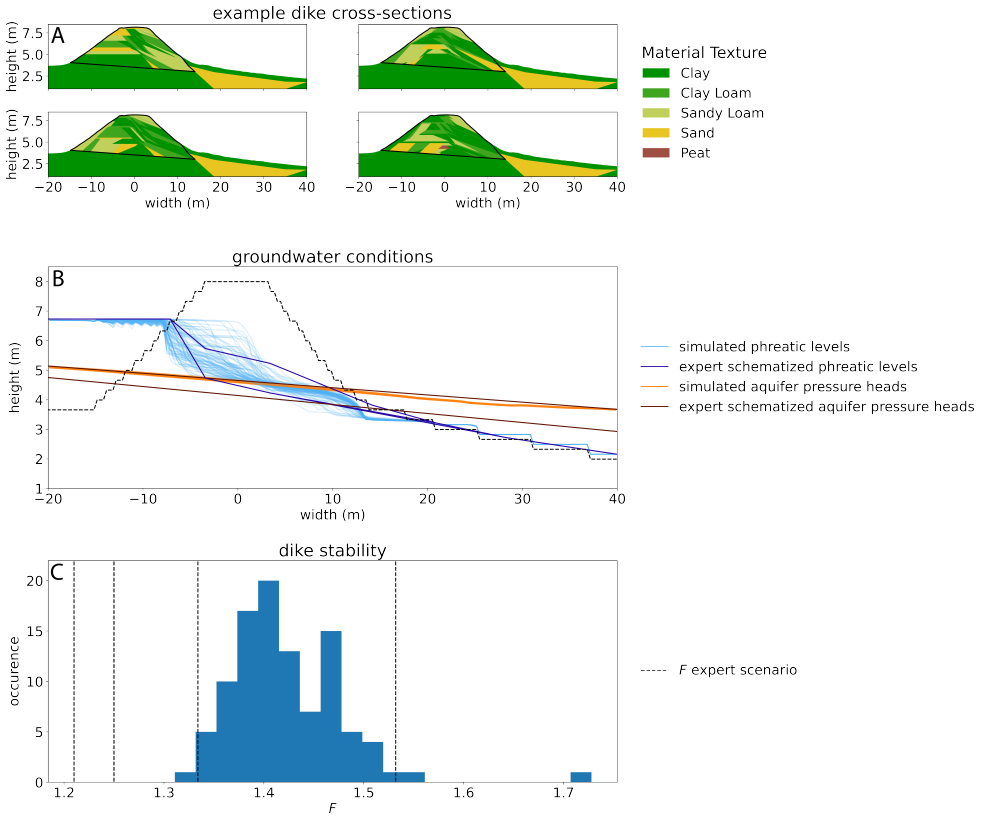

Figure 4.12 Results and implications of using DETRIS for dike stability simulation. The entire cross-section is shown in Figure 4.6. For 100 dike realizations using DETRIS (of which 4 realizations are shown as an example (panel A), the groundwater level (B) and dike stability (C) is calculated and compared against schematized expert scenarios. The simulated phreatic levels (B) (light blue) are mostly in-between the two expert schematized phreatic levels (dark blue). Similarly, the resulting dike stability safety factors (F, panel C) are also mostly in between the safety factors resulting from the two expert schematized phreatic levels (dotted lines).

4.4 Discussion

4.4.1 Relevance of local statistics for dike heterogeneity assessments

To assess the dike safety on a longer dike stretch, information on dike material variation along the dike on a small scale (several meters) is crucial. However, to our knowledge only a few observations exist from which the parameters needed for DETRIS can be derived, and these are often far apart. However, an indication of the

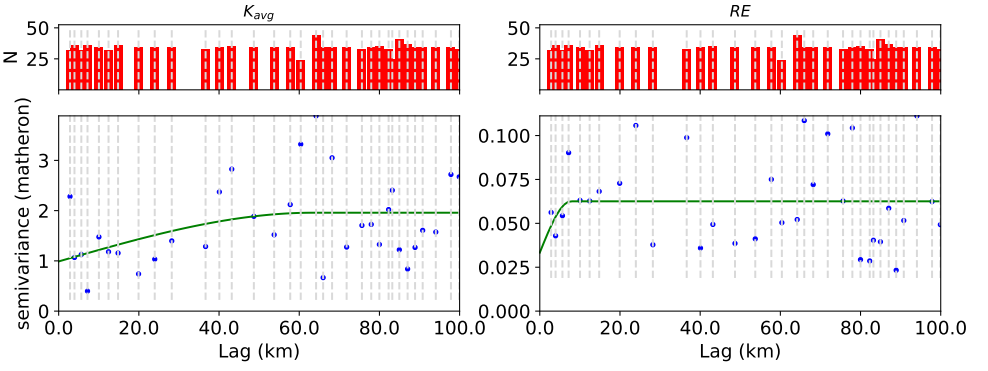

Figure 4.13 Variogram models of two dike properties. Both show a large nugget, indicating local variability at scales smaller than sampled in this research is significant.

spatial correlation of material properties is essential as it indicates how representative the local and regional statistics are that are used to parameterize DETRIS.

The spatial variability of dike buildup is analyzed based on the material types of all 66 cross-sections in the larger database (see Section 3.1), which include both the twelve detailed profiles used for the parametrization of DETRIS as well as other less detailed reports on historical dikes. Two parameters are assessed: the previously discussed RE, as a measure of dike material heterogeneity, and the average saturated conductivity K_{avg} based on Table 4.1, as a measure of average dike properties. The spatial similarity of these metrics between dikes is assessed using variograms (Matheron, 1963). A spherical variogram model is fitted including the nugget effect, with a maximum lag distance of 100 km and a uniform binning strategy.

The K_{avg} has a nugget of 0.989, which is 50.5% of the total sill of 1.958, and an effective range of 63.4 km. The RE has a nugget 0.033, which is 53.3% of the total sill of 0.063, and an effective range of 7.7 km (Figure 4.13).

The variograms of Figure 4.13 suggest that the use of local dike statistics is only useful within 7.7 km from a known dike cross-section, as at further distances no spatial similarity in dike buildup may be expected. Of the approximately 1850 km of primary river dike in the Netherlands, 17% is located within a radius of 7.7 km from a detailed dike cross-section. As the local statistics from detailed dike cross-sections substantially decrease the uncertainty in dike buildup and groundwater conditions, increasing the number of detailed cross-sections from which local statistics can be derived, would increase the overall accuracy. However, the high nugget-to-sill ratios (∼50%) indicate that even on smaller scales large variations can occur, and that ground truth data, in combination with a successfully applied interpolation or simulation model, is also needed for accurately predicting dike buildup. This was also shown by the balanced accuracy (BA), where for Vlaardingen, local statistics without ground truth data lead to a median balanced accuracy (BA) of 0.17, while regional statistics with three ground truth data cores for conditioning lead to a BA of 0.49 and local statistics with three ground truth data cores lead to a BA of 0.51 (Figure 4.11). Thus, the model

benefits more from adding ground truth data at multiple locations when regional statistics are used, than it benefits from adding a limited number of cross-sections to provide the local parameterization. Also, cross-sections are very destructive and often not allowed in primary dikes. However, we recommend a more intense collaboration with archaeologists to increase the density of high-quality data on dike material buildup to inform dike reconstructions, in particular as the delineation of the reconstruction phases is an open question in our method. Again, replacing it by aggregated statistics for the entire dike buildup and using ground truth data can solve this partly, but the results will deteriorate considerably without ground truth data conditioning.

4.4.2 Dike safety assessment improvements by DETRIS

DETRIS can provide more realistic heterogeneous dikes than those currently in use, as it does not assume uniform material characteristics in the entire dike. Its fast and effective algorithm can provide multiple realizations of dike buildup, based solely on input statistics of material and layer characteristics, and optionally incorporate ground truth data. As such, it produces a data-based approximation of the uncertainty in dike failure risk as a function of dike heterogeneity and groundwater conditions. This probabilistic approach results in a better informed assessment of dike slope stability. In addition, it can easily incorporate (more) local statistics, ground truth data, or knowledge on dike construction history in an objective manner, contrary to human-controlled expert schematizations. In this case, the probabilistic assessment resulted in a smaller uncertainty when compared to expert judgement (Figure 4.12). While this may vary from case to case, it reflects the strength of DETRIS in evaluating the effect of the buildup and the uncertainty therein on the stability of dikes in a mechanistic manner.

4.4.3 Suggestions for model improvements

DETRIS is currently capable of simulating realistic dike buildup on 2D cross-sections, but the algorithm is prone to simulate too large differences in composition between adjacent layers. In the observed cross-sections similar layers were often more clustered. Like conditioning on point data, adding conditional probabilities to represent interlayer dependencies can result in more realistic dike buildup realizations. The use of recent developments in continuous geophysical data interpretation, such as electrical resistivity tomography (Chavez Olalla et al., 2021) or ground penetrating radar (Di Prinzio et al., 2010) are promising to increase the availability of ground truth data too. In addition, coupling our object-based model to other geostatistical methods, such as multiple-point geostatistics (Tahmasebi, 2018) can provide more detailed indications of material uncertainty across but also along the dike. Such a coupling has already been successfully applied to simulate natural deposits (Michael et al., 2010).

4.4.4 Outlook and suggestions for further research

The explicit characterization of the legacy of dike construction on the material composition as implemented in the DETRIS algorithm can assist in obtaining better

informed safety calculations and improve our understanding of the governing processes on different temporal scales. An example of a short-term process as presented in this paper is the location of the phreatic line during high river water levels and the dike slope stability. Other stability related features, such as the presence of an erosion resistant core or small sand lenses in the dike can be better assessed using DETRIS as well. They are important as a source of residual strength after dike slope failure and for having a major influence on the intrusion length of pore pressures.

In terms of long-term processes such as soil formation and weathering, DETRIS can link the composition of a particular layer and its properties to material and age. In addition, compaction of the layers can change the dike buildup geometry and material properties. This, eventually, may alter the behavior of the dike during prolonged periods of droughts due to irreversible shrinkage of clay and peat and the formation of fissures, which could affect its ability to withstand high water levels that follow, thus introducing hysteresis.

4.5 Conclusion

In this work, we developed the Dike Erection Tessellation using Regionally Inherited Statistics (DETRIS) model to simulate dike buildup based on historical dike cross-sections. By applying this model, a new valuable source of information is added to improve estimates of dike material and its heterogeneity, and provide uncertainty estimates of flood safety of the corresponding dikes.

- The implementation of a process-based model (DETRIS) enables a probabilistic assessment of dike interior buildup based on observed characteristics of historic dikes, which goes beyond the current assumption of homogenous dikes.
- Dikes have a high internal heterogeneity which is captured by the model. Local information improves the predicting capacity of dike buildup, but regional statistics, nonetheless lead to representative dikes.
- Dike cross-sections only have a predictive capacity within several kilometers, and considerable variation is observed even on smaller scales. Conditioning to ground truth data cores or CTPs provides a good alternative at locations outside this range.
- Using DETRIS-based scenarios of dike buildup to simulate groundwater levels and dike stability provides a more comprehensive way of incorporating heterogeneity than arbitrary expert-based estimations and narrows down the uncertainty of dike slope stability analyses while incorporating local and adverse effects of more permeable or less competent layers.
- DETRIS is capable of simulating non-natural discrete lithology sequences, and it can be further improved by adding layer inter-dependency or possibly coupling it to a multiple-point geostatistics algorithm.

- We recommend a more intense collaboration with archaeologists and responsible institutions for dike maintenance to increase the density of high-quality data on dike buildup material and ages of dike erection phases than currently present.

Author contributions

T.v.W, R.v.B, M.F.P.B. and H.M. designed the research. T.v.W. and R.v.B. performed the primary data analysis and model development. H.M. and M.F.P.B. helped with result interpretation and all authors contributed to the manuscript.

Acknowledgements

We greatly appreciated the support of Martin van der Meer and Johan Hockx providing data on the case study and ideas on the application of the algorithm. We also greatly thank the late Michel Lascaris for providing references on archaeological dike cross-sections.

5 Effects and Implications of Transient Groundwater Model Simplifications for Dike Slope Stability

Abstract

The evolution of groundwater conditions that potentially cause dike slope instability is a three-dimensional process, thus a coarser subsurface schematization or the use of a 2D groundwater model is likely to provide a less realistic representation than detailed 3D approaches. This paper explores the impact of simplifications in subsurface schematization detail and model dimensions on pressure head estimations for dike slope stability, i.e. by applying these simplifications to a realistic and detailed 3D reference scenario: the Stuivenberg channel belt (Rhine-Meuse delta, the Netherlands). A 3D groundwater model with a hypothetical dike-river system was created for the entire mapping domain, from which a set was created of 373 cross-sectional 2D groundwater models perpendicular to that river. Also, we applied the 3D model to a downgraded version of the subsurface schematization. We found that using 2D groundwater models can result in severe underestimations of pressure heads compared to 3D groundwater models. These occur where river to groundwater infiltration is limited in the 2D model but not in the 3D model as water can bypass less pervious layers in the 3D simulations. For the same reason, large overestimations may occur using a 2D model if groundwater is impounded against impermeable geological units but can be deflected in the 3D model. Using a simplified geological schematization mostly resulted in larger pressure heads at the locations where the schematization changed. Related to dike slope safety assessments the use of the 2D groundwater models leads to an underestimation of groundwater pressure heads and thus are overly optimistic in assessing the failure probability of dikes, with possibly dangerous consequences.

5.1 Introduction

Dikes (i.e. earthen flood defenses) are raised to prevent flooding of many major lowland rivers. These dikes not only need to be higher than the extreme expected river water levels, but also need the structural integrity to withstand water at levels lower than the dike crest, as slope instability during high river water levels is one the major failure mechanisms of dikes (Jonkman et al., 2018). The probability of slope instability depends on the material properties of the dike and of the subsoil, and on the pore water pressure (pressure heads) at these locations. When river water levels increase during a high water event, seepage into the dike and subsoil increases pressure heads, reducing the soil's effective stress and strength and thus increasing the dike slope failure probability ('t Hart et al., 2016). With more extreme river water levels expected in the future worldwide (IPCC, 2022), and already 1500 km of primary flood defenses still to be assessed and possibly reinforced in the Netherlands alone (HWBP, 2022), accurate estimates of groundwater conditions remain crucial for assessing dike failure probabilities.

Both dike stability and groundwater flow are three-dimensional phenomena and thus 3D models for both slope stability and groundwater flow provide a more realistic representation than 2D approaches, especially when dealing with heterogeneous subsurface material (Hicks et al., 2014; Barnett et al., 2012). Despite this, to simulate pressure heads for dike slope stability assessments often 2D groundwater models are used (Meehan and Benjasupattananan, 2012; Lanzafame et al., 2017) as this coincides with the presumed largest gradient, being perpendicular to the river, across the dike, and is in agreement with the plane strain assumption used in limit-equilibrium slope stability models. However, for flow across a dike and its subsurface differences in permeability and storativity imply that flow paths are not constrained to the same 2D plane, thus decreasing the assumed validity of 2D groundwater models (Cheng et al., 2016; Jafari et al., 2016).

To make an accurate assessment of groundwater conditions that potentially cause dike slope instability, a detailed subsurface schematization is necessary. Creating such a schematization involves describing the subsurface architecture: the spatial distribution, occurrence depth and thickness variation of deposits, as well as their properties, such as lithology and hydraulic conductivity. However, the shallow subsurface around lowland rivers in a deltaic setting is very heterogeneous, due to both the temporal evolution of the river system on antecedent stratigraphy (Geleynse et al., 2011) as the interplay between these rivers and coastal processes (Hoitink et al., 2017). In our study area (the Rhine-Meuse delta in the Netherlands) a large part of the delta consists of clay and peat deposits from river floodplains intersected by sandy deposits from their past and present river systems (Berendsen and Stouthamer, 2000; Bierkens, 1996; Winkels et al., 2022). Within the sandy channel belts from these often meandering river systems, units with different lithological characteristics are present, related to the meander dynamics and abandonment of these systems, such as abandoned and residual channels (Toonen et al., 2012; Winkels et al., 2022). The latter are often relatively small (tens of meters) and therefore may be overlooked or ignored in subsurface schematizations for groundwater models.

Thus, the large natural variability of subsurface architecture poses a challenge for simulating accurate groundwater pressure heads around specific dike sections. This challenge is related to the complexity of the natural system, which due to practical reasons cannot always be fully captured in the groundwater simulation. The problem is twofold: First, the 3D groundwater models are often simplified to 2D groundwater models, possibly to constrain calculation time, which might produce inaccurate flow paths and pressure head evolution in the heterogeneous subsurface architecture. Second, the subsurface architecture is often simplified in the model schematizations as the number of subsurface observations is too small to capture the heterogeneous subsurface architecture in sufficient detail. Moreover, these two simplifications often co-occur.

The large natural variability of subsurface architecture poses a challenge for simulating accurate groundwater pressure heads around specific dike sections. Due to the complexity of the natural system, it often cannot be fully captured in terms of the finer detail and the heterogeneity of the material for practical reasons. Hence, the subsurface architecture is often simplified in the model schematizations as the number of subsurface observations is too small to capture the heterogeneous subsurface architecture in sufficient detail. Also, 3D groundwater models are often simplified to 2D groundwater models for computational expediency and to reduce the volume of input and output data. In many cases, these considerations result together in strongly generalized 2D groundwater models.

This paper explores the impact of simplifications in subsurface schematization detail and model dimension on pressure head estimations for dike slope stability in relation to a realistic and detailed 3D reference scenario. Based on the findings, we will suggest good practice choices for groundwater modelling related to the assessment of dike failure probability and infer the consequences when less suitable groundwater schematizations are used. First, we describe an extensive workflow for assessing both the impact of reduced detail in subsurface schematizations and reduced model dimensionality on groundwater conditions in section 5.2. This method includes the calculation of time-dependent pressure heads with the MODFLOW hydrological model. Second, we aim to explain the key factors causing differences in groundwater conditions when the detail in subsurface schematizations and model dimensionality are reduced in section 5.3. Hereafter section 5.5 discusses the effects on dike slope stability and the main implications for groundwater modelling near river dikes.

5.2 Methods

To assess the effect of simplifying subsurface architecture two subsurface schematizations of our study are considered with a different level of detail. The study area contains a geological architecture characteristic for the Rhine-Meuse delta and is mapped in high detail (Winkels et al., 2022). Given a subsurface schematization, 2D and 3D groundwater models are created. The influence of subsurface architecture detail is expected to decrease further away from the river, as groundwater gradients decrease. To capture the maximum influence of the subsurface architecture we created multiple model runs with a hypothetical river channel at different locations. Finally, the

model outcomes of these model runs are combined in composite images to highlight the influence of local subsurface architecture heterogeneity on groundwater conditions within, and between, 2D and 3D groundwater models.

5.2.1 Subsurface scenarios

The 2D and 3D subsurface schematizations for our analyses are based on a geological mapping (Cohen, 2017; Winkels et al., 2022) of the Stuivenberg channel belt (SCB). The SCB is a meandering channel belt in the central Rhine delta that was active between approximately 4300 and 3500 cal. yr BP (Winkels et al., 2022). Its internal architecture and lithology have been mapped in detail and includes an abandoned channel with a residual channel within the channel belt extent. The subsurface scenarios in our workflow contained either both the channel belt and its internal architecture (*complex*) or a simplification in which the internal architectural elements are ignored (*simple*) (Figure 5.1).

The Stuivenberg channel belt sand body has a thickness of approximately 8 m and is at the bottom connected to a different coarse-sandy unit deposited by an older (Pleistocene age) braided river system. The SCB is embedded in thick clayey floodplain deposits, which at the bottom are also connected to these Pleistocene sands. On top of the embedded SCB lay additional floodplain deposits with a thickness of 1 m (Figure 5.1). Within the boundaries of the SCB sands, an abandoned channel and a residual channel are present. The abandoned channel fill is characterised by finer sands and higher silt content that were deposited in the final stage of river activity. It indicates the full channel width just prior to its abandonment, in which the river discharge already decreased (Toonen et al., 2012). The residual channel is the final clayey infilling of the abandoned channel after it is disconnected from the main branch (Toonen et al., 2012).

5.2.2 General workflow to assess model dimension impact

To analyze the effect of model dimension given a subsurface scenario and its local architecture, a hypothetical present-day active river is incised into the geological schematization. This hypothetical river is schematized as a N-S oriented straight line at a given x-coordinate and is bordered by two parallel dikes, each at 100 meter distance from the river bank. The river incision was shaped as an upside-down trapezoid, with a depth of 6 meters, a base width of 100 meters, and a slope towards the riverbank of 1/5. The dikes were modelled as trapezoids too, with a height of 6 meters, a top width of 5 meters, and a slope of 1/3. Furthermore, outside the dikes, the surface elevation is assumed to be the same everywhere (Figure 5.2).

To assess the effect of geological transitions between different lithologies and with different orientations to the river, the dike-river system was step-wise re-positioned on the geological subsurface, by laterally shifting it to a different x-coordinate, with a spacing of 50 meters resulting in a total of 46 locations. For each position of the dike-river system on the subsurface, a 3D groundwater model was created for the entire mapping domain. In addition, an array of 373 W-E oriented 2D groundwater models was created at different y-coordinates, with a spacing of 3 meters (Figure 5.2).

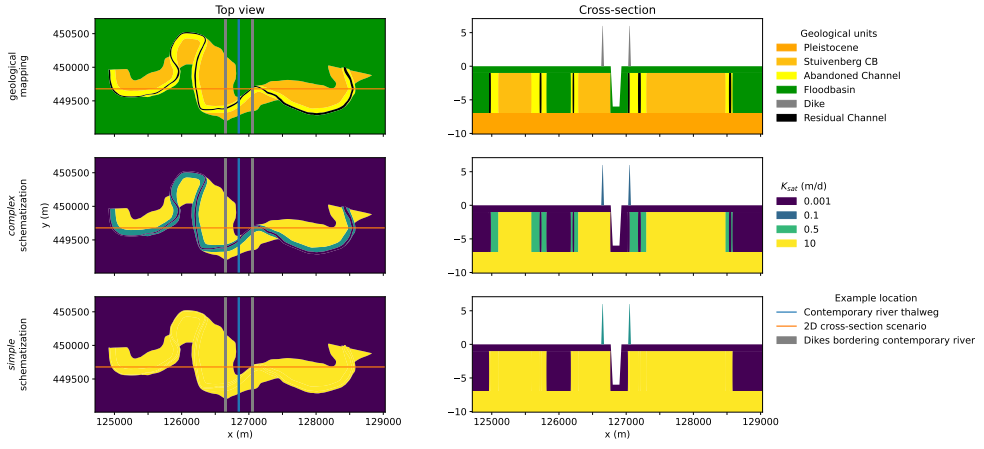

Figure 5.1 Schematized overview of subsurface schematizations. Given the Stuivenberg channel belt mapping (top row) two subsurface scenarios are created: a complete schematization including all geological units (complex, middle row) and a simplified schematization without the abandoned channel and residual channel (simple, bottom row). These schematizations are assigned a saturated conductivity (K_{sat}) based on hypothetical characteristic values. A 2D cross-section scenario is made on an y-coordinate transect (orange line). Note that the top view (left column) is a horizontal slice at a depth of -1 m, above which clayey floodplain deposits are found.

Using this layout, the 3D groundwater simulations can at many locations directly be compared to those resulting from the 2D groundwater models. Thus, in total per subsurface scenario, 46 3D groundwater model runs and 17158 2D groundwater model runs are performed. With this multiplicity of models many different orientations of the channel belt (and residual channel) were present between the river and the dikes on either side of that river. Thus, this approach covers many scenarios of realistic geological architecture that are encountered in the Rhine-Meuse delta.

5.2.3 Hydrological model setup and boundary conditions

The hydrological model setup and its boundary conditions were similar for the two-dimensional calculations and three-dimensional calculations. The groundwater model software MODFLOW 6 (Langevin et al., 2019) was used to simulate the pressure heads in the dike and subsurface. Initial groundwater levels were set to -1 meter, being 1 meter below the floodplain elevation. Changing river water levels were provided by a half sine function that is scaled between a minimum water level of -1 m and a maximum water level of 5 m, which is reached at time T = 15 days. The transient MODFLOW simulation ran on a 1-day timestep and had a total runtime of 30 days. The model grid was created by the GRIDGEN software (Lien et al., 2015) which creates layered quadtree grids. A quadtree grid contains refinements by continuously dividing an existing cell into four smaller cells until the desired level of refinement is reached. We used a maximum cell size of 32 m, a cell size of 4 meter near the

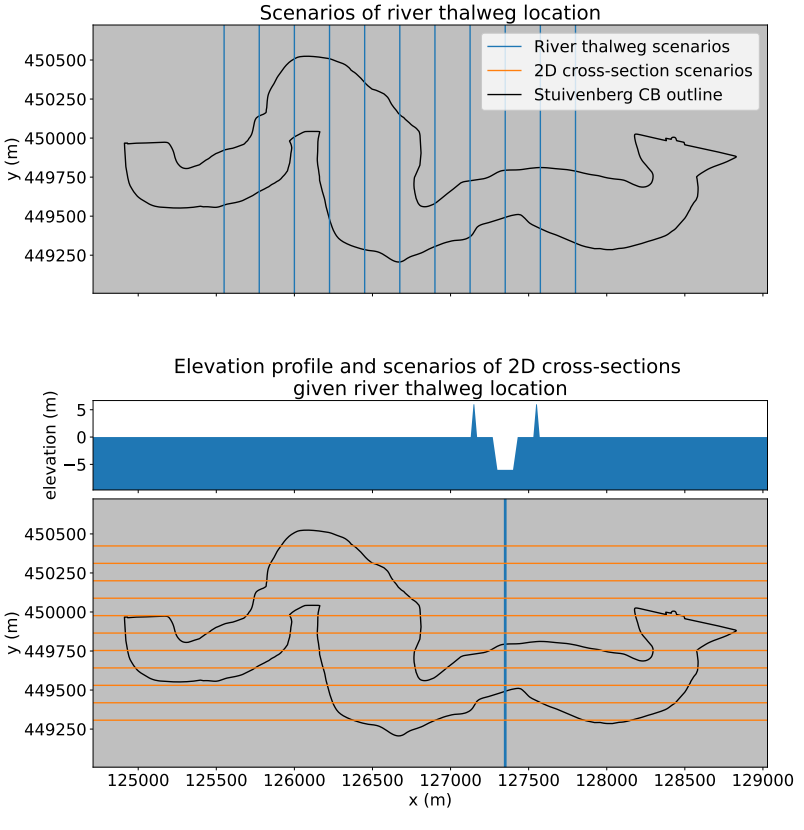

Figure 5.2 Schematized overview of general workflow with scenarios of river thalweg location (at a selected x-coordinate). For a selected river thalweg location, a 3D groundwater model is created and a multiplicity of 2D groundwater models over a cross-section (at a selected y-coordinate). Note that to increase clarity the number of visualized scenarios is less than actually computed.

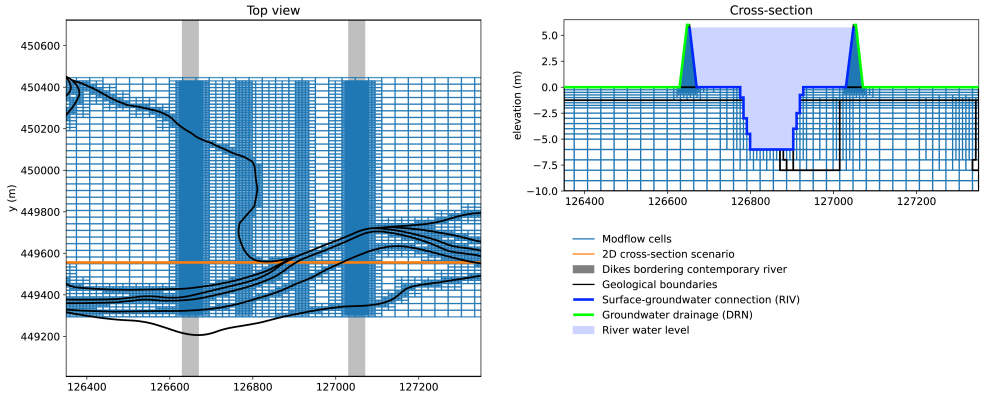

Figure 5.3 GRIDGEN model grid example and exemplary boundary condition schematization on a cross-section. The grid cell sizes are higher near geological boundaries and near the river thalweg.

Table 5.1 Values for hydrological and geo-mechanical parameters given the geological unit. Note that the Abandoned channel and Residual channel are not present in the simple schematization.

Geological Unit	K_{sat} (md^{-1})	ϕ (^{o})	c' (kPa)	γ_{sat} (kNm^{-3})
Dike	0.1	30.0	1.0	20.0
Floodplain	0.001	17.5	5.0	17.0
Channel belt	10	32.5	0.0	20.0
Pleistocene	10	32.5	0.0	20.0
Abandoned channel	0.5	30.0	0.0	20.5
Residual channel	0.001	17.5	5.0	17.0

river and near geological boundaries, and a cell size of 1 meter in the dike (Figure 5.3). The vertical cell size decreases from 1 m resolution at an elevation below -6 m to 0.5 m resolution between elevations of -6 m and -2.5 m and 0.25 m above that. A saturated conductivity (K_{sat}) is assigned to the subsurface material types based on typical values (Table 5.1). In the river channel and where the river water level is above the floodplain, the MODFLOW river package enables river-groundwater interaction (Figure 5.3). On the landward side, the drain package (Hughes et al., 2017) enables outflow only if pressure heads become higher than the surface elevation. For these interactions, the conductance (with unit m^2/day) is calculated according to $K_{sat} * A$ / M, with A as the cell surface area and M as the cell thickness. This package is also used to model a ditch (which permits unhampered outflow at a conductance of 1000 m^2/day) parallel to the river dike 50 meters inland from the inner dike toe.

5.2.4 Post-processing of groundwater conditions

Two types of post-processing are performed on the MODFLOW model output. First, for a single 3D groundwater model run (with a given subsurface scenario and the N-S river at a given x-coordinate) the corresponding set of 2D groundwater model runs (at y-coordinate W-E cross-sections) were combined into a three-dimensional composite of 2D model runs. As the 2D model cell size at the dike is smaller than the 3 m spacing between 2D model runs, not all 3D model nodes have a 2D counterpart. Nonetheless afterwards horizontal and vertical cross-sections were retrieved from the merged-2D and true-3D model outputs for further analyses and comparison. In this manuscript, we particularly evaluated horizontal cross-sections at a depth of 1 m (being at the top of the SCB) of either a single 3D model run or the composite of 2D model runs, and vertical cross-sections consisting of a single 2D model run or a slice of a 3D model run. As dike slope stability partly depends on the pressure heads underneath the dike, the pressure head at a depth of 1 meter beneath the dike is used as a representative and intuitive value for a first order model comparison.

In addition, a second type of composite is created to analyze the spatial influence of the model dimension and the geological schematization on pressure heads related to dike slope stability. In our workflow multiple groundwater simulations were performed with the river (and the bordering dikes) at different x-coordinates. Of all simulations, which is: for all 46 river positions with each one 3D and 373 2D groundwater simulations, the simulated pressure heads at an elevation of -1 m (top of the SCB) underneath the dike were combined into a composite image. This composite image provides an estimation of the maximum influence of subsurface architecture and model dimension on pressure heads for dike stability.

5.2.5 Slope stability model setup

To further assess the impact of simplifications in subsurface schematization detail and model dimension on pressure head estimations for dike slope stability, several slope stability calculations were made as well. These slope stability calculations were performed in the D-Stability software (Deltares, 2019) using a limit-equilibrium method. The hydraulic heads from the MODFLOW groundwater model were used as input for a detailed schematization of the groundwater pressure heads in D-Stability. The inner (landward) slope stability was calculated using the Uplift-Van method (Van, 2001), which accounts for long-shaped slip planes with strength loss due to uplifting of relatively thin clay blanket layers. A particle swarm search algorithm was used to select the most critical slip plane. The geomechanical parameters angle of internal friction (ϕ), cohesion (c') and saturated unit weight (γ_{sat}) (Table 5.1) are deterministic and based on EC7 (CEN, 2004).

5.3 Results

In this section, we will first present the groundwater pressure heads and differences for one model schematization (i.e. one river thalweg x-coordinate location). Subse-

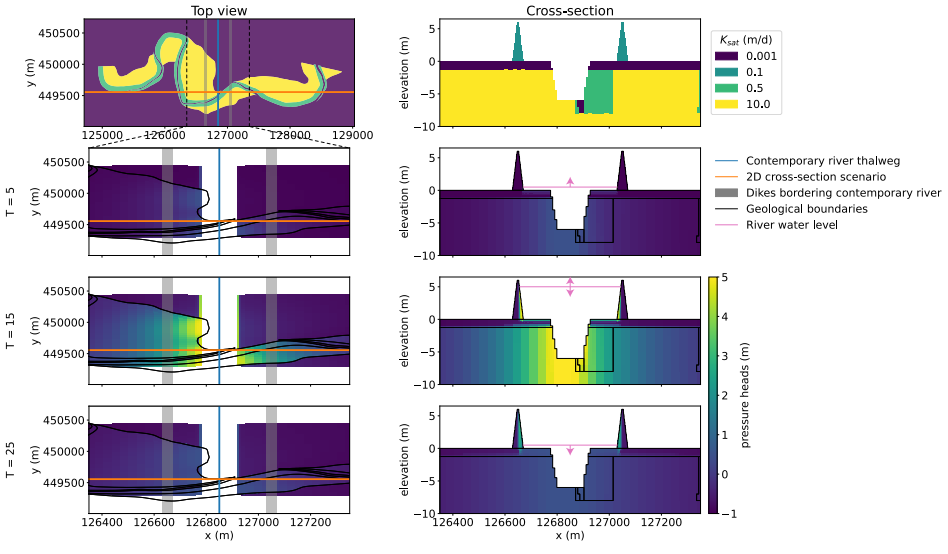

Figure 5.4 Subsurface schematization and pressure head evolution for the *complex 3D* scenario. The top view represents a horizontal cross-section at a depth of -1.0 m, above which an aquitard is located (see cross-section). The pink arrows indicate the direction of water level change at that timestep.

quently, we will present the combined results of all river thalweg locations and relate these to dike slope stability.

5.3.1 Evolution of pressure heads over time

For the most realistic reference scenario (*complex 3D*), consisting of a 3D groundwater model based on the detailed geological model of the channel belt, we first present the pressure head evolution over time (Figure 5.4). In the selected cross-section at T = 5 days, little response is observed in the dike and cover layer, but the pressure head at a depth of 1 meter beneath the dike are -0.28 m and -0.46 m below the left and right dike respectively. At T = 15 days the pressure head beneath the dikes are 2.32 m and 1.63 m and at T = 25 days 0.15 m and 0.04 m for the left and right dike respectively. The difference between the left and right dike is mostly induced by the variation in subsurface permeability and corresponding river to groundwater infiltration rates. In the falling limb of the flood wave, the delay in groundwater response may result in aquifer pressure heads that are larger than the river water levels. The same is true for pressure heads in the dike and cover layer, which due to their low K_{sat} have a smaller but more prolonged response to the river water level than the sandy deposits. In the selected cross-section at T = 25 days, the riverward side of the dikes still retain

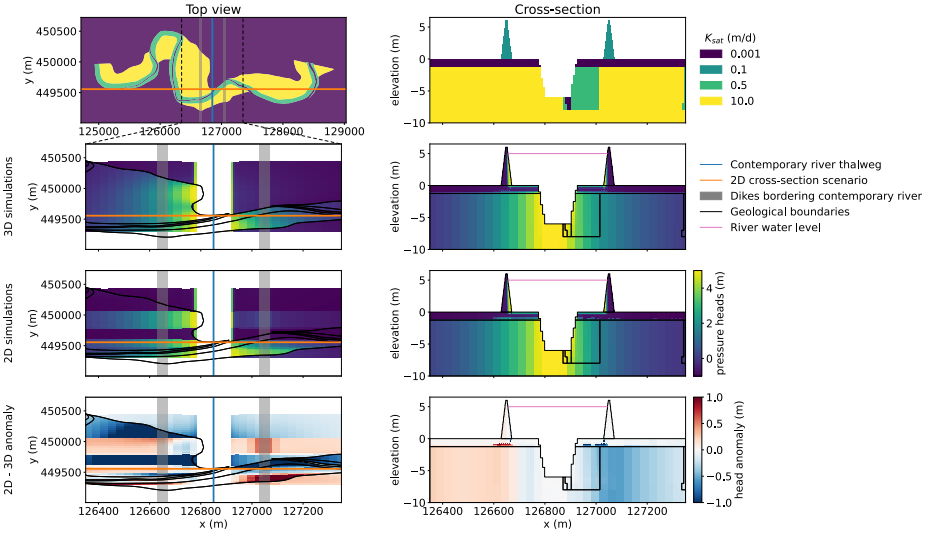

Figure 5.5 Pressure head of the *complex 3D* scenario versus the *complex 2D* scenario for T = 15. The top view represents a horizontal cross-section at a depth of -1.0 m, above which an aquitard is located (see cross-section). The pressure head anomalies indicate *complex 2D* - *complex 3D*, thus high (red) anomalies indicate higher values in the *complex 2D* scenario.

pressure heads up to 3 m, while the river water level already dropped to 0.5 m (Figure 5.4).

Focusing on the spatial pattern of pressure head evolution at the top of the aquifer, we observe similar patterns. First, with the same river water levels, pressure heads in the higher permeability area are higher at T = 25 days than at T = 5 days. Second, pressure heads are significantly lower (for example at x=127000, y=449800) if the river to groundwater infiltration is hampered by low permeabilities, but further away from the river this effect is partly diminished by groundwater flow not perpendicular to the river. As the largest pressure head differences seems to emerge at the timestep of maximum river water level (T = 15 days), we hereafter limit our analysis to this moment.

5.3.2 Reducing realism

In the following sections, we first simplify either the groundwater model dimension or the subsurface schematization. Afterwards we analyze the effect of simplifying both, thus additionally removing realism from the model schematization. We select the timestep with the highest river water level (T = 15 days) as representative for the observed patterns.

2D groundwater model

When comparing the *complex 3D* results to a *complex 2D* model run at the cross-section location and the composite aquifer heads of multiple 2D runs (Figure 5.5) the pressure head differences between the 3D and 2D groundwater model are small inside the river dike in the selected cross-section. However, larger differences occur in the subsurface, where the *complex 2D* resulted in a pressure head at a depth of 1 meter beneath the dike (at T = 15 days) of 2.51 m and 1.08 m on the left and right side of the river respectively, which is a difference of +0.18 and -0.55 compared to the *complex 3D* scenario. As such, the skewed infiltration pattern is amplified in the *complex 2D* scenario. This is caused by the less permeable (K_{sat} 0.5 m/d) abandoned channel deposit, which hampers flow in the 2D section, whereas lateral groundwater flow through the sandy aquifer will allow flow towards this lower-valued area in the 3D simulation.

The same process is also responsible for the large negative head differences (< -1 m) between the 3D and 2D groundwater simulation at the top of the aquifer (Figure 5.5, Top view): At those y-coordinate cross-sections where the river is completely embedded in low aquifer clays (at y = 449700), no water can infiltrate, and pressure heads remain low in that entire cross-section in a 2D simulation. On the other hand, lateral flow will partly level out these along-river differences from the locations where the river does touch the sandy channel belt deposits. The opposite is true too: high positive (> 1 m) pressure head differences occur if 2D simulations model impoundment of groundwater on a sand-clay interface, whereas groundwater will flow along that boundary in a 3D simulation. This effect is most visible on the channel belt to floodplain boundary (x=127100, y=449400). Thus, we can conclude that a 2D model is insufficient if the river channel is connected to a permeable deposit nearby, but this connection is not present in the 2D cross-section, or if the river channel is connected to the permeable deposit but a nearby transition to an impermeable deposit is not parallel to the river orientation and therefore absent in the 2D simulation.

Simple subsurface geology

In addition, we compare the *complex 3D* results to a *simple 3D* model, with the cross-section location and the composite aquifer heads given a less detailed geological schematization, in which the residual channel fill is absent (Figure 5.6). In the *simple 3D* scenario the pressure head at a depth of 1 meter beneath the left and right dike on the cross-section respectively (at T = 15 days) is 2.44 m and 2.08 m, which is a difference of +0.12 m and +0.44 m with respect to the *complex 3D* scenario. As expected, simplifying the geological schematization by not mapping relatively impermeable deposits result in a more equal infiltration pattern on both sides of the river. As a result, in the selected cross-section, where differences in geology occur on the right side of the channel (a K_{sat} of 10 m/d instead of 0.5 m/d), more water can infiltrate the subsurface resulting in pressure head increase. The maximum head difference between the complex and simple subsurface geology in the cross-section occurs directly next to the channel and is 0.83 m. In the top view the pressure heads at aquifer depth clearly only differ close to removed channel fill; removing the less per-

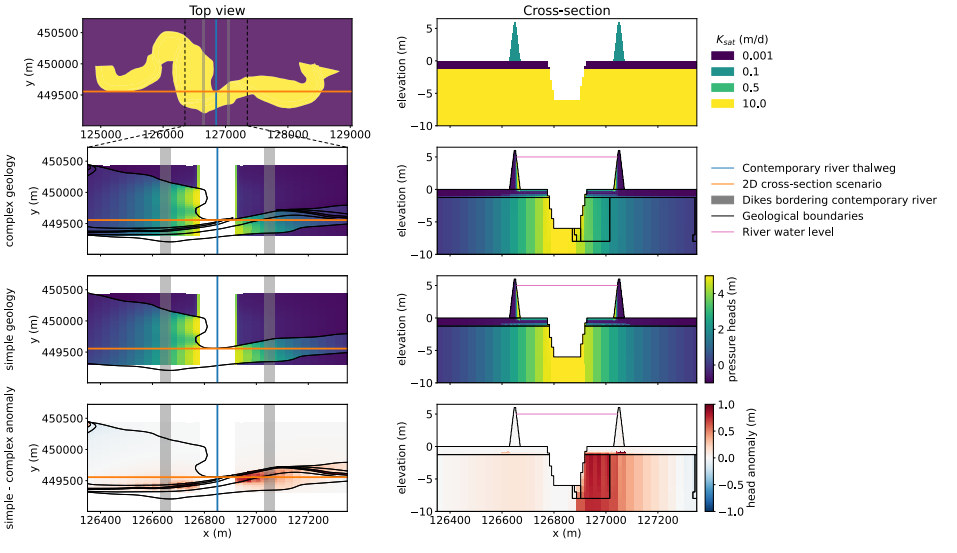

Figure 5.6 Pressure head of the *complex 3D* scenario versus the *simple 3D* scenario for T=15. The top view represents a horizontal cross-section at a depth of -1.0 m, above which an aquitard is located (see cross-section). The pressure head differences indicate *simple 3D* - *complex 3D* schematization, thus high (red) positive differences indicate higher values in the simple subsurface schematization.

meable residual channel from the detailed subsurface schematization generally results in higher pressure heads.

2D groundwater model and simple subsurface geology

Finally, we decrease the realism even further and perform 2D groundwater models with a simple subsurface geology (Figure 5.7, *simple 2D*). In the *simple 2D* scenario the pressure head at a depth of 1 meter beneath the left and right dike on the cross-section respectively (at T = 15 days) is 2.45 m and 2.25 m, which is a difference of +0.12 m and +0.62 m with respect to the *complex 3D* scenario. This is very similar to the differences observed between the *complex 2D* and 3D scenarios, however if we look at the top view of pressure head differences at an elevation of -1 m (top of the SCB), the differences contain patterns observed in the separate analyses (*complex 2D* and *simple 3D*). Nonetheless, the combined result is not simply an addition of these two. Overall, the pressure head difference resembles the *complex 2D – complex 3D* difference, with large positive differences where groundwater is impounded on transitions to impermeable units and large negative differences where river-groundwater infiltration does not occur in the 2D model runs. However, at the cross-section y-

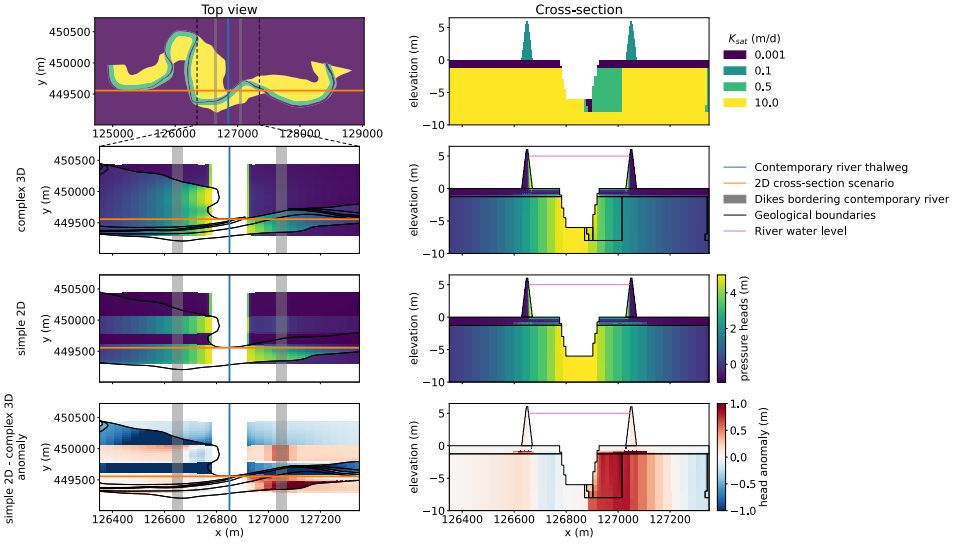

Figure 5.7 Pressure head of the *complex 3D* scenario versus the *simple 2D* scenario for T=15. The top view represents a horizontal cross-section at a depth of -1.0 m, above which an aquitard is located (see cross-section). The pressure head differences indicate *simple 2D - complex 3D*, thus large positive (red) differences indicate higher values in the *simple 2D* scenario.

coordinate, a different effect is prominent as the river-groundwater infiltration in the *simple 2D* scenario is no longer hampered by the low permeability of the residual channel in the complex geological schematization. Thus, large positive pressure had differences are observed, as clearly seen in the cross-section (Figure 5.7). Still, the influence of the simplified geological schematization remains small when compared to the removal of the third dimension in the modeling.

5.4 Results of combined model runs

The results previously discussed only represent a single river thalweg location scenario and the subsurface architecture in its close proximity. This section explores the maximum pressure heads underneath the dikes given the complete set of model runs. In this set, all time steps are considered in finding the maximum pressure heads, where the river was repositioned across the entire study area (see Section 5.2.4). The complete set of model runs thus encompasses many local configurations of model setup and subsurface architecture. We hereby focus on the dikes on top of the sandy SCB, as there the differences are much larger than around dikes on top of the clayey flood basin deposits (Figure 5.5, Figure 5.6, Figure 5.7).

With a simplified subsurface the 3D groundwater model (*simple 3D*) generally results in higher pressure heads. If a 2D groundwater model is used, the pressure

Table 5.2 Average maximum pressure heads (μ) and their standard deviation (σ) for the various schematization scenarios, and the (absolute) differences of the average pressure heads of the simplified scenarios relative to the reference *complex 3D* scenario.

Scenario	*complex 3D*	*simple 3D*	*complex 3D*	*simple 2D*
Value	2.09 ± 1.12	2.51 ± 0.80	2.09 ± 1.62	2.43 ± 1.43
Difference to *complex 3D*		0.42 ± 0.90	-0.01 ± 0.88	0.25 ± 1.28
Absolute difference to *complex 3D*		0.51 ± 0.85	0.60 ± 0.65	0.82 ± 1.02

head differences compared to the *complex 3D* model are almost equally positive and negative. The *complex 2D* scenario on average results in similar pressure heads but in absolute terms the differences are much larger. When both dimension and geological schematization are simplified (*simple 2D*), the (absolute) difference becomes even larger. Thus, if we look at the average absolute differences between the realistic *complex 3D* scenario and the other model schematizations, using a simple geological schematization produces as much of a bias as using a 2D groundwater model. Using a *simple 2D* model then combines the worst aspects of both and thus yields an even larger bias.

Both *simple 2D* and *simple 3D* scenarios result in large positive pressure head differences when compared to the complex subsurface scenarios (Table 5.2). These large positive differences occur where the complex subsurface scenario contains impermeable channel fill deposits and extends further in the direction of flow (left of the deposits in Figure 5.8). The differences occur because the simple geological schematization does not have impermeable internal deposits that hamper flow, resulting in higher pressure heads. Furthermore, large negative pressure head differences are more likely to occur in both *simple 2D* and *complex 2D* groundwater models. These large negative differences occur where in 2D groundwater cross-section the riverbed is mostly bordered by impermeable deposits disabling groundwater infiltration, whereas in the 3D groundwater model infiltration will occur elsewhere and partly replenish the groundwater deficit at this location (Figure 5.1). This occurs mostly just downstream of the floodplain to channel belt transition.

5.4.1 Effect on slope stability

We performed slope stability analysis (section 5.5.2) on the inner (landward) slope of the dike on each side of the river to assess the impact of pressure head differences due to simplifications in subsurface schematization detail and model dimension on dike slope stability. Slope stability calculations were made on each y-coordinate of the 2D groundwater models for the same river thalweg location scenario as presented in sections 5.3.1 and 5.3.2. Here we present the minimum dike safety factor F over all model time steps. We again differentiate between dikes on top of the sandy SCB and dikes on top of the clayey flood basin deposits.

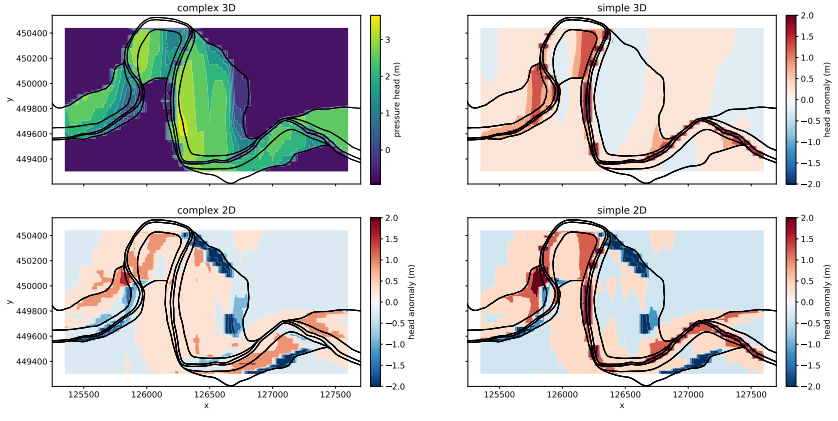

Figure 5.8 Composite image of the maximum pressure heads at the top of the channel belt (-1.0 m) underneath the 'left' dike for all groundwater simulations with the river (and the bordering dikes) at different x-coordinates. Therefore, the river location is slightly to the right of the plotted coordinate and all patterns in these composites represent flow towards the left. The pressure head differences indicate 'scenario' - *complex 3D*, thus high (red) positive differences indicate an overestimation in the corresponding scenario relative to the *complex 3D* scenario.

The average and standard deviation of the minimum dike safety factor F given the most realistic scenario (complex subsurface and 3D groundwater model) is 1.33 $\pm$ 0.04 and 1.08 $\pm$ 0.11 for dikes on top of the flood basin deposits and SCB deposits respectively (Figure 5.9). This difference is due to the higher pressure heads in the mostly sandy SCB, but also the overall lower geomechanical strength of these deposits. Considering the safety factor differences (with positive differences meaning higher F values in that scenario than in the *complex 3D* scenario) obtained for the other model schematizations, only small decreases in F arise when using the *simple 3D* schematization, with an F difference of -0.01 $\pm$ 0.02 and -0.05 $\pm$ 0.06 in the floodplain and channel belt respectively. A larger difference and higher F-values result from the 2D scenarios, with a floodplain and channel belt F-difference of 0.03 $\pm$ 0.09 and 0.06 $\pm$ 0.28 for the *complex 2D* scenario, and 0.03 $\pm$ 0.09 and 0.01 $\pm$ 0.29 for the *simple 2D* scenario respectively. The average difference for slope stability given the 2D groundwater models is low due to differences being approximately equally negative and positive. The absolute differences for the floodplain and channel belt are 0.09 $\pm$ 0.03 and 0.24 $\pm$ 0.15 or 0.09 $\pm$ 0.03 and 0.25 $\pm$ 0.15 for the *complex 2D* or *simple 2D* scenario respectively. These results clearly indicate that dikes on sand are most adversely affected by simplifications in subsurface schematization detail and model dimension, as their average safety factor is generally closer to failure ($F < 1$).

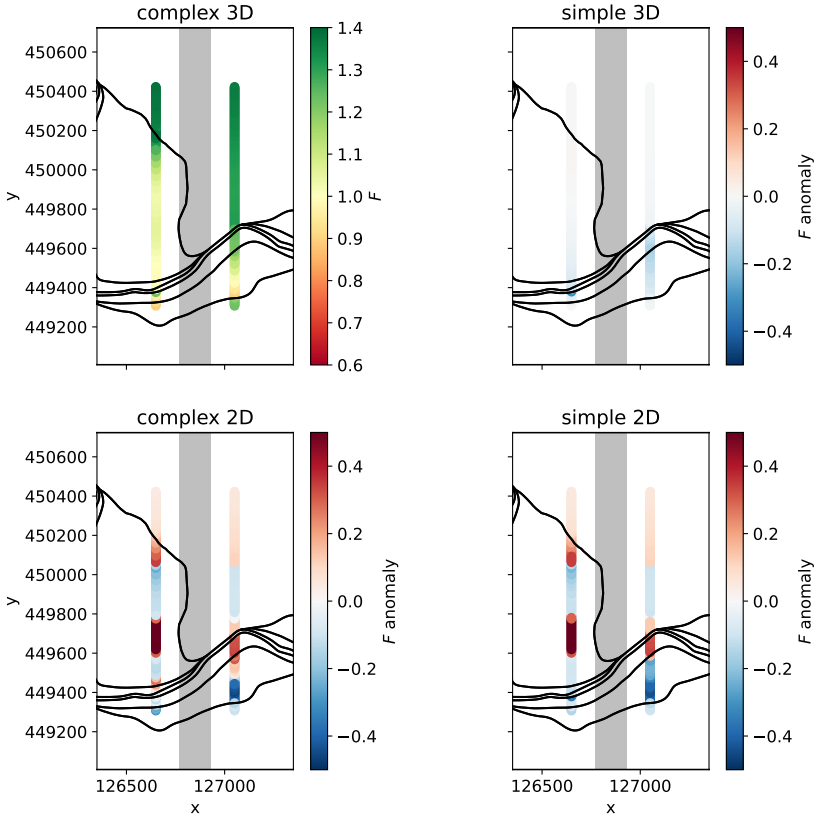

Figure 5.9 Minimum dike slope safety factors (F) for the *complex 3D* scenario and safety factor differences to the other scenarios given an example river thalweg location. The F differences are 'scenario' to *complex 3D* differences, thus high (red) values indicate a higher safety factor in the corresponding scenario than in the *complex 3D* scenario.

5.5 Discussion

5.5.1 Importance of parameters for explaining pressure head difference

The effect of the different model configurations on the predicted pressure heads underneath the dike is discussed by determining the relative influence of four parameters on the resulting pressure head differences with the *complex 3D* scenario. Four parameters are selected that relate to substrate lithology and its local configuration, and therefore likely influence these differences: saturated hydraulic conductivity of the subsurface corresponding to a geological unit (K_{sat}), distance from the dike to the nearest geological boundary (D_{edge}), angle to the nearest geological boundary (α_{edge}), and the percentage of the riverbed located in sandy material in the 2D cross-section ($2D\%_{sand}$). These parameters reflect important processes related to groundwater flow, respectively the likelihood of high pressure head buildup in a transient calculation, the nearby presence of subsurface heterogeneity, whether or not this transition is located perpendicular to the pressure head gradient from the river to the dike and to what extent river-to-groundwater infiltration is possible. The relative importance of these parameters is based on a regression tree, which iteratively creates two new branches (split the dataset into smaller subsets using the four parameters as features) to be able to best predict its target (pressure head difference). New branches are created based on a variance reduction objective function, i.e. the split in the dataset that results in the smallest value of the branch variance is made (Hastie et al., 2009). The iterative procedure ends if no further improvements can be made, the maximum splitting depth (5 in the selected regression tree) is reached or the minimum sample size on a branch is reached (10 in the selected regression tree). As the dataset is completely partitioned by a single decision tree, this method provides a powerful and intuitive method of regression (Hastie et al., 2009). The feature importance is calculated as the Gini-importance (Breiman et al., 1984).

The feature importance resulting from the decision tree analysis indicates that there are two parameters with a large effect on the pressure head differences (Figure 5.10): the percentage of the riverbed located in sandy material in the 2D cross-section ($2D\%_{sand}$) and the saturated hydraulic conductivity of the subsurface (K_{sat}). For explaining the difference between the 3D and 2D groundwater model dimension $2D\%_{sand}$ is most important while the difference between the complex and simple subsurface schematization is most explained by the K_{sat}. The differences from the *simple 2D* scenario are approximately equally influenced by both. The importance of $2D\%_{sand}$ for 3D – 2D differences can be explained by the large difference of river to groundwater infiltration if the river in the 2D cross-section is located in the clay deposit, whereas in the 3D deposit infiltration elsewhere will partly cover this. The importance of K_{sat} for simple – complex differences is closely related to the overestimation of pressure heads in the simple schematization where the clayey residual channel can be found in the complex scenario. Despite that most large differences are located directly next to a geological transition (Figure 5.10), the distance to the nearest geological transition (D_{edge}) and the angle to that transition (α_{edge}) only have a minor importance in our regression tree. This is likely related to the fact that although most pressure head differences are close to geological transitions, only

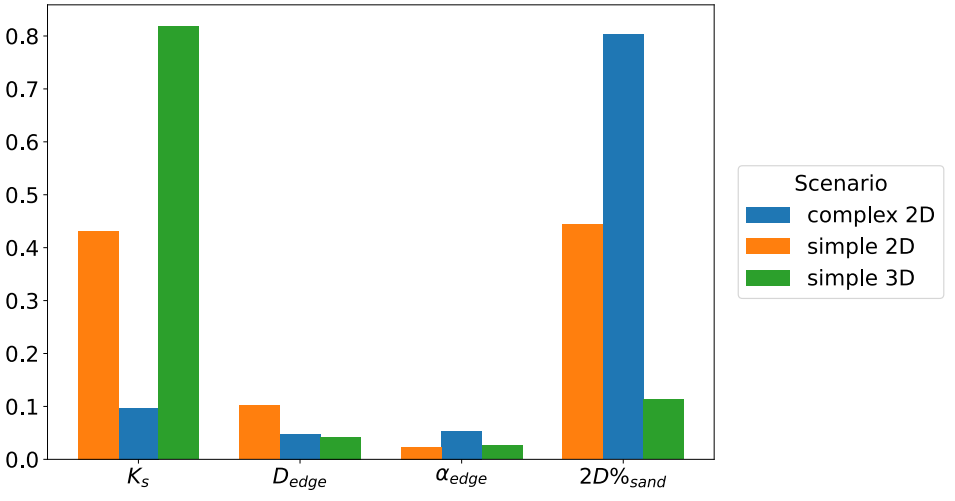

Figure 5.10 Feature importance of several subsurface architecture parameters for groundwater difference between the selected scenario and the *complex 3D* scenario.

geological transitions correlated with large changes in saturated conductivity (for example channel belt to floodplain, but not channel belt to abandoned channel) result in a large pressure head difference.

5.5.2 Slope stability differences related to groundwater head differences

We compared the slope stability and groundwater conditions in terms of their real values (for the *complex 3D* scenario) and in terms of the differences of these properties with that scenario (for the *simple 3D*, *complex 2D*, and *simple 2D* scenarios). The groundwater conditions are analyzed by means of the phreatic level and the pressure heads in the subsurface (at an elevation of -1 m, top of the SCB).

The pressure heads in the subsurface have a near-linear relation with dike slope stability in the *complex 3D* scenario (Figure 5.11). In the *complex 3D* scenario, two parallel relations exist for subsurface pressure head level versus F. The shift on the x-axis is related to the subsurface material, where in sandy material (right line) higher groundwater levels result in similar safety factors as in the clayey deposits (left line). A similar pattern is seen with the *simple 3D* to *complex 3D* differences, with a second group of scatter points on a positive groundwater difference related to clayey deposits. However, in the *complex 2D* and *simple 2D* scenarios a step in the relation between pressure head difference and differences in dike safety factors is observed towards lower pressure head differences. This step is related to the very limited river-to-groundwater infiltration in some 2D model runs, but it remains unclear why this leads to a break in the linear relation between groundwater head difference and F difference. Overall, the near linear relations between subsurface pressure head differences and F differences

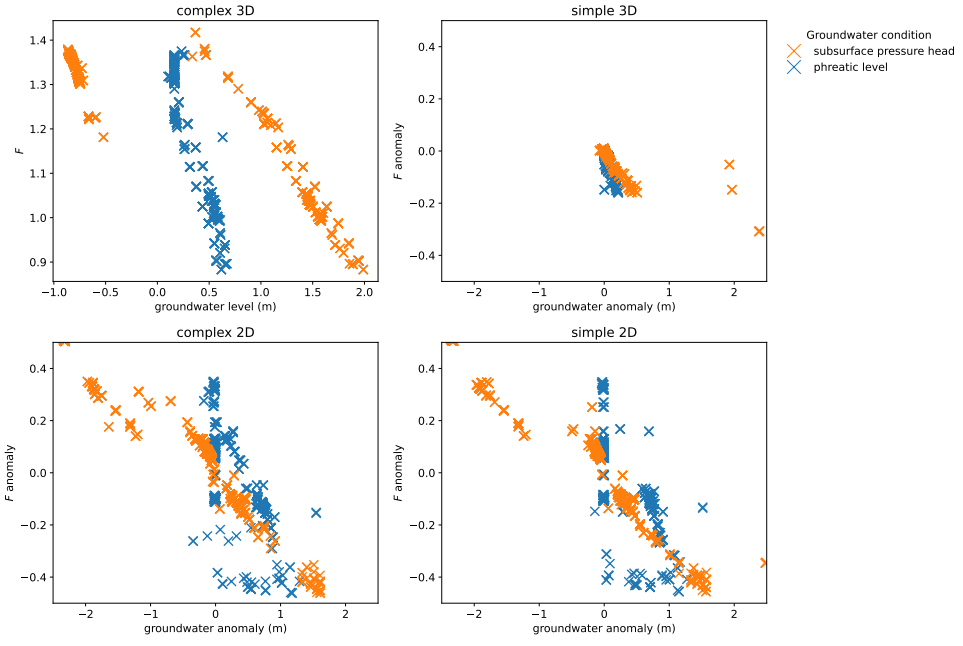

Figure 5.11 Correlation between groundwater conditions and safety factor F for the *complex 3D* scenario, and the correlation between the difference of groundwater conditions and safety factor F given different subsurface or model scenarios.

are similar over all scenarios and have a slope -0.34 $\pm$ 0.07, i.e. for every meter increase of pressure head difference the safety factor F difference decreases by 0.34.

Although the phreatic levels in the dike also seem to behave near-linear relation with dike slope stability in the *complex 3D* scenario (Figure 5.11), no near-linear pattern is observed in the phreatic level differences related to the dike slope stability differences in other scenarios. This indicates a smaller dependence of dike slope stability on phreatic levels than on the subsurface pressure head, which is reflected in the correlation coefficient (r^2) of the phreatic level differences, which is much smaller (r^2 0.57) than that of the subsurface pressure heads (r^2 0.92) (Figure 5.11). As already shown before (Figure 5.9), the small range for the *simple 3D* indicates very similar results as the reference *complex 3D* case. For the 2D schematizations, changes are substantial.

5.5.3 Implications for dike safety predictions

Groundwater conditions are one of the main drivers for dike (slope) instability (van Woerkom et al., 2023) and given known subsurface material characteristics the relation between subsurface pressure heads and dike slope stability can be considered as linear (section 5.5.2). Thus, an improved estimation of groundwater conditions directly leads to improved dike slope safety assessments. Where an overestimation

of pressure heads leads to underestimation of dike safety, new dike reinforcements are most likely over-dimensioned, i.e. made larger and more expensive than needed. This is undesirable, but less critical than an overestimation of dike safety due to too low predicted groundwater pressure heads. Deploying a 2D groundwater model for dike safety assessments thus may locally lead to considerable underestimation of groundwater pressure heads (Figure 5.8) and, hence, overestimating dike slope stability (Figure 5.9). On the other hand, a simpler geological schematization hardly results in too low pressure head estimates, but instead yields much higher pressure heads where impermeable deposits are missing. Based on this rationale, using a 2D groundwater model poses a larger potential risk of inaccurate dike safety estimates than using a simplified subsurface geology.

However, in our workflow, the simple schematization deviates from the complex schematization by not including several lower permeability units. In case the non-mapped units would have a high permeability, these units might have high negative pressure head differences compared to the complex situation, resulting in an overestimation of dike slope safety. Thus, the argument of a larger potential risk of 2D groundwater models assumes that a not complete, hence more simple, geological schematization often overlooks low permeability units. Often, sandy deposits in a delta are related to larger scale channel belts, which are not easily overlooked. Still, special attention should be paid to crevasse splay deposits (which form when sandy sediment is deposited on a floodplain when there is a breach in the river's natural or artificial levees). These deposits, when embedded within flood basin clay often have similar dimensions as residual channel deposits (Stouthamer, 2001).

To emphasize the need for 3D groundwater modeling, we assume that a maximum absolute error for F of 0.1 (dF) when simplifying either the groundwater model dimension or the subsurface schematization is still reasonably accurate, given for example uncertainty in material characteristics and associated model parameters that are not considered here (van der Krogt et al., 2019). Given the linear relation (with a slope of -0.34) between pressure head difference and dike slope F difference, a maximum absolute pressure head difference of $\frac{0.1}{0.34} = 0.29$ m is acceptable. In the *simple 2D* 41% and in the *complex 2D* 40% of the maximum pressure head differences are above the threshold of 0.29 m, and only 21% in the *simple 3D* scenario. However, within the channel belt extent these percentages increase to 61%, 61% and 43% for the *simple 2D*, *complex 2D* and *simple 3D* scenarios respectively. The similar values for the *simple 2D* and *complex 2D* scenarios are caused by relatively identical patterns of groundwater differences that arise due to the 2D model simplification. In addition, respectively, 81%, 84% and 95% of the pressure head differences above the threshold occur within 100 m of a geological boundary. However, due to limited field data, the position of these boundaries can often not be determined with less than 100 m accuracy. Therefore, we recommend using 3D groundwater models for dike slope stability assessments wherever local differences in geology and subsurface saturated conductivity can be expected, especially in sandy deposits.

5.5.4 Suggestions for model improvements and future research

2D groundwater simulations mostly seem to underestimate pressure heads, and thus overestimate dike slope stability. Therefore, 3D groundwater models are preferred over 2D simulations, but 3D models are computationally much more expensive in terms of memory usage and computation time, and this is not always possible. However, as they decrease the likelihood of underestimating the dike safety, future research should focus on how to restrain computational burden while retaining model accuracy, for example by looking at the minimum model extent, maximum transient time-step and maximum cell size resulting in accurate model results.

Furthermore, changes in subsurface architecture schematization have a large local effect on the pressure head calculations. In line with that, we expect local changes in material characteristics to have a similar effect, but each architectural unit in our analysis is homogeneous. For example, we know for the Stuivenberg study area that throughout the channel belt scroll bar deposits have significant internal variation in terms of local grain size differences or vertical trends in grain sizes. In addition, relatively coarse patches can be found on the inside of the abandoned channel meanders (Winkels et al., 2022). These grain size differences are likely to alter the permeability of the deposits, but it is unclear to what extent they will change the simulated groundwater conditions. Thus, the current analysis could be expanded by adding local heterogeneity to the saturated conductivity.

Overall, to up-scale the results of this study to the entire Rhine-Meuse delta we should consider regional variability in channel belt architecture and meander dynamics (Winkels et al., 2022; Stouthamer et al., 2011). In short two channel belt types occur. First, there are lower delta channel belts, which were active for a short (800 to 1200 years (Stouthamer, 2001)) period and are generally narrow channel belts, such as the SCB. Second, there are upper delta channel belts, which were active for a longer period of time and actively migrated in their floodplain, thereby reworking their own extensive sandy deposits and for example creating oxbow lakes. Despite the fact that these upper delta channel belts will have similar variation in permeability as lower delta channel belts, they often contain more complicated architectures (Hesselink et al., 2003) that might have unexpected implications for groundwater flow patterns.

Independent of the detail in groundwater model dimension and subsurface schematization, the presented results are a result of our selected model workflow. This workflow schematizes the river and dike as straight lines, with a fixed floodplain width between the river channel and the dike. Despite that we are confident that repositioning the river over the model domain with the meandering channel belt in the subsurface results in a large range of orientations of the river to the channel belt, this does not include an actual meandering river channel. For example, a dike on the inner side of a river meander might be subject to more extreme groundwater pressure heads than found in our analysis (Wösten et al., 2001). In addition, a change in floodplain width results in a smaller response time of pressure heads underneath the dike, also possibly leading to more extreme pressure heads, and the corresponding larger underestimates when a 2D groundwater model is used. Despite that the current analysis can thus be expanded, we do not expect significant differences to occur in the

observed patterns if 2D rather than 3D groundwater models are used in a complex and heterogeneous delta setting.

5.6 Conclusion

In this work, we performed a combined transient analysis on the influence of model dimensionality and complexity of subsurface schematization on pressure head estimations was carried out. This analysis evaluated the consequences for dike stability assessments. While a simpler subsurface schematization locally resulted in larger differences in terms of the pressure head, it was found that the use of 2D groundwater models had far stronger implications in terms of the simulated pressure head and the associated dike slope safety. In particular we find that:

- pressure heads in sandy river channel deposits are strongly influenced by river-to-groundwater infiltration, which can be hampered by low permeabilities directly bordering the river;
- using 2D groundwater models can result in large differences in pressure heads found with 3D models in case of a heterogeneous subsurface. Large underestimates of pressure heads compared to 3D groundwater models occur where river to groundwater infiltration is limited in the 2D model but flow perpendicular to the 2D cross-section level out this deficit in reality (as represented in the 3D model). Large overestimates occur using a 2D model if groundwater is impounded against impermeable geological units, whereas the flow is able to be deflected in the 3D model;
- using a simplified geological schematization can result in large head differences compared to a full heterogeneous model schematization, but these occur mostly at the locations where the subsurface shows large contrasts. In our simplification, ignoring small, less permeable geological units, groundwater pressure heads are mostly overestimated;
- the described differences are most prominent in sandy deposits as their high permeability enables a fast response to rising and falling river water levels;
- hydraulic heads (and thus pore pressures) in the subsurface have a direct linear relation to dike slope stability safety factors, resulting in large differences in dike slope stability assessments between the different model configurations;
- when used for dike slope safety assessments, using 2D groundwater models is found to be possibly dangerous, as these models tend to underestimate groundwater pressure heads and thus overestimate dike safety. This is especially the case if a permeable deposit is connected to the river channel but this connection is not present in the 2D cross-section. The corresponding overestimation of dike safety might lead to insufficient reinforcements and higher risks of dike failure. This effect can be severe, in our assessment 61% of the area within the sandy channel belt was underestimated and the effect was more pronounced towards the edges of the channel belt;

- on the basis of this evidence, we recommend that 3D groundwater modelling is used as a basis to assess dike stability and attention is given to a proper schematization of the subsurface in relation to the dike position and river orientation during a high water event.

Author contributions

T.v.W. designed the research and performed the primary data analysis and model development. R.v.B. and M.F.P.B. helped with result interpretation and H.M. significantly improved the written text in the manuscript.

Acknowledgements

We greatly appreciated the support of Tim Winkels and Willem-Jan Dirkx, whose ideas on subsurface geology schematization and implications of subsurface heterogeneity on groundwater hydrology formed the initial idea of this research project.

6 Synthesis

The main objective of this study was **to assess and quantify the contribution of various parameters to uncertainty in dike failure probabilities resulting from variability in groundwater conditions in a delta setting**. Several of these parameters were investigated individually and found to be partly responsible for the uncertainty in groundwater conditions and dike failure probabilities. In this synthesis, I will summarize these findings and assess their relative influence. In addition, I will elaborate on the implications of these findings for flood risk management and provide recommendations for further research.

6.1 Research questions and main conclusions

In the preceding chapters, I consecutively looked at the importance of subsurface lithology and geometry, variable flood wave shapes, a heterogeneous dike interior, and 3D geological architecture for dike stability, and their contribution to uncertainty in dike failure probabilities and are summarized here with respect to the slope stability of the dike.

Which subsurface and geometrical properties influence dike stability estimates the most under steady-state conditions?

Dike stability is most sensitive to the steepness of the dike slope, closely followed by the dike material. These parameters have a dual influence; they have a direct effect on slope stability through the downslope component of the potentially unstable mass and the shear resistance that can be mobilized along the slip plane; and they have an indirect effect by altering the local pressure head conditions through the permeability and porosity. Other parameters have a more limited influence; for example groundwater drainage to nearby ditches only affects dike slope stability if the ditches are close to the dike. Finally, some parameters have a negligible influence on dike slope stability, such as the dike crest width and the thickness of sandy deposits at deeper depths underneath the dike. The uppermost subsurface material has a very specific influence, as it is of main importance for dissipating high pressure heads in the dike. As geometric parameters, such as drainage location and dike slope, can be more precisely determined, the dike material type and the first subsurface material type are a larger source of uncertainty in high-resolution groundwater modelling for estimating dike slope stability.

What is the influence of flood wave shapes on probabilistic dike slope stability under transient groundwater conditions?

Including the variability of flood wave shapes in a time-dependent analysis of both groundwater flow and dike slope stability results in a more realistic failure probability than analyses under steady-state groundwater conditions. Moreover, when compared to using a single design flood wave, considering multiple variable flood wave shapes leads to a higher failure probability, as the combined failure probability of multiple flood waves is more strongly influenced by the most adverse flood wave shapes. Overall, flood wave shape uncertainty can be as much an important source of uncertainty

for dike slope stability as material properties, especially in case of extreme water levels. The transient analysis of pressure head conditions given variable flood wave shapes reveals a delay in the lowest dike slope stability of at least 2.5 days after the peak water level, which suggests that the highest dike slope failure probability occurs after the peak water level passed. The most important flood wave shape parameters for dike slope stability are respectively a prolonged high water level and a large decrease in water levels after the peak for inner and outer slope stability.

How can we incorporate the heterogeneous dike interior?

We can incorporate dike interior heterogeneity by using data from archaeological cross-sections of historical dikes. These data can create, when incorporated in a newly developed object-based and process-based model simulating dike construction history, multiple scenarios of dike interior heterogeneity. The Dike Erection Tessellation using Regionally Inherited Statistics (DETRIS) method simulates similar patterns of heterogeneity as observed in real dikes and provides a more comprehensive way of incorporating heterogeneity than arbitrary expert-based estimates. The dike interior heterogeneity can be incorporated even more accurately when local statistics of dike buildup or ground truth data (e.g. from core penetration tests) are available. As such, it produces a data-based approximation of the uncertainty in dike failure risk as a function of dike heterogeneity and groundwater conditions, which results in a better informed assessment of dike slope stability.

To what extent do the downgraded information from 2D groundwater simulations and simplified geological schematizations bias the results of a hydrological model and stability assessment?

Often 2D groundwater simulations are deemed sufficiently accurate for dike stability analyses in case of a relatively homogeneous subsurface or at large distances from geological boundaries. However, when a complex subsurface architecture is present, 2D groundwater models can result in large differences in pressure heads when compared to a 3D model with a more complex geological architecture. We found that a more complex geological schematization mostly results in local changes in groundwater conditions at the specific location of the increased complexity. However, 2D modelling can severely underestimate groundwater pressure heads if the river channel is connected to a permeable deposit but this connection is not present in the 2D cross-section. In addition, an overestimation of pressure heads occurs if the river channel is connected to the permeable deposit but a nearby transition to an impermeable deposit is not parallel to the river orientation. Since these differences between 2D and 3D models have large impacts on estimated safety factors it is advisable to always use 3D models when hydrogeological heterogeneity is present.

Table 6.1 Values for hydrological and geomechanical parameters given the material texture. Note that the dike, cover layer and subsurface scenario consist of different material textures in different model runs.

Material textures	K_{sat} (md^{-1})	ϕ (^{o})	c' (kPa)	γ (kNm^{-3})	γ_{sat} (kNm^{-3})
Clay	0.01	17.5	5.0	17.0	17.0
Clay Loam	0.05	30.0	1.0	20.0	20.0
Sandy Loam	0.26	30.0	0.0	18.5	20.5
Sand	5.75	32.5	0.0	18.0	20.0
Peat	0.10	15.0	3.75	12.5	12.5

6.2 Relative importance of parameters influencing groundwater induced dike slope instability

The various parameters and processes that influence dike slope stability by altering groundwater conditions are separately discussed throughout this thesis, but not yet combined. To assess the relative contribution of each of those parameters on groundwater induced dike slope instability, I selected the most important yet difficult to determine parameters from each of the chapters and combined them in one exploratory sensitivity analysis. Thus, I selected the material of the first subsurface layer (chapter 2), the flood wave shape (chapter 3), the dike interior (chapter 4), the level of detail in subsurface architecture (chapter 5) and the dimension of the groundwater simulation model (chapter 5). These important parameters and schematizations were used as variables, and their values were varied in a modelling chain consisting of a groundwater model (MODFLOW) and dike slope stability model (D-stability).

6.2.1 Baseline scenario and variables for the sensitivity analysis

The baseline scenario for this analysis encompasses an area of 1600 m by 1600 m, which in its center is intersected by a north-south oriented river channel (Figure 6.1). The overall elevation of the area was set to 0 m, with exceptions for the river channel and the dike. The river channel has the shape of an upside down trapezoid and is 6 m deep, has a flat base with a width of 100 m and slopes up with a 1:5 ratio to the riverbank. On each side of the river a dike is located 100 meters from the river bank. The dike has the shape of an upright trapezoid and is 5 m high, has a flat crest with a width of 5 m and a slope at a 1:3 ratio. Relative to this baseline setup several parameters were varied between predefined values in different scenarios.

First of all, the subsurface architecture has two schematizations with different levels of detail and can thus take either the simple schematization or the complex schematization. The subsurface architecture is hypothetical but heavily based on characteristics of the Stuivenberg channel belt in the central Rhine-Meuse delta (Section 5.2.1). The simple schematization consists of a sandy 'channel belt' intersecting a clay 'overbank deposit'. The complex schematization also includes a hypothetical 'abandoned channel' and 'residual channel'. These deposits are characteristic of the

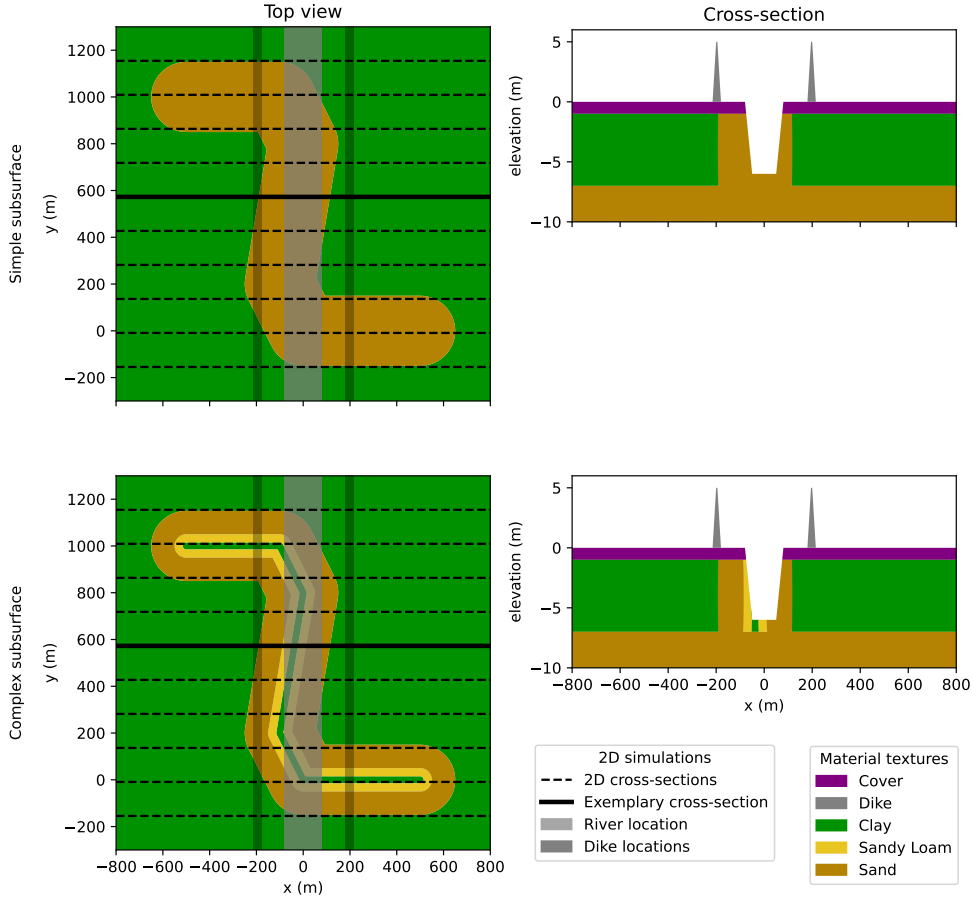

Figure 6.1 Schematized overview of subsurface schematizations. Given the hypothetical subsurface architecture, two subsurface scenarios are created: a simplified schematization without the abandoned channel and residual channel (simple) and a complete schematization including all geological units (complex). At the exemplary cross-section located a depth transect is also shown. Note that the top view (left column) is actually a horizontal slice at a depth of -1 m, above which a cover layer is found.

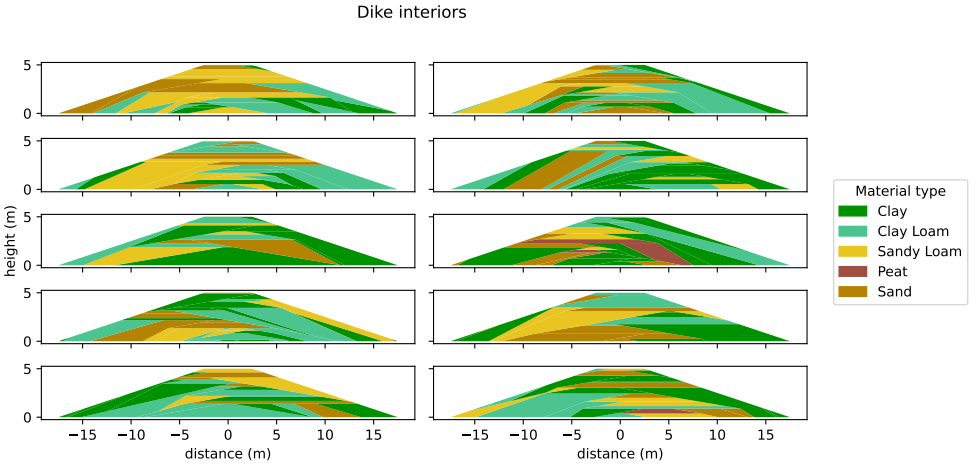

Figure 6.2 The 10 dike buildup schematizations created by the DETRIS algorithm used in the sensitivity analysis.

last phase of river activity in the channel belt and are sometimes overlooked in subsurface schematization due to their limited extent or the inability to identify their position. In the subsurface schematization used, these deposits can be found between 1 and 7 meters depth. Below these deposits sandy material can be found. On top of these deposits, the subsurface schematization has two additional scenarios (Figure 6.1): a homogeneous layer of either clay or sand is schematized.

Second, the dike buildup has 10 schematizations (Figure 6.2) created by the DETRIS algorithm (section 4.2.2). These dike buildup schematizations were created using the dike surface geometry described in the previous paragraph and the combined 'regional' characteristics derived from all available historical archaeological dike cross-section excavations. As such, the average occurrence of material textures and layer geometry in the simulated schematizations mimics that of the observed dikes (section 4.3.1, Figure 4.8).

Third, the groundwater conditions were forced with 10 different flood wave shapes with a maximum water level at the dike crest (5 m). These flood wave shapes were selected from the GRADE database (Hegnauer et al., 2014) using the method described in (section 3.2.1, Figure 3.1). Given a set of 1000 flood wave shapes with the same maximum water level, this method divides these flood waves into 10 subsets. The subsets were created with k-means clustering, which aims at minimizing the combined within-cluster variance given five flood wave shape parameters: H_0, A_{peak}, A_{tot}, ΔH_{ds}, Ds_{max} (Table 3.1, Figure 3.1, Section 3.2.1). From each subset, one flood wave was randomly selected for this analysis, which is assumed to be representative of its corresponding subset (Figure 6.3).

Last, the groundwater model dimension is either three-dimensional or two-dimensional. In the 3D model, calculations are performed on the entire model domain. In the 2D

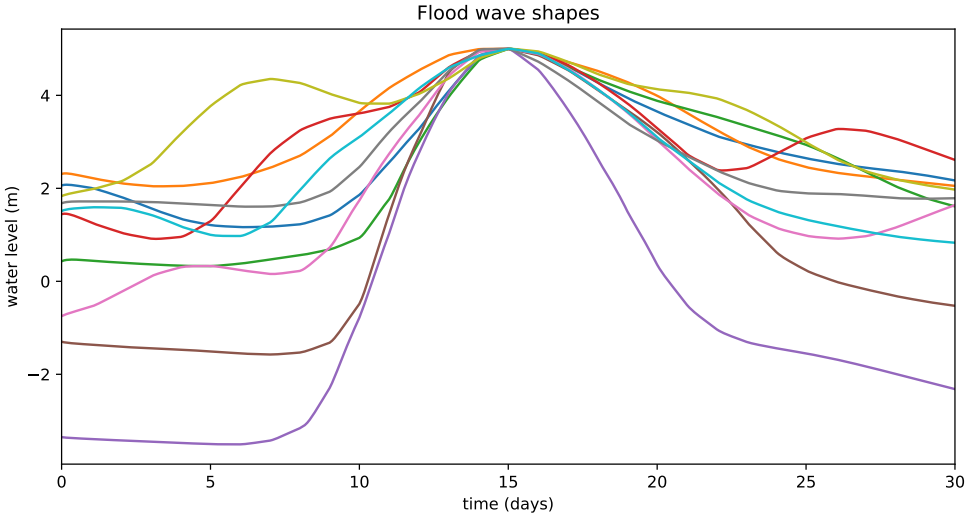

Figure 6.3 The 10 flood wave shapes used in the sensitivity analysis. These flood waves were selected from a total set of 1000 flood wave shapes in such a way that the total variation in possible flood wave shapes is represented.

model, calculations are performed on a cross-section perpendicular to the river. In total 10 2D models were created, each on a different y-coordinate of the model domain.

6.2.2 Model parameterization of groundwater and dike slope stability

The groundwater hydrology was simulated using MODFLOW 6 software (Langevin et al., 2019), with the same setup and boundary conditions for 2D and 3D simulations. The transient MODFLOW simulation was initiated with groundwater levels and river water levels set at -1 m. The model runs with a temporal resolution of two hours and stops 15 days after the maximum water level is reached (Figure 6.3). The vertical resolution is 0.25 m in the dike and increases towards 2 m in the deepest subsurface layer. The horizontal calculation grid also has a variable resolution created by the GRIDGEN software (Lien et al., 2015). This software creates quadtree grids, which in our model have a maximum resolution of 32 m and a minimum resolution of 0.5 meter in the dike. River-groundwater interaction is governed by the MODFLOW river package and surface-seepage is governed by the MODFLOW drain package (Hughes et al., 2017). Saturated conductivities (K_{sat}) are assigned to all material types based on typical values (Table 6.1).

The dike slope stability was assessed on the inner (landward) slope of the dike and expressed in terms of the safety factor F. It was always calculated on a 2D cross-section at specific y-coordinates, but given the groundwater scenario the pore pressure heads from either the 2D groundwater simulation or the 3D groundwater simulation were used. The Uplift-Van limit equilibrium method (Van, 2001) was used for slope stability calculations (see Appendix A.2) within in the D-Stability slope

stability software (Deltares, 2019). Shear stresses are calculated with a C-Phi model, of which the parameters cohesion (c'), friction angle (ϕ), material weight (γ) and saturated material weight (γ_{sat}) have a characteristic value per material type (Table 6.1).

6.2.3 Sensitivity indices to analyze parameter importance

I used the Delta Moment-Independent measure (DMI) as sensitivity index (Borgonovo, 2007). The DMI represents the non-overlapping area between the resulting probability density function $f_Y(y)$ given an unconditional input vector X, including all parameter values, and a conditional input vector X_i, consisting of a subset of parameter values (section 2.2.4). It returns the measure δ_i, mathematically expressed as:

$$\delta_i = \frac{1}{2} E_{X_i}[s(X_i)] \tag{6.1}$$

with

$$E_{X_i}[s(X_i)] = \int f_{X_i}(x_i)[\int |f_Y(y) - f_{Y|X_i}(y)|dy]dx_i \tag{6.2}$$

6.2.4 Outcome of combined sensitivity analysis; parameter influence on groundwater-related dike slope safety

Parameter influence on dike phreatic levels

The influence of the variables in the sensitivity analysis on the uncertainty in groundwater conditions was first assessed for the phreatic level at the center of the dike (Figure 6.4). The phreatic level is most influenced by the uncertainty of the dike interior, which is of course expected to be the factor most directly influencing the seepage inside the dike. Especially the presence of low permeability units that hamper infiltration or the presence of high permeability units near the riverward side of the dike that increase the infiltration length seems to be important. Additionally, the flood wave shape and material of the first subsurface layer have a substantial influence on the phreatic level. The influence of the first subsurface layer on the phreatic level is less widely acknowledged, although an increase in permeability both enables seepage from the aquifer towards the dike given high water levels in the river and enables a more rapid decrease of the phreatic level in the dike when river water levels drop. Finally, the level of detail in subsurface architecture and groundwater model dimension hardly have an influence on the phreatic level.

Parameter influence on subsurface groundwater heads

The influence of the variables on the uncertainty in groundwater conditions is secondly assessed on the pressure heads at a depth of 1.5 meters underneath the inner (landward) toe of the dike. The pressure heads are most sensitive to the material of the first subsurface layer; a more permeable material enables infiltration into the underlying sandy aquifer not only in the river channel, but also on top of the (silty or

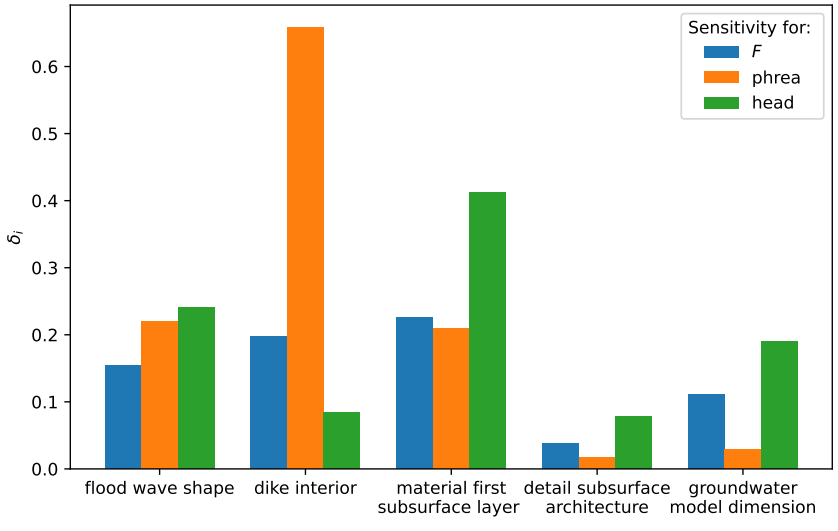

Figure 6.4 Sensitivity of groundwater conditions and inner (i.e., landward) dike slope safety factor (F) to the different subjects studied in this thesis. Note that the sum of all δ_i values is greater than unity, indicating dependency and interactions between parameters.

sandy) floodplain (Figure 6.4). As such, the distance between the dike and a direct infiltration point is much shorter and pressure heads underneath the dike are higher than in case of a clayey floodplain cover layer. In addition, the flood wave shape and groundwater model dimension have a significant impact on the pressure heads. Both of these variables influence the groundwater flow patterns in the subsurface, by either causing different temporal patterns of river-to-groundwater infiltration due to various flood wave shapes or, for example, by inhibiting infiltration into this aquifer in the 2D model cross-section while in a 3D situation the river channel is connected to this aquifer. The level of detail in subsurface architecture has little influence on the subsurface pressure heads, which is in line with the large (but very local) influence on the groundwater conditions observed in chapter 5. Finally, the sensitivity to the dike interior is limited, acknowledging that groundwater flow through the dike to the subsurface is of little importance for the occurrence of the maximum pressure heads below the surface.

Parameter influence on dike slope stability

The influence of the variables in the sensitivity analysis on the uncertainty in dike slope stability was assessed for the safety factor F for inner (landward) slope stability. There is no clear parameter to which the safety factor is most sensitive, contrary to the effect of the parameters on the groundwater conditions (Figure 6.4). This

again emphasizes the complex processes related to dike slope stability, being directly influenced by the geomechanical soil properties and indirectly by the hydrological soil properties due to groundwater flow. In that regard, the flood wave shape and groundwater model dimension only influence the dike slope safety by altering the groundwater pressure heads. Additionally, the dike interior and the material of the subsurface layer also directly influence the geomechanical soil properties important for the dike slope safety. Only the level of detail in subsurface architecture seems to play a minor role in accurately estimating the safety factor F.

6.3 Advances in dealing with uncertainties related to groundwater conditions for dike slope safety

This thesis demonstrates and quantifies the contribution of various parameters and drivers to uncertain dike failure probabilities caused by variability in groundwater conditions in a delta setting. In this light, I recall the various levels of uncertainty regressing from 'know' to 'no-know' (Walker et al., 2003): determinism, statistical uncertainty, scenario uncertainty, recognized ignorance, and total ignorance. First, I found that the main parameters that are non-deterministic are the material types (which are subject to scenario uncertainty), with more complex interactions between the type of dike material and the subsurface material. This study increased our knowledge of these interactions, thus decreasing the recognized ignorance. Second, I concluded that the uncertainty in flood wave shape can be as important as the uncertainty in geotechnical material parameters for the final uncertainty in dike slope stability. The initial scenario uncertainty in flood wave shapes can be incorporated in the dike slope safety assessment in a statistical manner with a newly developed method. Third, I found that dike buildup uncertainty contributes substantially to dike slope stability uncertainty. Currently, the dike material is assumed to be homogeneous, and the material uncertainty is captured in probability density functions, but I have developed a new realistic method to simulate layers of different material types with representative geomechanical parameters. This is especially important for accurately simulating the phreatic groundwater conditions in the dike (Figure 6.4). Thereby, I decreased the statistical uncertainty by developing a more comprehensive way of incorporating uncertainty in dike buildup heterogeneity and characteristics. Fourth, I found that 2D groundwater models or groundwater models based on a simplified geological schematization can cause large differences in the estimated dike safety when compared to more realistic 3D groundwater models. Although more research is needed to set specific guidelines on this matter, this investigation has made some essential first steps in moving this issue from recognized ignorance to determinism, as using a 3D groundwater model improves the model results and thus decreases the uncertainty. Finally, when all of these factors are combined, we can observe that multiple parameters contribute to the uncertainty in dike stability due to the variability in groundwater conditions in a delta setting. Whereas the material in the dike and upper subsurface seem to have the largest influence (by small margins), all of them need to be considered in an integrated manner to accurately estimate the uncertainty caused by groundwater conditions.

6.4 Future groundwater conditions for dike slope stability and flood safety

This research focused mainly on understanding interactions and qualifying uncertainties between river water levels, subsurface characteristics, groundwater flow and dike slope stability. These interactions and uncertainties are valid for the current situation but might change towards the future when climate change may lead to situations unseen in the present and recent history. First of all, extreme river water levels (and thus also the pressure heads in and below dikes) are likely to increase, which - without adaptation measures applied - would be followed by a projected increase in direct flood damages of by 1.4 to 2 times at 2^oC and 2.5 to 3.9 times at 3^oC compared to 1.5^oC global warming (IPCC, 2022). The river dike network thus needs to be extensively reinforced towards the future, but the effects of higher river water levels on dike stability in the future can be relatively well captured by models, especially when taking groundwater conditions into account in more detail. At global warming of 4^oC on the other hand, not only extremely high river flows but also extremely low river flows are projected to occur globally (IPCC, 2022), also causing periods of extremely low groundwater levels in and below river dikes. From 2050 onwards, the Rhine-Meuse delta might experience an increase in severe streamflow deficits of 20 to 50% (Forzieri et al., 2014). These prolonged periods of low groundwater levels may eventually alter the behavior of the dike due to irreversible shrinkage of clay and peat and the formation of fissures, which could affect its ability to withstand future extreme high flows. To understand the local occurrence probability of drought shrinkage, the developed DETRIS algorithm might provide suitable information on the dike buildup material. Thus future challenges for managing groundwater conditions and safety of river dikes do not only include reinforcing dikes for extreme high flows, but also preventing the deterioration of these dikes during extremely dry conditions.

6.5 Towards a better incorporation of uncertainty in groundwater conditions in dike safety practice

Given the possibly more extreme discharge conditions in the future, increasing knowledge on processes related to flood safety and the implementation of this knowledge is expected to lead to a more robust safety assessment. Since the transition to safety standards in terms of acceptable probabilities of flooding, many parameters related to dike slope stability are now being assessed in a probabilistic manner. The uncertainty related to these parameters, most strikingly geotechnical material properties such as angle of internal friction or shear strength increase exponent, is thus considered (Huber et al., 2017). In addition, uncertainty in geological architecture is taken into account as 1D scenarios over depth (Hijma and Lam, 2015). On the other hand, groundwater conditions are often deterministically schematized or assessed for two extreme (high and low) design scenarios given a baseline subsurface buildup (TAW, 2004). The concepts and knowledge explicated in this thesis can significantly refine these approximations, but they currently require extensive knowledge of the processes

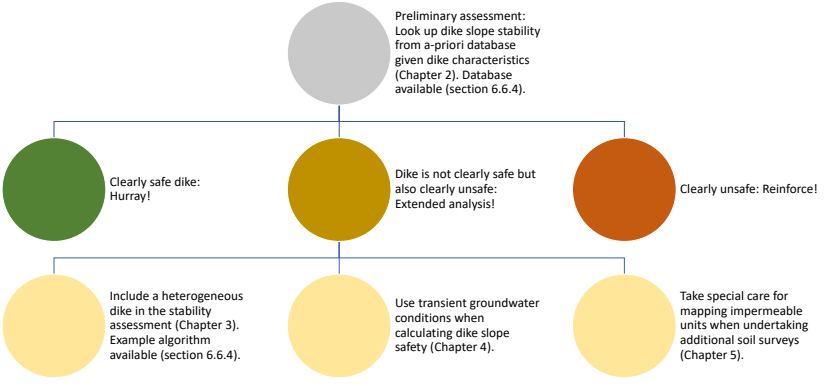

Figure 6.5 Suggested workflow for implementing the algorithms and results described in this thesis.

and modelling algorithms. This section provides several suggestions for making them more operable and easily utilizable in dike safety assessments.

When assessing dike safety, first a preliminary assessment is made using a rough approximation of all parameters involved (Figure 6.5); if this preliminary assessment indicates a more than sufficiently safe dike, no detailed assessment needs to be performed. Currently such a preliminary assessment is solely based on geometrical parameters of the dike surface and subsurface layers. However, a preconstructed database of dike slope safety factors derived from a Monte-Carlo analysis (chapter 2) including dike geometry, subsurface geometry, material parameters and a physics-based groundwater model is found to also provide a quick a-priori analysis of the dike stability. As shown in Figure 6.4, the material properties of the shallow subsurface should definitely be incorporated into such a database. With even more processes and parameters included, such a database could already provide a more detailed overview of sufficiently safe dikes.

In case this assessment points to a dike of which the strength is near the minimum safety standard a detailed analysis needs to be performed to indicate whether or not it meets the required protection level (Figure 6.5). In case of an insufficiently safe dike, a detailed analysis can indicate the necessary reinforcements needed to reach the required safety standard. Before the detailed analysis, often additional soil surveys are performed to make more accurate subsurface schematizations. Our research on the effect of complexity in geological architecture on groundwater conditions (chapter 5) indicates that special care should be taken to map impermeable units, especially when they are likely to hamper river-to-groundwater infiltration.

In such a detailed analysis schematizations of groundwater conditions should be (based on) transient groundwater conditions instead of steady-state conditions, as steady-state conditions are prone to underestimating dike slope stability (chapter 3). The transient groundwater conditions can be simulated using a single design discharge wave, such as taking the vertical average of multiple waveforms, but ideally multiple flood wave shape scenarios are considered. In order to simplify this approach, a designated flood wave shape can be selected, taking into account a certain uncertainty margin, and ensuring it accurately reflects the uncertainty in groundwater conditions arising from the variability in flood wave shape.

In addition, a detailed analysis should include dike buildup heterogeneity, as it is crucial to accurately assess the phreatic groundwater level in the dike (Figure 6.4). However, currently applied model schemes assume a homogeneous dike. The DETRIS algorithm produces a data-based approximation of the uncertainty in dike failure risk as a function of dike heterogeneity and groundwater conditions, and it allows for incorporating local information from e.g. a few cores or CTPs (cone penetration tests) to reduce uncertainty (chapter 4). Groundwater simulation results with DETRIS-built dikes indicate that the location and extent of highly permeable units in the dike have a large effect on the phreatic level and it is therefore questionable to what extent the influence of dike buildup can be captured in a purely statistical manner. As calculating multiple dike buildup scenarios for every dike section would produce the most reliable results but is practically less desirable, I would recommend developing multiple dike heterogeneity scenarios. In a similar way the subsurface scenarios are used (Hijma and Lam, 2015), these can be compared to local statistics, ground truth data, or knowledge of dike construction history. The feasible dike heterogeneity scenarios can subsequently be used to determine groundwater conditions.

Whether or not the previously mentioned aspects are considered, guidelines should be proposed on the appropriate method for estimating groundwater conditions. In case of a very homogenous subsurface, when looking in the expected direction of groundwater flow, the current 2D and steady-state analytical approximation (TAW, 2001) might be adequate. In other situations, at least a physics-based groundwater model is required to model the transient (time-dependent) response of groundwater conditions on river water levels. Moreover, especially in case of horizontally nearby geological boundaries, a 3D groundwater model should be created to accurately assess the groundwater pressure heads. The conditions in which any of these methods should be applied are roughly known but should be stated more clearly in succinct guidelines.

6.6 Research recommendations

The research presented in this thesis helped to increase the understanding of processes influencing groundwater conditions related to dike slope stability, thereby decreasing the uncertainty related to these processes. Therefore, it provides useful insights that can improve the current approximations for groundwater conditions. However, not all required parameters have miraculously become perfectly determinable, thus dealing with uncertainty will always be part of estimating groundwater conditions for dike slope stability. Hence, I recommend several subjects that need additional work, either

to further decrease the remaining uncertainty or to provide further handles on how to deal with this remaining uncertainty.

6.6.1 River dike data incorporation and derivation

To further decrease the uncertainty in groundwater conditions for dike slope stability, further research is recommended on understanding the processes that occur or have occurred inside the dike. First, data on dike cross-sections is sparse, thus our notion of dike heterogeneity is mostly based on point observations. To improve our knowledge of what the interior of a dike looks like, and to further include this knowledge in dike reinforcement practice, I would encourage any cooperation between specialists in the fields of dike safety and dike history, as they proved to be much more intertwined than previously thought. This can increase the spatial density of high-quality data on dike buildup material and ages of dike erection phases and decrease the uncertainty on dike heterogeneity in river dikes.

Less destructive ways of decreasing the uncertainty of groundwater conditions in river dikes are by either directly monitoring groundwater conditions or by performing borehole drillings or cone penetration tests. With the former, a time-dependent response is observed that can be used to calibrate a groundwater model (White et al., 2020) and as such it has predicting capacities over a larger area beyond the observation point. With the latter, probabilistic information on soil texture and geotechnical parameters are frequently derived (van der Krogt et al., 2019) and in recent years permeability estimations from combined cone penetration test and groundwater measurements are more widely used (McCall and Christy, 2020). However, these methods are often only used to approximate average values over larger depth ranges, not fully capturing the realistic heterogeneity within river dikes. The development of novel methods for saturated conductivity estimations from geophysical techniques would greatly improve schematizations of groundwater conditions inside the dike body.

6.6.2 Small-scale heterogeneity in subsurface properties and efficient groundwater modelling

The research in this thesis includes various geometries and parameterizations of geological units, but generally (except for chapter 4 on dike interior simulation) uses a homogeneous parameterization over larger spatial domains. However geotechnical and hydrological parameters are known to vary substantially within these geological units as well. A dike failure slip plane tends to be attracted to weaker zones, but the influence of weak zones is typically small compared to other sources of uncertainty, allowing for the use of layer-average estimations of geotechnical properties (van der Krogt, 2022). For groundwater conditions, the scale of the considered problem matters: large-scale problems can be sufficiently parameterized by average properties, but small-scale problems require the inclusion of local heterogeneity (de Marsily et al., 2005). Other groundwater-related dike failure mechanisms (such as piping) are known to be influenced by this local heterogeneity (Dirkx et al., 2020), but for dike slope stability, this has remained relatively unattended and requires further study. Further research on the required scale of heterogeneity to accurately assess groundwater con-

ditions for dike slope stability is therefore needed. However, to capture the effect of subsurface heterogeneity, it is probably required to use 3D groundwater models and increase the spatial resolution of those models. This might lead to infeasible calculation times or memory usage, but further research on effective parallel computing for these small-scale hydrological problems might overcome this problem (Verkaik et al., 2021).

6.6.3 Timing of dike failure and residual strength

A time-dependent analysis of dike slope stability indicated that the highest probability for dike slope failure occurs several days after the maximum water level, which is self-evident for outer (riverward) slope failure but less so for inner (landward) slope failure. As water levels may have dropped substantially by that time and are likely to decrease further in the days after failure, this has a large influence on the development of the dike breach and the probability of extensive flooding in the area behind the dike. Thus, we would argue to reconsider the effect of a dike slope failure on flood probability, also in relation to other stability-related features of the dike, such as the presence of an erosion-resistant core or small sand lenses in the dike. The effect of these features can be assessed using DETRIS as well. They are important as a source of residual strength after dike slope failure and have a major influence on the intrusion length of pore pressures. I have already found that the flood wave shape has a large effect on dike slope safety. Additionally, since a dike with a slope failure is vulnerable to fast re-occurring high water levels, we recommend analyzing the return times of high river water levels shortly after a possible dike failure. Finally, the evolution of pore pressures and soil behavior during deformation could also influence the residual strength of the dike.

Long term changes in dike reliability

From a methodological point of view, the effect of collecting data on changing dike strength properties for long-term dike safety assessments is now being covered (Klerk et al., 2019). However, the processes that change the dike strength are still poorly understood. More precisely, understanding the timing and rate at which soil properties change is important for estimating future dike safety. In terms of long-term processes such as soil formation and weathering, DETRIS can link the composition of a particular layer and its properties to material and age. Additionally, compaction of the layers can change the dike buildup geometry and material properties. This, in turn, may alter the behavior of the dike during prolonged periods of drought due to irreversible shrinkage of clay and peat and the formation of fissures. These changes could affect the dike's ability to withstand high water levels that follow, thus introducing hysteresis.

6.6.4 Script and data availability

Database global sensitivity analysis dike parameters and safety factor

A global sensitivity analysis of dike stability under adverse loading is performed using a coupled hydro-stability model to indicate relations between the geometry, material

characteristics, groundwater hydrology and stability for three different failure processes (van Woerkom et al., 2021). The database created by this extensive Monte Carlo analysis contains parameter combinations and the corresponding safety factor F. The datasets are CSV files containing parameter values and their resulting safety factor (F) given a certain macro-stability related failure mechanism and are stored online (van Woerkom, 2020).

DETRIS; Dike Erection Tessellation using Regionally Inherited Statistics

The DETRIS algorithm is an object-based and process-based model simulating dike construction history on archaeological dike cross, yielding similar patterns of heterogeneity as observed in real dikes, and applying it in a dike safety assessment. The DETRIS code (in the Python programming language) and example input datasets (consisting of CSV-files) can be downloaded from `https://github.com/TvWoerkom/Detris`.

A Supplements to Chapter 4

A.1 Used sources containing dike cross-sections (in Dutch)

Location Name	Source
Pernis, Oud Pernis	Jacobs, E. (2000): Pernis, een doorsnede van de dijk van de polder 'Oud-Pernis' (11-76). DANS. https://doi.org/10.17026/dans-zrj-gh2m (11-76).
Kampen, N50 Ramspol	ADC Archeoprojecten; Ridder, J.A.A. de ; (2010): Kampen N50 Proefsleuvenonderzoek. DANS. https://doi.org/10.17026/dans-xnt-fsfk
Spijkenisse, Schenkeldijk	Burnier, C.Y.; (2003): Spijkenisse Schenkeldijk. DANS. https://doi.org/10.17026/dans-xyt-z4av
Vianen, Diefdijk	Genabeek, R.J.M. van; Schorn, E.A.; (2004): Project Verbreding A2: tracebegeleiding Diefdijk. DANS. https://doi.org/10.17026/dans-zdv-586d
Reitdiep, Kanaaldijken	Huis in t Veld, J.Y.; (2011): De dijken van het Reitdiep. Een archeologisch onderzoek bij een nieuwe fietsbrug over het Reitdiep te Groningen (GR). DANS. https://doi.org/10.17026/dans-zxr-astj
Breda, Buitendijks Slangwijk	Nollen, J.; Jonge, L. de; Gemeente Breda; (2010): Breda Buitendijks Slangwijk. DANS. https://doi.org/10.17026/dans-z82-d8jf
Angeren, Rijndijk	Mulder, J.R., P.F.J. Franzen, L.J. Keunen en A.J.M. Zwart, (2003): In de ban van de Betuwse dijken. Deel 4 Angeren. Een bodemkundig, archeologisch en historisch onderzoek naar de opbouw en ouderdom van de Rijndijk te Angeren (Over-Betuwe). Wageningen, Alterra.
Malburgen, Rijndijk	Mulder, J.R., L.J. Keunen en A.J.M. Zwart (2004): In de ban van de Betuwse dijken.Deel 5. Malburgen. Een bodemkundig, archeologisch en historisch onderzoek naar de opbouw en ouderdom van de Rijndijk te Malburgen/Bakenhof, Arnhem. Wageningen, Alterra.
Opheusden, Rijndijk	Mulder, J.R., P.F.J. Franzen, (2006): In de ban van de Betuwse dijken. Deel 6 Opheusden. Een bodemkundig, archeologisch en historisch onderzoek naar de opbouw en ouderdom van de Rijndijk te Opheusden (Neder-Betuwe). Wageningen, Alterra.
Vlaardingen, Maassluissedijk	Louwe, drs E. (Vestigia); Pierik, MSc H.J. (Vestigia); Flamman, drs J.P. (Vestigia) (2013): Dijkdoorgraving Maassluissedijk in het kader van de realisatie van de Doorverbinding Vettenoord - Centrum Westwijk te Vlaardingen; Een archeologische begeleiding (protocol opgraven) van de graafwerkzaamheden. DANS. https://doi.org/10.17026/dans-2x5-feem
Bunschoten, Westdijk	van Benthem, Drs A. (ADC ArcheoProjecten) (2017): Eemdijk Dijkverbetering Een coupure door de Eemdijk bij Bunschoten-Spakenburg. DANS. https://doi.org/10.17026/dans-zc3-f6vf
Lent, Bemmelsedijk	Rondags, drs. E.J.N. (RAAP) (2019): Lent zones K en L, archeologisch dijkonderzoek, gemeente Nijmegen. DANS. https://doi.org/10.17026/dans-ze9-ars8

A.2 Example D-Stability model including DETRIS dike

This supplementary material contains screenshots of one of the D-Stability models based on a previously conducted soil survey and a DETRIS dike simulation. These

screenshots provide insight in how the DETRIS dike simulation and pressure heads from the MODFLOW groundwater model are implemented in D-Stability. For readers without experience with the software I recommend to have a look at the software user manual first Deltares (2019). The cross-section, the material types and the corresponding hydro-geo-mechanical parameters are explained in detail in the main body of the manuscript. A short description will be provided here as well.

The cross-section mainly consists of sandy material below 0 m (above Dutch Ordnance Datum), but a clay cover can be found near the dike with a thickness of approximately 4 m (Figure A.1). On the landward side of the dike a sandy wedge is present. The dike itself consists of many layers (as simulated by the DETRIS algorithm) with lithologies ranging from clay to sand, but some peat is present too (Figure A.2).

In the D-Stability software, groundwater conditions are defined by head lines and reference lines. The head line represents a pressure head, and the reference line represents the corresponding location in the cross-section where this pressure head is valid. Linear interpolation of pressure heads in the z direction is applied in between reference lines Deltares (2019). Contrary to common practice, in which only a phreatic head line and one head line corresponding to a reference line in a deeper sand body are schematized, we inserted many reference lines with a maximum z-interval of 1 meter to fully capture the variability in groundwater conditions (Figure A.3). At depths of special interest, such as the base of the dike or the top of the sandy aquifer, this z-interval is further decreased. The transformation of the pixel-based MODFLOW pressure head output to the line-based D-Stability schematization was automated using python scripts.

Given two initial search areas, a particle swarm search algorithm aims to find the center points of two circles, which together with a horizontal bar form the critical slip plane using the Uplift Van method Van (2001). In this example a relatively shallow slip plane is found to be most critical with a Safety Factor of 1.466 (Figure A.4).

To further analyze the forces acting on this slip plane, the software includes a slip plane inspector. Here, we show the hydrostatic pressures (Figure A.5), with a clear deflection at the inner toe of the dike. In the calculated shear stress (Figure A.6) this deflection is observed as well. Additionally, variable the material type at the slip plane results in small jumps in calculated shear stress, as the material parameters (cohesion and internal friction angle) change as well (Figure A.6).

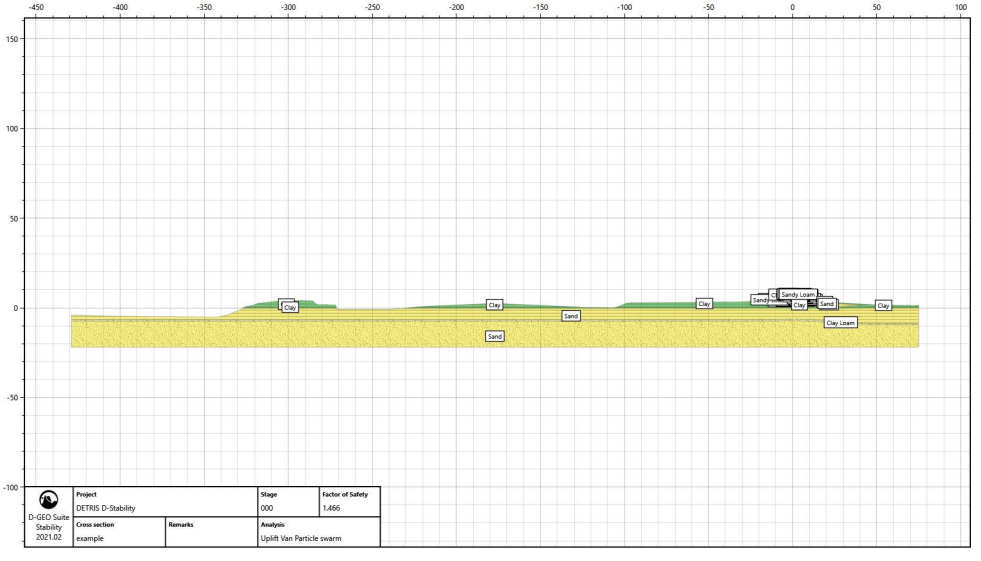

Figure A.1 Overview of cross-section geometry and subsurface schematization. The location of the dike is on the right of the cross-section. The river channel is located on the far left of the cross-section.

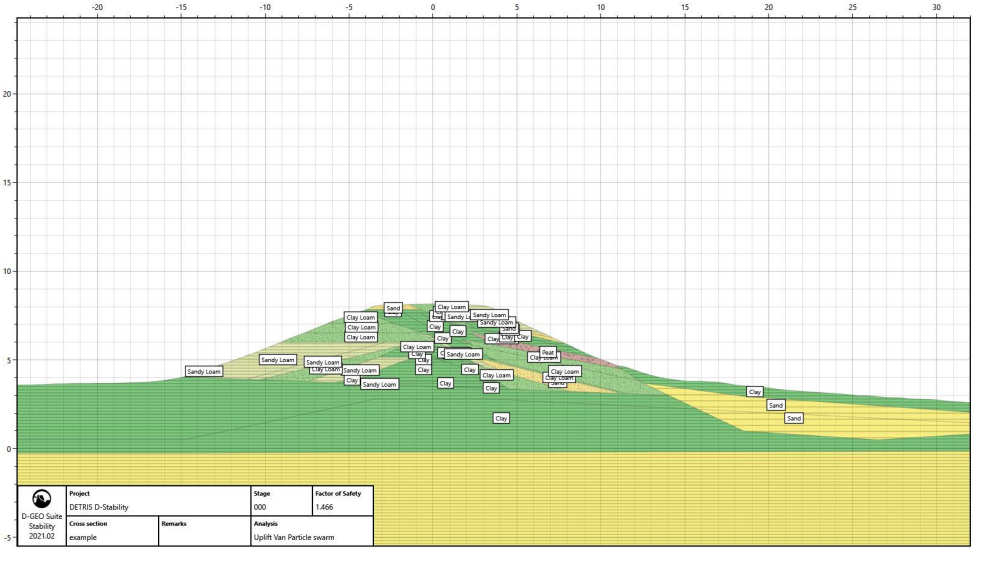

Figure A.2 Overview of cross-section dike geometry and subsurface schematization. Note again that the river is located on the left side of the dike.

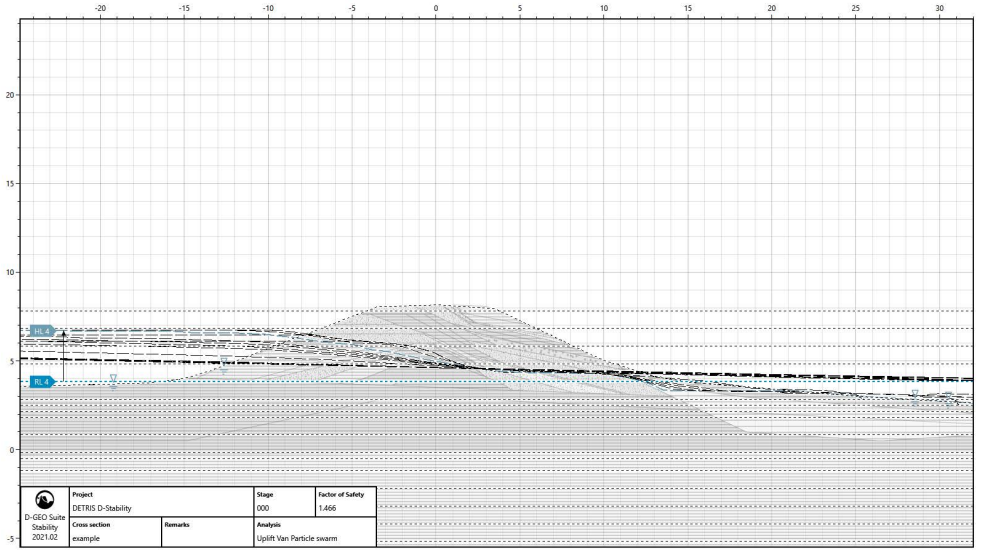

Figure A.3 Groundwater conditions as implemented in D-Stability. At an interval of maximum 1 meter reference lines are drawn to which the spatially variable piezometric head is assigned. Note how (in blue) A reference line (RL 4) corresponds to a certain pressure head line (HL 4).

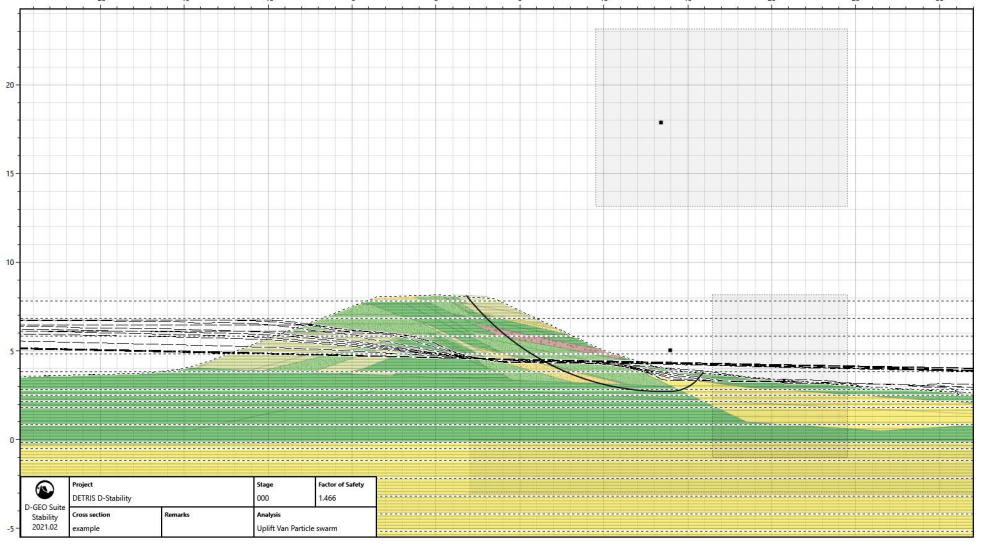

Figure A.4 Overview of D-Stability result, including the search algorithm starting condition and the circle centers for the critical slip plane according to the Uplift Van method Van (2001).

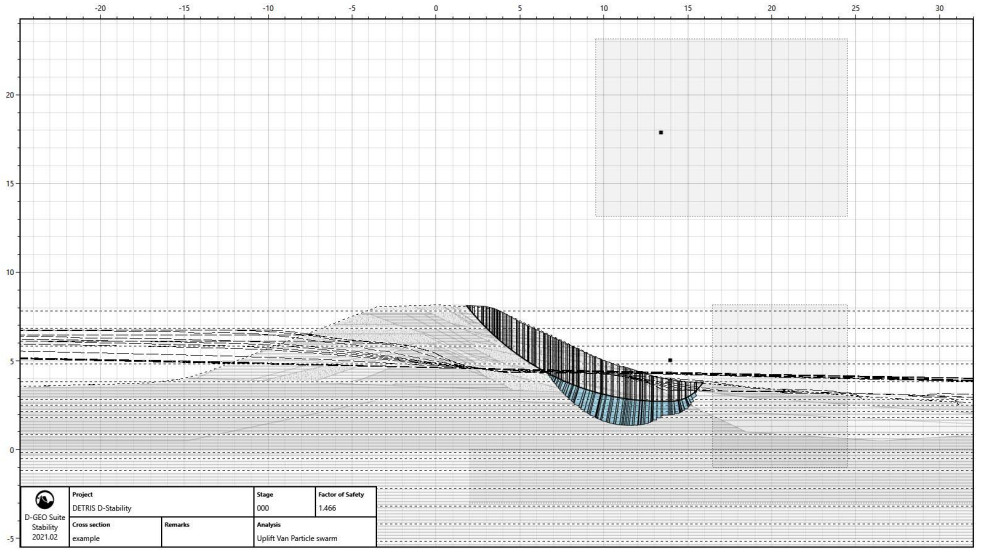

Figure A.5 Hydrostatic pressures (blue bars) at the base of the critical slip plane for each slice as used in the stability calculation.

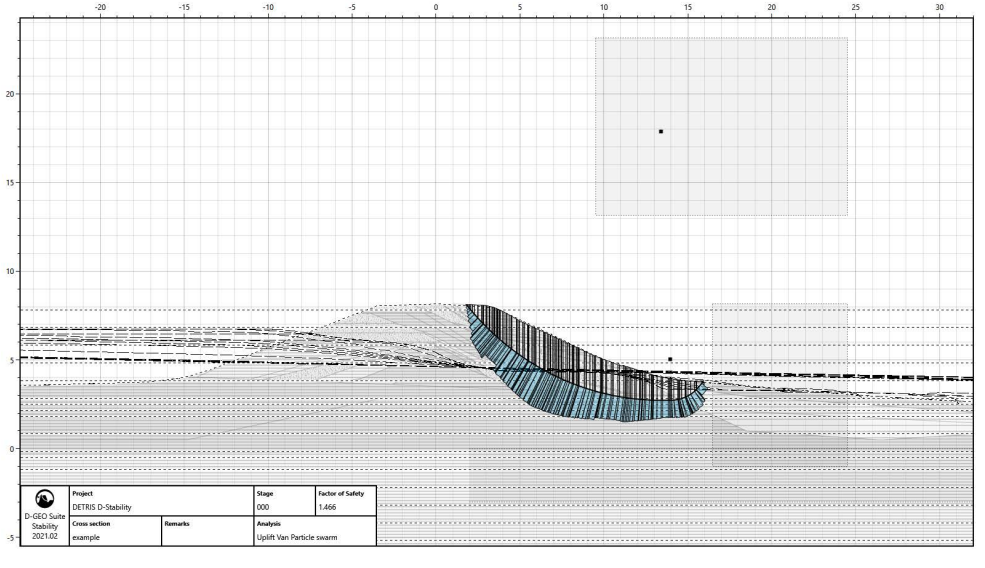

Figure A.6 Calculated shear stress at the base of the critical slip plane for each slice as used in the stability calculation. Note the sudden jumps in the calculated shear stress (length of the blue bars) where the material type at the base of the critical slip plane changes.

Bibliography

Andres, T. H. (1997), Sampling methods and sensitivity analysis for large parameter sets. Journal of Statistical Computation and Simulation 57, 77–110.

Baecher, G. B. (2016), Uncertainty in Dam Safety Risk Analysis. Georisk 10, 92–108. URL https://www.tandfonline.com/doi/abs/10.1080/17499518.2015.1102293.

Balistrocchi, M., G. Moretti, S. Orlandini and R. Ranzi (2019), Copula-based Modeling of Earthen Levee Breach due to Overtopping. Advances in Water Resources 134, 103433.

Barnett, B., L. Townley, V. Post, R. Evans, R. Hunt, L. Peeters, S. Richardson, A. Werner, A. Knapton and A. Boronkay (2012), Australian groundwater modelling guidelines. Tech. Rep. 82, National Water Commission, Canberra. URL file:///R:/LITERATURE/Angela/hydrogeologymethods/Waterlines-82-Australian-groundwater-modelling-guidelines.pdf.

Been, K. and M. G. Jefferies (1993), Towards systematic CPT interpretation. Predictive soil mechanics. Proc. of the Wroth memorial symposium, Oxford, 1992 , 121–134.

Begemann, H. K. (1965), The friction jacket cone as an aid in determining the soil profile. 6th ICSM&FE I, 17–20.

Berendsen, H. J. and E. Stouthamer (2000), Late Weichselian and Holocene palaeogeography of the Rhine-Meuse delta, the Netherlands. Palaeogeography, Palaeoclimatology, Palaeoecology 161, 311–335.

Bianchi Janetti, E., L. Guadagnini, M. Riva and A. Guadagnini (2019), Global sensitivity analyses of multiple conceptual models with uncertain parameters driving groundwater flow in a regional-scale sedimentary aquifer. Journal of Hydrology 574, 544–556.

Bierkens, M. F. (1996), Modeling hydraulic conductivity of a complex confining layer at various spatial scales. Water Resources Research 32, 2369–2382. URL http://doi.wiley.com/10.1029/96WR01465.

Bishop, A. (1955), The stability of earth dams. Ph.D. thesis, University of London. URL https://spiral.imperial.ac.uk/bitstream/10044/1/12453/2/Bishop-AW-1952-PhD-Thesis.pdf.

Bom, S. and B. van Leeuwen (2019), Opstellen Qf relaties 2018; Data-analyse en modelstudie. Tech. Rep., Svašek Hydraulics.

Borgonovo, E. (2007), A new uncertainty importance measure. Reliability Engineering and System Safety 92, 771–784.

Borgonovo, E., X. Lu, E. Plischke, O. Rakovec and M. C. Hill (2017), Making the Most out of a Hydrological Model Data Set: Sensitivity Analyses to Open the Model Black-box. Water Resources Research 53, 7933–7950. URL http://doi.wiley.com/10.1002/2017WR020767.

Botterhuis, T., R. Waterman and C. Geerse (2017), Gebruikershandleiding Waterstandsverloop. Tech. Rep., Rijkswaterstaat WVL.

Breiman, L., J. H. Friedman, R. A. Olshen and C. J. Stone (1984), Classification and regression trees. In: Classification and Regression Trees, CRC Press, 368. URL https://www.taylorfrancis.com/books/mono/10.1201/9781315139470/classification-regression-trees-leo-breiman-jerome-friedman-richard-olshen-charles-stone.

Butera, I. and M. G. Tanda (2006), Analysing River Bank Seepage with a Synthetic Design Hydrograph. Proceedings of the Institution of Civil Engineers: Water Management 159, 119–127. URL https://www.icevirtuallibrary.com/doi/abs/10.1680/wama.2006.159.2.119.

Butera, I., M. Climaci and M. G. Tanda (2020), Numerical analysis of phreatic levels in river embankments due to flood events. Journal of Hydrology 590, 125382.

Campolongo, F., J. Cariboni and A. Saltelli (2007), An effective screening design for sensitivity analysis of large models. Environmental Modelling and Software 22, 1509–1518.

Canli, E., M. Mergili, B. Thiebes and T. Glade (2018), Probabilistic landslide ensemble prediction systems: Lessons to be learned from hydrology. Natural Hazards and Earth System Sciences 18, 2183–2202. URL https://doi.org/10.5194/nhess-18-2183-2018.

Cao, Z., Y. Wang and D. Li (2016), Probabilistic approaches for geotechnical site characterization and slope stability analysis. Springer Berlin Heidelberg.

CEN (2004), Eurocode 7: Geotechnical design - Part 1: General rules. Tech. Rep., CEN.

Chavez Olalla, J., T. G. Winkels, D. J. Ngan-Tillard and T. J. Heimovaara (2021), Geophysical tomography as a tool to estimate the geometry of soil layers: relevance for the reliability assessment of dikes. Georisk URL https://www.tandfonline.com/doi/abs/10.1080/17499518.2021.1971252.

Cheng, H.-P., S. M. England and C. M. Murray (2016), Seepage and Piping through Levees and Dikes Using 2D and 3D Modeling Codes. Tech. Rep. ERDC/CHL TR-16-6, US Army Corps of Engineers. URL https://usace.contentdm.oclc.org/digital/collection/p266001coll1/id/3717/.

Ciriello, V., I. Lauriola and D. M. Tartakovsky (2019), Distribution-Based Global Sensitivity Analysis in Hydrology. Water Resources Research 55, 8708–8720. URL https://onlinelibrary.wiley.com/doi/10.1029/2019WR025844.

Cohen, K. (2017), Laaglandgenese boringendatabase Universiteit Utrecht. URL https://easy.dans.knaw.nl/ui/datasets/id/easy-dataset:74935.

Collison, A. J. and M. G. Anderson (1996), Using a combined slope hydrology/stability model to identify suitable conditions for landslide prevention by vegetation in the humid tropics. Earth Surface Processes and Landforms 21, 737–747.

Consortium DOT (2014), Veiligheid Nederland in Kaart 2, overstromingsrisico dijkring 16 Alblasserwaard en de Vijfheerenlanden. Tech. Rep., RoyalHaskoningDHV.

Curran, A., K. M. De Bruijn and M. Kok (2020), Influence of Water Level Duration on Dike Breach Triggering, Focusing on System Behaviour Hazard Analyses in Lowland Rivers. Georisk 14, 26–40. URL https://www.tandfonline.com/doi/abs/10.1080/17499518.2018.1542498.

de Marsily, G., F. Delay, J. Gonçalvès, P. Renard, V. Teles and S. Violette (2005), Dealing with spatial heterogeneity.

De Waal, J. P. (2016), Basisrapport WBI 2017. Tech. Rep., Deltares.

Deltacommissie (2008), Samen werken met water. Een land dat leeft, bouwt aan zijn toekomst. Bevindingen van de Deltacommissie 2008. Tech. Rep., Deltacommissie. URL http://www.deltacommissie.com/doc/2008-09-03AdviesDeltacommissie.pdf.

Deltares (2019), D-Stability User Manual. Tech. Rep., Deltares.

Deutsch, C. V. and L. Wang (1996), Hierarchical object-based stochastic modeling of fluvial reservoirs. Mathematical Geology 28, 857–880.

Di Prinzio, M., M. Bittelli, A. Castellarin and P. R. Pisa (2010), Application of GPR to the monitoring of river embankments. Journal of Applied Geophysics 71, 53–61.

Dirkx, W. J., R. van Beek and M. Bierkens (2020), The influence of grain size distribution on the hydraulic gradient for initiating backward erosion. Water (Switzerland) 12, 2644. URL https://www.mdpi.com/2073-4441/12/9/2644.

Eijgenraam, C., J. Kind, C. Bak, R. Brekelmans, D. Den Hertog, M. Duits, K. Roos, P. Vermeer and W. Kuijken (2014), Economically efficient standards to protect the netherlands against flooding. Interfaces 44, 7–21.

Elfeki, A. M. and F. M. Dekking (2005), Modelling subsurface heterogeneity by coupled Markov chains: Directional dependency, Walther's law and entropy. Geotechnical and Geological Engineering 23, 721–756. URL http://link.springer.com/10.1007/s10706-004-2899-z.

Erkens, G. and K. M. Cohen (2009), Quantification of intra-Holocene sedimentation in the Rhine-Meuse delta: A record of variable sediment delivery. Nederlandse Geografische Studies , 117–171.

Ferretti, F., A. Saltelli and S. Tarantola (2016), Trends in sensitivity analysis practice in the last decade. Science of the Total Environment 568, 666–670. URL http://dx.doi.org/10.1016/j.scitotenv.2016.02.133.

Feyen, L. and J. Caers (2006), Quantifying geological uncertainty for flow and transport modeling in multi-modal heterogeneous formations. Advances in Water Resources 29, 912–929.

Forzieri, G., L. Feyen, R. Rojas, M. Flörke, F. Wimmer and A. Bianchi (2014), Ensemble projections of future streamflow droughts in Europe. Hydrology and Earth System Sciences 18, 85–108.

Fredlund, D. G. and J. Krahn (1977), Comparison of Slope Stability Methods of Analysis. Canadian Geotechnical Journal 14, 429–439. URL http://www.nrcresearchpress.com/doi/10.1139/t77-045.

Fredlund, D. G., J. Krahn and D. E. Pufahl (1981), The relationship between limit equilibrium slope stability methods. In: Soil mechanics and foundation engineering. Proc. 10th international conference, Stockholm, June 1981. Vol. 3, (A.A.Balkema), Stockholm, 409–416. URL https://www.soilvision.com/subdomains/unsaturatedsoil.com/Docs/ResearchPapers/1981/ConferencePapers/Therelationshipbetweenlimitequilibriumslopestabilitymethods.pdf.

Gao, X., H. Liu, W. Zhang, W. Wang and Z. Wang (2019), Influences of Reservoir Water Level Drawdown on Slope Stability and Reliability Analysis. Georisk 13, 145–153. URL https://www.tandfonline.com/doi/abs/10.1080/17499518.2018.1516293.

Geleynse, N., J. E. Storms, D. J. R. Walstra, H. R. Jagers, Z. B. Wang and M. J. Stive (2011), Controls on river delta formation; insights from numerical modelling. Earth and Planetary Science Letters 302, 217–226.

Gong, W., H. Tang, H. Wang, X. Wang and C. H. Juang (2019), Probabilistic analysis and design of stabilizing piles in slope considering stratigraphic uncertainty. Engineering Geology 259.

Gouw, M. J. (2008), Alluvial architecture of the Holocene Rhine-Meuse delta (the Netherlands). Sedimentology 55, 1487–1516. URL https://onlinelibrary.wiley.com/doi/full/10.1111/j.1365-3091.2008.00954.x.

Gui, S., R. Zhang, J. P. Turner and X. Xue (2000), Probabilistic Slope Stability Analysis with Stochastic Soil Hydraulic Conductivity. Journal of Geotechnical and Geoenvironmental Engineering 126, 1–9. URL https://ascelibrary.org/doi/abs/10.1061/%28ASCE%291090-0241%282000%29126%3A1%281%29.

Guo, X., D. Dias and Q. Pan (2019), Probabilistic stability analysis of an embankment dam considering soil spatial variability. Computers and Geotechnics 113, 103093.

Hamm, N. A., J. W. Hall and M. G. Anderson (2006), Variance-based sensitivity analysis of the probability of hydrologically induced slope instability. Computers and Geosciences 32, 803–817.

Hasofer, A. M. (1974), Reliability Index and Failure Probability. Journal of Structural Mechanics 3, 25–27. URL https://www.tandfonline.com/doi/abs/10.1080/03601217408907254.

Hasofer, A. M. and N. C. Lind (1974), Exact and Invariant Second-Moment Code Format. ASCE J Eng Mech Div 100, 111–121. URL https://ascelibrary.org/doi/abs/10.1061/JMCEA3.0001848.

Hastie, T., R. Tibshirani and J. Friedman (2009), The Elements of Statistical Learning. Springer Series in Statistics, New York, NY: Springer New York. URL http://link.springer.com/10.1007/978-0-387-84858-7.

Hegnauer, M., J. Beersma, H. van den Boogaard, T. Buishand and R. Passchier (2014), Generator of Rainfall and Discharge Extremes (GRADE) for the Rhine and Meuse basins. Final report of GRADE 2.0. Tech. Rep., Deltares. URL http://projects.knmi.nl/publications/fulltexts/1209424004zws0018rgenerator_of_rainfall_and_discharge_extremes_grade_for_the_rhine_and_meuse_basins_definitief.pdf.

Hesselink, A. W., H. J. Weerts and H. J. Berendsen (2003), Alluvial architecture of the human-influenced river Rhine, The Netherlands. Sedimentary Geology 161, 229–248.

Hicks, M. A., J. D. Nuttall and J. Chen (2014), Influence of heterogeneity on 3D slope reliability and failure consequence. Computers and Geotechnics 61, 198–208.

Hijma, M. and K. S. Lam (2015), Globale stochastische ondergrondschematisatie (WTI-SOS) voor de primaire waterkeringen. Tech. Rep., Deltares.

Hoitink, A. J., Z. B. Wang, B. Vermeulen, Y. Huismans and K. Kästner (2017), Tidal controls on river delta morphology. URL https://www.nature.com/articles/ngeo3000.

Huber, M., M. van der Krogt and W. Kanning (2017), Probabilistic Slope Stability Analysis Using Approximative FORM. In: 14th International Probabilistic Workshop, Springer, Cham, 299–316. URL https://link.springer.com/chapter/10.1007/978-3-319-47886-9_21.

Hughes, J., C. Langevin and E. Banta (2017), Documentation for the MODFLOW 6 Framework. Tech. Rep., U.S. Geological Survey. URL https://pubs.er.usgs.gov/publication/tm6A57.

HWBP (2022), HWBP in cijfers (stand per 31 december 2021). URL https://www.hwbp.nl/projecten/kengetallen-hwbp.

ICOLD (2018), Twenty-Sixth Congress on Large Dams Vingt-Sixieme Congrès Des Grands Barrages. CRC Press, 1 edn.

Iooss, B. and P. Lemaître (2015), A review on global sensitivity analysis methods. Operations Research/ Computer Science Interfaces Series 59, 101–122. 1404.2405.

IPCC (2022), Climate Change 2022: Impacts, Adaptation, and Vulnerability. Contribution of Working Group II to the Sixth Assessment Report of the Intergovernmental Panel on Climate Change. Tech. Rep., IPCC, Cambridge, UK.

Isaaks, H. and R. Srivastava (1989), An Introduction to Applied Geostαtistics. New York: Oxford University Press.

Jafari, N. H., T. D. Stark, A. L. Leopold and S. M. Merry (2016), Three-dimensional levee and floodwall underseepage. Canadian Geotechnical Journal 53, 72–84.

Jonkman, S. N., H. G. Voortman, W. J. Klerk and S. van Vuren (2018), Developments in the management of flood defences and hydraulic infrastructure in the Netherlands. Structure and Infrastructure Engineering 14, 895–910. URL https://www.tandfonline.com/doi/abs/10.1080/15732479.2018.1441317.

Klerk, W. J., T. Schweckendiek, F. Den Heijer and M. Kok (2019), Value of information of structural health monitoring in asset management of flood defences. Infrastructures 4, 56. URL https://www.mdpi.com/2412-3811/4/3/56/htmhttps://www.mdpi.com/2412-3811/4/3/56.

Kok, M., R. Jongejan, M. Nieuwjaar and I. Tanczos (2017), Fundamentals of Flood Protection. Tech. Rep., Expertisenetwerk Waterveiligheid. URL https://puc.overheid.nl/rijkswaterstaat/doc/PUC_155243_31/.

Kok, M., J. Cortes Arevalo and M. Vos (2022), Towards Improved Flood Defences: Five Years of All-Risk Research into the New Safety Standards. TU Delft OPEN Books.

Kuriqi, A., M. Ardiçlioglu and Y. Muceku (2016), Investigation of seepage effect on river dike's stability under steady state and transient conditions. Pollack Periodica 11, 87–104. URL www.akademiai.comhttp://www.akademiai.com/doi/abs/10.1556/606.2016.11.2.8.

Langevin, C. D., J. D. Hughes, E. R. Banta, A. M. Provost, R. G. Niswonger and S. Panday (2019), MODFLOW 6 Modular Hydrologic Model version 6.1.1. URL https://www.usgs.gov/software/modflow-6-usgs-modular-hydrologic-model.

Lanzafame, R., H. Teng and N. Sitar (2017), Stochastic Analysis of Levee Stability Subject to Variable Seepage Conditions. In: Geotechnical Special Publication, GSP 283, 554–563.

Lendering, K., T. Schweckendiek and M. Kok (2018), Quantifying the Failure Probability of a Canal Levee. Georisk 12, 203–217. URL https://www.tandfonline.com/doi/abs/10.1080/17499518.2018.1426865.

Li, H. and J. F. Reynolds (1993), A new contagion index to quantify spatial patterns of landscapes. Landscape Ecology 8, 155–162. URL https://link.springer.com/article/10.1007/BF00125347.

Li, W., C. Zhang, J. E. Burt, A.-X. Zhu and J. Feyen (2004), Two-dimensional Markov Chain Simulation of Soil Type Spatial Distribution. Soil Science Society of America Journal 68, 1479–1490.

Lien, J.-M., G. Liu and C. D. Langevin (2015), GRIDGEN Version 1.0 : A Computer Program for Generating Unstructured Finite-Volume Grids. Tech. Rep., U.S. Department of the Interior; U.S. Geological Survey. URL http://dx.doi.org10.3133/ofr20141109.http://pubs.usgs.gov/of/2014/1109/.

Malet, J. P., T. W. van Asch, R. van Beek and O. Maquaire (2005), Forecasting the behaviour of complex landslides with a spatially distributed hydrological model. Natural Hazards and Earth System Science 5, 71–85. URL https://hal.archives-ouvertes.fr/hal-00330904.

Malkawi, A. H., W. F. Hassan and S. K. Sarma (2001), An efficient search method for finding the critical circular slip surface using the Monte Carlo technique. Canadian Geotechnical Journal 38, 1081–1089. URL http://www.nrcresearchpress.com/doi/10.1139/t01-026.

Mateo-Lázaro, J., J. Á. Sánchez-Navarro, A. García-Gil, V. Edo-Romero and J. Castillo-Mateo (2016), Modelling and layout of drainage-levee devices in river sections. Engineering Geology 214, 11–19. URL http://dx.doi.org/10.1016/j.enggeo.2016.09.011.

Matheron, G. (1963), Principles of geostatistics. Economic Geology 58, 1246–1266. URL http://pubs.geoscienceworld.org/segweb/economicgeology/article-pdf/58/8/1246/3481854/1246.pdf.

McCall, W. and T. M. Christy (2020), The Hydraulic Profiling Tool for Hydrogeologic Investigation of Unconsolidated Formations. Groundwater Monitoring and Remediation 40, 89–103. URL https://onlinelibrary.wiley.com/doi/full/10.1111/gwmr.12399.

Meehan, C. L. and S. Benjasupattananan (2012), An analytical approach for levee underseepage analysis. Journal of Hydrology 470-471, 201–211. URL http://dx.doi.org/10.1016/j.jhydrol.2012.08.050.

Michael, H. A., H. Li, A. Boucher, T. Sun, J. Caers and S. M. Gorelick (2010), Combining geologic-process models and geostatistics for conditional simulation of 3-D subsurface heterogeneity. Water Resources Research 46, 5527. URL http://doi.wiley.com/10.1029/2009WR008414.

Middelkoop, H., K. Daamen, D. Gellens, W. Grabs, J. C. Kwadijk, H. Lang, B. W. Parmet, B. Schädler, J. Schulla and K. Wilke (2001), Impact of Climate Change on Hydrological Regimes and Water Resources Management in the Rhine Basin. Climatic Change 49, 105–128. URL http://link.springer.com/10.1023/A:1010784727448.

Moellmann, A., P. A. Vermeer and M. Huber (2011), A Probabilistic Finite Element Analysis of Embankment Stability under Transient Seepage Conditions. Georisk 5, 110–119. URL https://www.tandfonline.com/action/journalInformation?journalCode=ngrk20.

Morgenstern, N. R. and V. E. Price (1965), The analysis of the stability of general slip surfaces. Geotechnique 15, 79–93. URL http://www.icevirtuallibrary.com/doi/10.1680/geot.1965.15.1.79.

Morris, M. D. (1991), Factorial sampling plans for preliminary computational experiments. Technometrics 33, 161–174.

Nossent, J., P. Elsen and W. Bauwens (2011), Sobol' sensitivity analysis of a complex environmental model. Environmental Modelling and Software 26, 1515–1525.

O'Neill, R. V., J. R. Krummel, R. H. Gardner, G. Sugihara, B. Jackson, D. L. DeAngelis, B. T. Milne, M. G. Turner, B. Zygmunt, S. W. Christensen, V. H. Dale and R. L. Graham (1988), Indices of landscape pattern. Landscape Ecology 1, 153–162. URL https://link.springer.com/article/10.1007/BF00162741.

Pachepsky, Y. and Y. Park (2015), Saturated Hydraulic Conductivity of US Soils Grouped According to Textural Class and Bulk Density. Soil Science Society of America Journal 79, 1094–1100.

PEÑUELA, W. F. M. (2013), River Dike Failure Modeling under Transient Water Condition. Ph.D. thesis, ETH-Zürich. URL https://www.research-collection.ethz.ch/handle/20.500.11850/78428.

Pianosi, F., K. Beven, J. Freer, J. W. Hall, J. Rougier, D. B. Stephenson and T. Wagener (2016), Sensitivity analysis of environmental models: A systematic review with practical workflow.

Pierik, H. J., E. Stouthamer, T. Schuring and K. M. Cohen (2018), Human-caused avulsion in the Rhine-Meuse delta before historic embankment (The Netherlands). Geology 46, 935–938. URL https://doi.org/10.1130/G45188.1.

Pleijster, E.-J., C. van der Veeken and LOLA Landscape Architects (2014), Dutch dikes. nai010. URL https://discovery.upc.edu/iii/encore/record/C__Rb1501734__Sdutchdikes__Orightresult__U__X7?lang=cat.

Polanco, L. and J. Rice (2014), A Reliability-Based Evaluation of the Effects of Geometry on Levee Underseepage Potential. Geotechnical and Geological Engineering 32, 807–820. URL https://link.springer.com/content/pdf/10.1007%2Fs10706-014-9759-2.pdf.

Powell, M. J. D. (1964), An efficient method for finding the minimum of a function of several variables without calculating derivatives. The Computer Journal 7, 155–162. URL https://academic.oup.com/comjnl/article-lookup/doi/10.1093/comjnl/7.2.155.

Pyrcz, M. J., J. B. Boisvert and C. V. Deutsch (2009), ALLUVSIM: A program for event-based stochastic modeling of fluvial depositional systems. Computers and Geosciences 35, 1671–1685.

Ratto, M., P. C. Young, R. Romanowicz, F. Pappenberger, A. Saltelli and A. Pagano (2007), Uncertainty, Sensitivity Analysis and the role of Data Based Mechanistic Modeling in Hydrology. Hydrology and Earth System Sciences 11, 1249–1266. URL https://hess.copernicus.org/articles/11/1249/2007/.

Rijkswaterstaat (2021), Schematiseringshandleiding Macrostabiliteit. Tech. Rep., Ministerie van Infrastructuur en Waterstaat.

Romme, W. H. (1982), Fire and Landscape Diversity in Subalpine Forests of Yellowstone National Park. Ecological Monographs 52, 199–221.

Saltelli, A., M. Ratto, T. Andres, F. Campolongo, J. Cariboni, D. Gatelli, M. Saisana and S. Tarantola (2008), Global Sensitivity Analysis. The Primer. John Wiley & Sons Ltd.

Schweckendiek, T., M. G. van der Krogt, A. Teixeira, W. Kanning, R. Brinkman and K. Rippi (2017), Reliability Updating with Survival Information for Dike Slope Stability Using Fragility Curves. In: Geo-Risk 2017, American Society of Civil Engineers, 494–503. URL https://ascelibrary.org/doi/10.1061/9780784480700.047.

Scott, D. W. (2015), Multivariate Density Estimation : Theory, Practice, and Visualization. John Wiley & Sons Ltd. URL https://www.wiley.com/en-us/Multivariate+Density+Estimation%3A+Theory%2C+Practice%2C+and+Visualization%2C+2nd+Edition-p-9780471697558.

Soil Science Division Staff (2017), Soil survey manual. Tech. Rep., USDA, Washington, D.C.

Song, X., J. Zhang, C. Zhan, Y. Xuan, M. Ye and C. Xu (2015), Global sensitivity analysis in hydrological modeling: Review of concepts, methods, theoretical framework, and applications.

Stafleu, J. and C. W. Dubelaar (2016), Product specification – Subsurface model GeoTOP (TNO 2016 R10133 — 1.3). Tech. Rep., TNO. URL www.tno.nl.

Stanisz, J., A. Borecka, Z. Pilecki and R. Kaczmarczyk (2017), Numerical simulation of pore pressure changes in levee under flood conditions. In: E3S Web of Conferences, vol. 24, 03002. URL https://www.e3s-conferences.org/articles/e3sconf/pdf/2017/12/e3sconf_ag2017_03002.pdf.

Stouthamer, E. (2001), Sedimentary products of avulsions in the Holocene Rhine-Meuse Delta, The Netherlands. Sedimentary Geology 145, 73–92.

Stouthamer, E., K. M. Cohen and M. J. Gouw (2011), Avulsion and its Implications for Fluvial-Deltaic Architecture: Insights from the Holocene Rhine–Meuse Delta. In: From River to Rock Record; The preservation of fluvial sediments and their subsequent interpretation, SEPM Society for Sedimentary Geology, 215–231.

Stuij, S., T. de Wit and R. Huting (2017), Dijkversterking Grebbedijk. Tech. Rep., HASKONINGDHV NEDERLAND B.V.,Waterschap Vallei en Veluwe.

't Hart, R., H. de Bruijn and G. de Vries (2016), Fenomenologische beschrijving Faalmechanismen WBI. Tech. Rep., Deltares. URL https://www.helpdeskwater.nl/onderwerpen/waterveiligheid/primaire/beoordelen/@205760/fenomenologische/.

Tabarroki, M., J. Ching, K. K. Phoon and Y. Z. Chen (2021), Mobilisation-based characteristic value of shear strength for ultimate limit states. Georisk .

Tahmasebi, P. (2018), Multiple point statistics: A review. In: Handbook of Mathematical Geosciences: Fifty Years of IAMG, Springer, Cham, 613–643. URL https://link.springer.com/chapter/10.1007/978-3-319-78999-6_30.

Tang, Y., P. Reed, K. Van Werkhoven and T. Wagener (2007), Advancing the identification and evaluation of distributed rainfall-runoff models using global sensitivity analysis. Water Resources Research 43. URL http://doi.wiley.com/10.1029/2006WR005813.

TAW (2001), Technisch Rapport Waterkerende Grondconstructies; Geotechnische aspecten van dijken, dammen en boezemkaden (in Dutch). Tech. Rep., Technische Adviescomissie voor de Waterkeringen.

TAW (2004), Technisch Rapport Waterspanningen bij dijken. Tech. Rep., TAW. URL https://repository-tudelft-nl.ezproxy2.utwente.nl/islandora/object/uuid:bf74eeaf-dc41-43fc-9c94-acd70f4a8340?collection=research.

TeBrake, W. H. (2002), Taming the waterwolf: Hydraulic engineering and water management in the Netherlands during the middle ages. Technology and Culture 43, 475–499.

Toonen, W. H., M. G. Kleinhans and K. M. Cohen (2012), Sedimentary architecture of abandoned channel fills. Earth Surface Processes and Landforms 37, 459–472.

Tourment, R. (2018), European and US levees and flood devences; Characteristics, Risks and Governance. Tech. Rep., EUCOLD Working Group on Levees and Flood Defences. URL www.barrages-cfbr.eu.

U.S. Army Corps of Engineers (2003), Slope stability - Engineering Manual. Tech. Rep., U.S. Army Corps of Engineers, Washington, D.C. URL https://www.publications.usace.army.mil/Portals/76/Publications/EngineerManuals/EM_1110-2-1902.pdf.

Vahedifard, F., S. Sehat and J. V. Aanstoos (2017), Effects of rainfall, geomorphological and geometrical variables on vulnerability of the lower Mississippi River levee system to slump slides. Georisk 11, 257–271. URL http://www.tandfonline.com/action/journalInformation?journalCode=ngrk20.

Van, M. A. (2001), New Approach for Uplift Induced Slope Failure. In: 15th International Conference on Soil Mechanics and Foundation Engineering, Istanbul, 2285–2288. URL https://www.issmge.org/publications/publication/new-approach-for-uplift-induced-slope-failure.

van der Krogt, M. (2022), Reliability updating for slope stability: Improving dike safety assessments using performance information. Ph.D. thesis, TU Delft. URL https://repository.tudelft.nl/islandora/object/uuid%3A2af85b15-9208-47bc-851d-9313d65cefcb.

van der Krogt, M. G., T. Schweckendiek and M. Kok (2019), Uncertainty in Spatial Average Undrained Shear Strength with a Site-specific Transformation Model. Georisk 13, 226–236. URL https://www.tandfonline.com/doi/abs/10.1080/17499518.2018.1554820.

van der Meer, A. W. (2020), Macrostabiliteit Buitenwaarts; een verkennende studie. Tech. Rep., POVM actuele sterkte.

van der Meer, A. W., A. Teixeira, A. P. Rozing and W. Kanning (2021), Probability of Flooding Due to Instability of the Outer Slope of a Levee, vol. 153 LNCE. Springer International Publishing. URL http://dx.doi.org/10.1007/978-3-030-73616-3_48.

van Gerven, K. (2004), Dijkdoorbraken in Nederland. Ontstaan, voorkómen en bestrijden. Tech. Rep., TU Delft; Royal Haskonig.

van Heiningen, H. (1978), Dijken en dijkdoorbraken in het Nederlandse rivierengebied. Boekencentrum. URL https://www.archieven.nl/nl/zoeken?mivast=0&mizig=64&miadt=102&miaet=14&micode=0623&minr=856387&miview=ldt.

van Leeuwen, P. (2019), An Analysis of the Influence of the Flood Duration on Slope Stability. Tech. Rep., Delft University of Technology, Delft.

van Woerkom, T. (2020), Monte-Carlo simulation of dike stability based on a coupled steady-state hydro-stability model. URL https://zenodo.org/record/4275401#.Y4nF4nbMJPZ.

van Woerkom, T., R. van Beek, H. Middelkoop and M. F. P. Bierkens (2021), Global Sensitivity Analysis of Groundwater Related Dike Stability under Extreme Loading Conditions. Water 13, 3041. URL https://www.mdpi.com/2073-4441/13/21/3041/htmhttps://www.mdpi.com/2073-4441/13/21/3041.

van Woerkom, T., M. van der Krogt and M. F. Bierkens (2023), Effects of flood wave shape on probabilistic slope stability of dikes under transient groundwater conditions. Georisk URL https://www.tandfonline.com/doi/abs/10.1080/17499518.2023.2222540.

Verkaik, J., J. D. Hughes, P. E. van Walsum, G. H. Oude Essink, H. X. Lin and M. F. Bierkens (2021), Distributed memory parallel groundwater modeling for the Netherlands Hydrological Instrument. Environmental Modelling and Software 143, 105092.

Walker, W. E., P. Harremoes, J. Rotmans, J. P. Van Der Sluijs, M. B. A. Van Asselt, P. Janssen and M. P. Krayer Von Krauss (2003), Defining Uncertainty. Integrated Assessment 4, 5–17. URL https://www.narcis.nl/publication/RecordID/oai:tudelft.nl:uuid:fdc0105c-e601-402a-8f16-ca97e9963592.

Wang, X., H. Wang and R. Y. Liang (2018), A method for slope stability analysis considering subsurface stratigraphic uncertainty. Landslides 15, 925–936.

White, J. T., R. J. Hunt, M. N. Fienen, J. E. Doherty and U. S. G. Survey (2020), Approaches to highly parameterized inversion: PEST++ Version 5, a software suite for parameter estimation, uncertainty analysis, management optimization and sensitivity analysis:. Techniques and Methods 5, 64. URL http://pubs.er.usgs.gov/publication/tm7C26.

Winkels, T., E. Stouthamer and K. Cohen (2022), Planform architecture, meander evolution and grain-size variability of a deltaic channel belt in the Rhine-Meuse delta, The Netherlands. Sedimentology URL https://onlinelibrary.wiley.com/doi/full/10.1111/sed.13022.

Wösten, J., G. Veerman, W. D. Groot and J. Stolte (2001), Waterretentie- en doorlatendheidskarakteristieken van boven-en ondergronden in Nederland: de Staringsreeks. Tech. Rep., Wageningen Environmental Research, Wageningen. URL http://edepot.wur.nl/359376http://library.wur.nl/WebQuery/clc/1611658.

Xu, Z., X. Zhou and Q. Qian (2020), The uncertainty importance measure of slope stability based on the moment-independent method. Stochastic Environmental Research and Risk Assessment 34, 51–65. URL https://doi.org/10.1007/s00477-019-01752-5.

Yue, S., T. B. M. J. Ouarda, B. Bobée, P. Legendre and P. Bruneau (2002), Approach for Describing Statistical Properties of Flood Hydrograph. Journal of Hydrologic Engineering 7, 147–153. URL https://ascelibrary.org/doi/abs/10.1061/%28ASCE%291084-0699%282002%297%3A2%28147%29.

About the author

Teun van Woerkom (11 June 1995) was born and raised in Tilburg, The Netherlands. During rainy days, he spent his childhood viewing atlas maps. He obtained his high school diploma at the Theresia Lyceum in the same city. It was during this period that his curly hair started to appear, and he developed an interest in system understanding, such as the co-occurrence of certain plant and animal species or the temporal development of lowland creek meanders between his yearly new-years-day hikes. Therefore, it was no surprise that he started his bachelor Earth Sciences at Utrecht University in 2012.

Two years later, while working in the Austrian Alps during the winter season as a ski instructor, he discovered his interest in comprehensive and creative explanations of difficult and counter-intuitive mechanisms. In addition, he was introduced to the effect and relevance of natural hazards (such as avalanches) and their risk management. After completing his Bachelor of Science (cum laude) with a focus on physical geography, he continued at Utrecht University with a Master in Earth Surface and Water in the direction of Geohazards and Earth Observation. Keeping a wide interest in all facets of natural hazards, he graduated (cum laude) in 2022 with a master thesis on moraine erosion and debris-covered glaciers in the Himalayas and an internship at a consultancy firm on modelling pluvial flood hazard in a part of the Netherlands.

After an extended summer holiday (during which he had his job interview online for this PhD project in an abandoned barn on the top of a hill in Romania, for it was the only spot with sufficient internet connection) he started his PhD within the All-Risk project. Within this project, being a cooperation between many universities, other institutions, and companies, he performed research on subjects within a triangle with its vertices on subsurface heterogeneity – groundwater flow – dike slope stability. In addition, he enjoyed supervising student field works, teaching other courses, and mentoring a master thesis project. Teun shortly worked as a post-doc at Utrecht University on developing a serious game on sediment budget management, before starting as a groundwater researcher and consultant at Deltares.

Acknowledgements

Allereerst wil ik mijn vaste begeleidingsteam Rens, Marc en Hans bedanken voor hun inzet, inbreng en energie in een onderwerp dat ook aan de grenzen van hun expertise lag. Door de gemixte inbreng, dan wel op de rode lijn, het algemene proces, een statistische analyse of de geotechnische modellering, was er altijd wel één van jullie die me terug de juiste kant op kon duwen (of liet inzien dat mijn eigen ingeslagen weg nog niet zo gek was). Daarnaast ben ik heel blij de kans te hebben gehad Ylva te begeleiden bij haar scriptie, en de kans om te proberen mijn kennis over processen in ruimte en tijd over te brengen aan een achttal eerstejaars studenten tijdens hun veldwerk.

Voor wat afleiding was het fijn dat mijn kantoortje naast de koffiehoek zat, daar was altijd wel een collega in voor een praatje. De tot-ietwat-voor-tien-opstartkoffies zijn daarnaast wel het vermelden waard, waarin een brug werd geslagen tussen het wel en wee van verschillende promovendi en de voor-uitwerking van de ideeën voor die dag. Een van de belangrijkere pijlers van die brug, Job, zat aan het eind van mijn promotietraject in een gelijke fase en was daarin een goede steunpilaar. De andere belangrijke steunpilaar, Bas, was ook altijd in de buurt om te sparren over allerhande onderwerpen. Hij leerde me vanaf het begin wat je allemaal met geotop kan, wat kickrolls zijn en op de valreep ook nog dat je op krukken prima paranimf kan zijn. De laatste twee 'dijkenjongens', Willem-Jan en Tim, zorgden daarnaast voor de nodige relativering van werkgerelateerde problemen en voor de nodige versnaperingen na afloop van lang uitgetrokken vergaderingen en congressen. Not only the current state of things, but mainly ideas for the future were a reoccurring topic with Tatjana, who I someday hope to meet in an old Spanish farmhouse.

Niet alleen op sociaal vlak, maar ook op wetenschappelijk gebied was er hulp en samenwerking. De meetings met de All-Risk gebruikerscommissie waren niet alleen een goed moment om eens uit te zoomen en van een afstandje naar mijn eigen onderzoek te kijken, maar vormden soms ook waardevolle discussiemomenten en zorgden voor eenvoudig benaderbare contacten bij verschillende instanties. Rondom de dijken-TETRIS ben ik Martin (en in een later stadium ook Johan) dankbaar voor het planten van het historie-zaadje en het actief meedenken over het opzetten van dit onderzoek. Besides that, the excursions and meetings with the other All-Risk researchers were fun and educative, met een speciale shoutout naar Mark door me mee te nemen in de wereld van probabilistische stabiliteitsberekeningen vanuit geotechnisch perspectief.

In the university I also had a fun time organizing FEST-lectures, together with the variable composition of the FEST-committee. Despite the approachable atmosphere and relaxed Friday drinks I unfortunately never managed to attract and involve a continuous flow of physical geographers... I do wish my successor Safaa good luck to

be more fortunate, and I am happy to have met you and been able to see you grow in your PhD during our shared office time in the VMA.

Daarnaast is er liefde en dankbaarheid voor mijn verrassingsprinsessen, Boris, -(spreek uit als 'streepje') en mijn ouders; jullie waren dan niet direct betrokken bij mijn promotie, maar zorgden wel voor blijdschap, vakanties, fietstochten en mooie momenten gedurende deze periode! Marjolein, fijn dat je vol enthousiasme mijn paranimf wilde zijn, blijf zo door de dag huppelen! Thuis was er altijd Benthe, die me (ondanks dat ze geen kaas heeft gegeten van grondwater dan wel dijken) gevraagd en ongevraagd advies gaf over het promoveer-proces en me daarmee vaak de goede kant op stuurde. Tenslotte was er de eeuwige steun van Muts de kat, die in de roerige thuiswerk-COVID-tijden mijn schoot tot een van haar favoriete slaapplekken had gemaakt. All these things did not only make the 4+ years of my PhD educational, but also fulfilling, grateful and fun! Thank you all :)

List of publications

Scientific publications

de Haas, T. and T. van Woerkom (2016), Bed scour by debris flows: experimental investigation of effects of debris-flow composition. Earth Surface Processes and Landforms 41, 1951–1966.

van Woerkom, T. (2020), Monte-Carlo simulation of dike stability based on a coupled steady-state hydro-stability model. URL https://zenodo.org/record/4275401#.Y4nF4nbMJPZ.

Van Woerkom, T., J. F. Steiner, P. D. Kraaijenbrink, E. S. Miles and W. W. Immerzeel (2019), Sediment supply from lateral moraines to a debris-covered glacier in the Himalaya. Earth Surface Dynamics 7, 411–427.

van Woerkom, T., R. van Beek, H. Middelkoop and M. F. P. Bierkens (2021), Global Sensitivity Analysis of Groundwater Related Dike Stability under Extreme Loading Conditions. Water 13, 3041. URL https://www.mdpi.com/2073-4441/13/21/3041/htmhttps://www.mdpi.com/2073-4441/13/21/3041.

van Woerkom, T., R. van Beek, H. Middelkoop and M. F. Bierkens (2022), Assessing lithological uncertainty in dikes: Simulating construction history and its implications for flood safety assessment. Journal of Flood Risk Management , e12848URL https://onlinelibrary.wiley.com/doi/full/10.1111/jfr3.12848.

van Woerkom, T., M. van der Krogt and M. F. Bierkens (2023), Effects of flood wave shape on probabilistic slope stability of dikes under transient groundwater conditions. Georisk URL https://www.tandfonline.com/doi/abs/10.1080/17499518.2023.2222540.

Conference Proceedings

van Woerkom, T., R. van Beek, M. F. P. Bierkens and H. Middelkoop (2019), Incorporating subsurface heterogeneity in hydrological models for assessing dike stability. In: Land of Rivers; Book of Abstracts NCR Days 2019, Utrecht, 34–35.

van Woerkom, T., R. van Beek, H. Middelkoop and M. F. P. Bierkens (2020), A coupled hydro-stability model for a sensitivity analysis on dike stability. In: Managing changing rivers; Book of Abstracts NCR Days 2020, Nijmegen, 75–76.

van Woerkom, T. A. A., M. G. van der Krogt and M. F. P. Bierkens (2022), On the incorporation of transient groundwater conditions resulting from variable flood wave shapes in probabilistic slope stability assessments of dikes. In: EGU General Assembly 2022, Vienna. URL https://meetingorganizer.copernicus.org/EGU22/EGU22-3099.html.

Other Publications

van Woerkom, T., J. Cortes Arevalo and P. Buter (2021), From dike history to reinforcement practice. URL https://storymaps.arcgis.com/stories/2d14e8423ce445ffa336dcb24f04ca1f.

van Woerkom, T., M. G. van der Krogt, M. van der Meer and M. F. P. Bierkens (2022), Reflection: Data-driven dike enforcements; Constructive feedback from new and historical sources. In: M. Kok, J. Cortes Arevalo and M. Vos, eds., Towards Improved Flood Defences; Five Years of All-Risk Research into the New Safety Standards, 121–125. URL https://kbase.ncr-web.org/all-risk/updates/reflection-data-driven-dike-enforcements-constructive-feedback-from-new-and-historical-sources/.